

Electronic Thesis and Dissertation Repository

---

6-22-2023 1:00 PM

## Water Decontamination via Electrodialysis

Baian Almusned,

Supervisor: Noël, James J., *The University of Western Ontario*

A thesis submitted in partial fulfillment of the requirements for the Master of Science degree in Chemistry

© Baian Almusned 2023

Follow this and additional works at: <https://ir.lib.uwo.ca/etd>

---

### Recommended Citation

Almusned, Baian, "Water Decontamination via Electrodialysis" (2023). *Electronic Thesis and Dissertation Repository*. 9606.

<https://ir.lib.uwo.ca/etd/9606>

This Dissertation/Thesis is brought to you for free and open access by Scholarship@Western. It has been accepted for inclusion in Electronic Thesis and Dissertation Repository by an authorized administrator of Scholarship@Western. For more information, please contact [wlsadmin@uwo.ca](mailto:wlsadmin@uwo.ca).

## **Abstract**

The single best water decontamination technique continues to be researched for by scientists globally. The purpose and subject of the decontamination determine the preferred technique to be used. For example, nanometre-sized contaminants require a different technique than those used for micrometer-scale contaminants. Recently, electrochemical membrane filtration techniques, such as electrodialysis, have gained great interest due to their capability to capture ionic contaminants. However, a lack of selective membranes continues to be a setback and so, novel polymers are under development. For this research, the sequestration behaviours of a commercial membrane and a novel phosphorus-based membrane are characterized for the application as potential metal decontaminants. A series of surface analytical and electrochemical techniques are applied to analyze the membranes and to explore their electrodialysis performance, respectively.

This work provides insight into the polymers' ion exchange capabilities, chemical and electrochemical, contributing to the advancements required when developing ion exchange membranes for water decontamination.

**Keywords:** electrodialysis, water treatment, ion-exchange membranes, decontamination techniques, surface analysis, electrochemistry

## Summary for Lay Audience

Contaminants, organic and inorganic, pave their way into masses of water either naturally or through human interventions, a result of the agricultural or electronics industries, for example. Various techniques have been employed over the years to decontaminate water and although advancements are on the rise, a universal solution has yet to be established. Specifically, a universal solution has yet to be established for heavy metals contaminants, which are comprised of elements with high atomic weights such as nickel, arsenic, or mercury. Heavy metals are commonly used in various industries, including the automotive industry, electronics, and mining operations. The demand for heavy metals is on the rise and this increases living beings' exposure. Heavy metal ion contaminants are especially concerning due to their toxicity to life, in all forms, as they can cause countless serious health and environmental problems. Consequently, scientists continue to investigate the best water treatment method, in terms of performance, environmental impact, and economical value. Electrochemical water purification techniques have gained large interest recently because of their ease of operation, low maintenance cost, and their ability to target contaminants on the picometer scale, along with other advantages. Electrodialysis, which uses electrochemistry and ion-permeable polymers, is one such technique. Interestingly, electrodialysis uses a membrane that cannot be crossed by water and other chemicals, but with assistance from an electric field, ionic contaminants can be made to cross the membrane, leaving clean water behind.

In this thesis, the concept of electrodialysis was applied to investigate its capabilities in removing nickel and strontium ions from water. A commercial ion-exchange polymer was compared to a novel phosphorus-based polymer prepared at Western University. Chemical and electrochemical tests as well as surface characterization techniques were applied to evaluate the metal ion uptake behaviour of the polymers. The results presented in this thesis provide considerations required for commercialising a novel class of polymers as ion-exchangers, expanding the field of electrodialysis, and facilitating the advancement of water decontamination techniques.

## **Co-Authorship Statement**

Chapter one: Written by Baian Almusned (100%); reviewed by Dr. James Noël.

Chapter two: Written by Baian Almusned (100%); reviewed by Dr. James Noël.

Chapter three: Experimental design by Baian Almusned (85%); with input from Dr. James Noël. Data was plotted by Baian Almusned (100%) and results were interpreted with input from Dr. James Noël. This chapter was written by Baian Almusned (100%); reviewed by Dr. James Noël.

Chapter four: Written by Baian Almusned (100%); reviewed by Dr. James Noël.

## Acknowledgments

This thesis was mostly completed during a time of uncertainty and many challenges and without the help of numerous important people in my life, it would not have been possible.

First and foremost, I would like to thank my supervisor Dr. James J. Noël. Thank you for your continuous support and wisdom throughout the years. Ever since you and Dr. David Shoesmith offered me a summer position in your group, you ignited my interest in research. Thank you for your witty jokes and for always being there for your students. You believed in me before I ever did.

Thank you to the Noël/Shoesmith group members. I am grateful for your support. In particular, Dr. Xuijie Li, Dr. Mengnan Guo, and Dr. Fraser Filice. Dr. Dmitrij Zagidulin and Dr. Jian Chen, thank you for your troubleshooting and advice.

Thank you to Dr. Paul Ragona and Dr. Johanna Blacquiere for your insight on the side of the project with the CapturePhos. Many thanks to J-W for providing me with the phosphorus polymers to test.

I would also like to thank the staff at SSW for always willing to help. Each scientist helped me in one way or another. Specifically, thank you to Dr. Jonas Hedberg for the help with ICP-MS, Mr. Brad Kobe and Dr. Jeff Henderson for your help with SEM/EDX, Ms. Becky Sarazen and Dr. Thalia Standish for your help with FT-IR and Raman Spectroscopy, and Ms. Heather Bloomfield for always checking-in and for your advice.

Thank you to my dear friends and family. You always push me to do better, stand by my side, and motivate me to try my best. I am grateful for every single one of you. Without your support, this thesis would not be possible.

Charlie, thank you for listening to my rants over the years and for your encouraging words.

This research was funded by NWMO, ORF, and IAEA MSCFP.

# Table of Contents

Abstract.....	ii
Summary for Lay Audience.....	iii
Co-Authorship Statement.....	iv
Acknowledgments.....	v
Table of Contents.....	vi
List of Tables.....	x
List of Figures.....	xii
List of Abbreviations and Symbols.....	xvi
1. Introduction.....	1
1.1 Water Contamination and Decontamination.....	1
1.2 Decontamination Methods.....	2
1.2.1 Physical Decontamination Methods.....	2
1.2.1.1 Screening and Filtration.....	3
1.2.1.2 Flotation.....	4
1.2.1.3 Membrane Filtration.....	4
1.2.2 Chemical Decontamination Methods.....	4
1.2.2.1 Precipitation.....	5
1.2.2.2 Advanced Oxidation.....	5
1.2.2.3 Ion Exchange.....	5
1.2.3 Electrochemical Decontamination Methods.....	6
1.2.3.1 Electrochemical Oxidation and Reduction.....	6
1.2.3.2 Electrocoagulation.....	7
1.2.3.3 Electrodialysis.....	7
1.3 Ion Exchange Membranes.....	9

1.4	Radioactive Contamination.....	11
1.5	Gaps in Research and Research Objectives.....	12
2.	Methods and Materials.....	14
2.1	Fundamentals of Electrochemistry.....	14
2.1.1	Concentration Polarization and ED Current-Potential Curves.....	15
2.2	Electrochemical Techniques.....	16
2.2.1	Open Circuit Potential (OCP).....	16
2.2.2	Polarization Techniques.....	16
2.2.2.1	Galvanostatic Polarization.....	17
2.2.2.2	Galvanodynamic Polarization.....	17
2.3	Surface and Solution Analysis Techniques.....	17
2.3.1	Scanning Electron Microscopy (SEM) and Energy Dispersive X-ray (EDX) Analysis.....	17
2.3.2	Fourier Transform Infrared (FTIR) Spectroscopy.....	18
2.3.3	Raman Spectroscopy.....	20
2.3.4	Inductively Coupled Plasma-Mass Spectrometry (ICP-MS).....	21
2.4	Experimental Conditions and Setup.....	22
2.4.1	Benchtop Experiments.....	22
2.4.2	Glovebox Experiments.....	23
2.5	Materials.....	23
2.5.1	Nafion 117 Membrane.....	23
2.5.2	CapturePhos.....	24
3.	Results and Discussion.....	25
3.1	Nafion Experiments.....	26
3.1.1	Chemical Sequestration.....	26
3.1.2	Electrochemical Sequestration.....	28

Control Experiments.....	28
LCD Determination.....	30
OCP Measurements.....	31
Potential-time Curves.....	32
Effect of Pre-Treatment.....	34
Effect of Applied CD: Experiments Above the LCD.....	35
Effect of applied CD: Experiments Below the LCD.....	37
Effect of Agitation Rate.....	37
Effect of Initial Concentration.....	39
Effect of Applied CD.....	40
Effect of Metal Ion.....	41
Effect of Generating an Electric Field: Galvanostatic (GS) or Potentiostatic (PS).....	42
Effect of ED Duration.....	43
Effect of pH.....	46
3.1.3 Surface Analysis and Membrane Characterization.....	50
FT-IR.....	50
SEM/EDX.....	51
Raman.....	53
Discussion.....	53
3.2 CapturePhos Experiments.....	56
3.2.1 Chemical Sequestration.....	56
3.2.2 Electrochemical Sequestration.....	59
3.2.3 Surface Analysis and Membrane Characterization.....	61
FTIR.....	61
SEM/EDX.....	62

Discussion.....	68
4. Conclusions and Future Work.....	69
4.1 Conclusions.....	69
4.2 Future Work.....	71
5. References.....	73
Curriculum Vitae.....	78

## List of Tables

Table 1.1. Various filtration techniques and the targeted particles' specifications.....	3
Table 2.1. Formulation ratios and amounts cured for CapturePhos polymers tested.....	25
Table 3.1. Chemical sequestration data for 1000 ppm Ni <sup>2+</sup> solution for various durations and agitation speeds.....	27
Table 3.2. Chemical sequestration data for 500 ppm Sr <sup>2+</sup> solution for various durations and agitation speeds.....	27
Table 3.3. Concentrations in the concentrate and diluate compartments for the three-hour experiment, with standard deviation values.....	29
Table 3.4. Measured limiting current densities (LCD) for the solutions listed.....	30
Table 3.5. Various pre-treatments tested, for Nafion 117 subjected to 500 ppm Ni <sup>2+</sup> test solution.....	35
Table 3.6. Removal efficiency and energy consumption data for two experiments, with and without pre-treatment, for 1000 ppm Ni <sup>2+</sup> systems performed at 1.67 mA/cm <sup>2</sup> for two hours.....	36
Table 3.7. Removal efficiency and energy consumption data for an experiment performed using 500 ppm Sr <sup>2+</sup> solution at a constant potential of 300 mV, 250 rpm agitation speed, and for three hours.....	43
Table 3.8. Removal efficiency and energy consumption for experiments performed using 500 ppm Sr <sup>2+</sup> solution at 0.33 mA/cm <sup>2</sup> for three and five hours.....	44
Table 3.9. Removal efficiency and EC data for experiments performed using 1000 ppm Ni <sup>2+</sup> solution at 0.167 mA/cm <sup>2</sup> for three and twenty hours.....	45
Table 3.10. pH measured in the concentrate and diluate compartments, over the span of the twenty-hour experiment.....	46
Table 3.11. EDX semi-quantitative elemental analysis of Nafion 117.....	52
Table 3.12. Chemical sequestration data for first-generation CapturePhos polymer (P-91).....	56
Table 3.13. Chemical sequestration data for second-generation CapturePhos polymer (P-05).....	57
Table 3.14. Chemical sequestration data for third-generation CapturePhos polymer (P-40).....	57

Table 3.15. Chemical sequestration data for third-generation CapturePhos polymer (P-40) to investigate the effect of agitating the solution at 250 rpm.....	58
Table 3.16. Chemical sequestration data from a ninety-six hour soak of the fourth-generation CapturePhos polymer (P-65).....	58
Table 3.17. Amount of Ni <sup>2+</sup> desorption in NaCl post soak experiment for P-40.....	58
Table 3.18. Measured Ni <sup>2+</sup> concentrations and removal efficiency for the electrochemical sequestration experiment performed at 9.2 mA/cm <sup>2</sup> for fifteen minutes, on a fourth-generation CapturePhos polymer (P-65).....	60
Table 3.19. EDX semi-quantitative data for P-91.....	63
Table 3.20. EDX semi-quantitative data for P-05.....	63
Table 3.21. EDX semi-quantitative data P-40.....	65
Table 3.22. EDX semi-quantitative data for P-65.....	67

## List of Figures

Figure 1.1. Schematic of an ED stack. Positive symbols represent cations, and negative symbols represent anions. Arrows indicate direction of ion flow.....	8
Figure 1.2. CEM schematic under the influence of an electric field. Arrow indicates the direction of electric field, positive charges depict cations, and negative charges depict anions.....	9
Figure 2.1. Representation of a typical electro dialysis current-potential curve.....	15
Figure 2.2. Schematic of primary electron beam interactions with a specimen.....	18
Figure 2.3. Schematic of FT-IR spectrometer components.....	19
Figure 2.4. Diagram of three possible transitions in Raman spectroscopy.....	20
Figure 2.5. Schematic of ICP-MS instrument components.....	21
Figure 2.6. Example calibration curve generated from ICP-MS standards with Ni <sup>2+</sup> concentrations between 1 ppb and 400 ppb.....	22
Figure 2.7. Four-electrode electrochemical cell setup.....	23
Figure 2.8. Schematic of Nafion 117 structure.....	24
Figure 2.9. Chemical reaction scheme for the preparation of the CapturePhos network.....	24
Figure 3.1. Change in Ni <sup>2+</sup> concentration from a 500 ppm Ni <sup>2+</sup> control experiment performed without an electric field .....	28
Figure 3.2. Change in Sr <sup>2+</sup> concentration from a 500 ppm Sr <sup>2+</sup> control experiment performed with a PTFE sheet instead of the Nafion 117 polymer.....	29
Figure 3.3. Limiting current densities (LCD) for the four solutions investigated.....	30
Figure 3.4. Example open circuit potential (OCP) transients for the four solutions investigated.....	31
Figure 3.5. Example potential-time curves corresponding to the indicated applied current densities for the experiments performed in 1000 ppm Ni <sup>2+</sup> solution.....	32
Figure 3.6. Example potential-time curves corresponding to the indicated applied current densities for the experiments performed in 500 ppm Ni <sup>2+</sup> solution.....	33
Figure 3.7. Example potential-time curves corresponding to the applied current densities for the experiments performed in 100 ppm Ni <sup>2+</sup> solution.....	33

Figure 3.8. Example potential-time curves corresponding to the applied current densities for the experiments performed in 500 ppm $\text{Sr}^{2+}$ solution.....	34
Figure 3.9. $\text{Ni}^{2+}$ concentration and removal efficiency changes from two experiments performed using 1000 ppm $\text{Ni}^{2+}$ solutions, with and without pre-treatment, at 1.67 $\text{mA}/\text{cm}^2$ for two hours.....	37
Figure 3.10. $\text{Sr}^{2+}$ concentration and removal efficiency changes from stationary (no stirring) and stirred experiments, agitation speed of 250 rpm, performed using 500 ppm $\text{Sr}^{2+}$ solution at 0.083 $\text{mA}/\text{cm}^2$ , for two hours.....	38
Figure 3.11. $\text{Ni}^{2+}$ concentration and removal efficiency changes from two experiments, with agitation speeds of 250 and 500 rpm, performed using 500 ppm $\text{Ni}^{2+}$ solution at 0.58 $\text{mA}/\text{cm}^2$ , for three hours.....	39
Figure 3.12. $\text{Ni}^{2+}$ concentration and removal efficiency changes for two experiments performed in 500 ppm and 1000 ppm $\text{Ni}^{2+}$ solutions, at 0.75 $\text{mA}/\text{cm}^2$ for three hours and 250 rpm agitation speed.....	40
Figure 3.13. $\text{Ni}^{2+}$ concentration and removal efficiency changes for two experiments performed using 1000 ppm $\text{Ni}^{2+}$ solutions at two current densities, 0.75 and 0.77 $\text{mA}/\text{cm}^2$ for two hours.....	41
Figure 3.14. $\text{Ni}^{2+}$ and $\text{Sr}^{2+}$ concentration and removal efficiency changes from experiments performed using 500 ppm $\text{Ni}^{2+}$ and 500 ppm $\text{Sr}^{2+}$ solutions at 0.33 $\text{mA}/\text{cm}^2$ for two hours.....	41
Figure 3.15. $\text{Sr}^{2+}$ concentration and removal efficiency changes from an ED experiment performed using 500 ppm $\text{Sr}^{2+}$ solution, at a constant potential of 350 mV, 250 rpm agitation speed, and for three hours.....	42
Figure 3.16. $\text{Sr}^{2+}$ concentration and removal efficiency changes for experiments performed using 500 ppm $\text{Sr}^{2+}$ solution at 0.33 $\text{mA}/\text{cm}^2$ for three and five hours.....	44
Figure 3.17. Time-potential curve for an experiment performed using 1000 ppm $\text{Ni}^{2+}$ solution at 0.167 $\text{mA}/\text{cm}^2$ , 250 rpm stirring speed, and for twenty hours.....	45
Figure 3.18. Pourbaix diagram for Ni-Cl system at 25 °C, indicating water stable region (dashed lines) and stable species at the given potential and pH values.....	47
Figure 3.19. Electrochemical cell diagram demonstrating the precipitation of nickel hydroxide.....	47
Figure 3.20. $\text{Ni}^{2+}$ concentration and removal efficiency changes for a pH-controlled experiment performed using 500 ppm $\text{Ni}^{2+}$ solution at 0.58 $\text{mA}/\text{cm}^2$ , 250 rpm agitation speed, and for three hours.....	48

Figure 3.21. Comparison between the removal efficiency and EC for 100 ppm, 500, and 1000 ppm Ni <sup>2+</sup> solutions investigated, at an applied CD of 0.58 mA/cm <sup>2</sup> , 250 rpm, 500 rpm, and pH controlled at 2.....	49
Figure 3.22. FT-IR spectra of an as-received Nafion 117 membrane and a Nafion 117 membrane post experimentation.....	50
Figure 3.23. BSE micrographs of Nafion 117. Areas marked correspond to EDX areas in Table 3.11.....	51
Figure 3.24. Cross-section BSE micrographs of Nafion 117.....	52
Figure 3.25. Raman spectrum of the collected and centrifuged Ni(OH) <sub>2</sub> precipitate.....	53
Figure 3.26. Pourbaix diagram for Sr-Cl system at 25 °C, indicating the water stability region (lines a and b) and stable species at the given potential and pH values.....	55
Figure 3.27. Digital image of the punctured P-91 polymer after a failed electrochemical experiment.....	59
Figure 3.28. Potential recorded for fifteen minutes in response to the application of 9.2 mA/cm <sup>2</sup> for polymer P-65.....	60
Figure 3.29. FT-IR spectrum of polymer P-40.....	61
Figure 3.30. Top-down SEM micrographs of a first-generation CapturePhos polymer (P-91). The areas marked indicate the EDX areas in Table 3.19.....	62
Figure 3.31. Cross-section SEM micrographs of a first-generation CapturePhos polymer (P-91).....	63
Figure 3.32. Top-down SEM micrographs of a second-generation CapturePhos polymer (P-05). The areas marked indicate the EDX areas in Table 3.20.....	64
Figure 3.33. Cross-section SEM micrographs of a second-generation CapturePhos polymer (P-05).....	64
Figure 3.34. Top-down SEM micrographs of a third-generation CapturePhos polymer (P-40). The areas marked indicate the EDX areas in Table 3.21.....	65
Figure 3.35. Cross-section SEM micrographs of a third-generation CapturePhos polymer (P-40).....	66
Figure 3.36. Cross-section SEM micrographs of a third-generation CapturePhos polymer (P-46).....	66
Figure 3.37. Top-down SEM micrographs of a fourth-generation CapturePhos polymer (P-65). The areas marked indicate the EDX areas in Table 3.22.....	67

Figure 3.38. Cross-section SEM micrographs of a fourth-generation CapturePhos polymer (P-65).....68

## List of Abbreviations and Symbols

AEM	Anion exchange membrane
AO	Advanced oxidation
$A_m$	Membrane area
ATR	Attenuated total reflectance
BSE	Backscattered electron
$C_{d,i}$	Initial diluate concentration
$C_{d,f}$	Final diluate concentration
$C_i$	Ion concentration
CEM	Cation exchange membrane
CC	Constant current
CD	Current density
CV	Constant potential
$D_i$	Diffusion coefficient
DI	Deionized
$e^-$	Electron
E	Potential difference
EC	Energy consumption
ED	Electrodialysis
EDX	Energy dispersive X-ray
EO	Electrochemical oxidation

ER	Electrochemical reduction
F	Faraday constant
FTIR	Fourier transform infrared spectroscopy
GS	Galvanostatic
HCl	Hydrochloric acid
HER	Hydrogen evolution reaction
HNO <sub>3</sub>	Nitric acid
I	Current
i	Ion concentration
I <sub>app</sub>	Applied current
ICP-MS	Inductively coupled plasma-mass spectrometry
IEM	Ion exchange membrane
J <sub>i</sub>	Flux density
LCD	Limiting current density
MAC	Maximum acceptable concentration
NWMO	Nuclear Waste Management Organization
OCP	Open circuit potential
P	Productivity
PS	Potentiostatic
PVDF	Polyvinylidene fluoride
Q <sub>d</sub>	Diluate flow rate
R	Electrical resistance

RO	Reverse osmosis
rpm	Revolutions per minute
SCE	Saturated calomel electrode
SE	Secondary electron
SEM	Scanning electron microscopy
SHE	Saturated hydrogen electrode
T	Temperature
t	Time
TEGDAE	Tetra ethylene glycol diallylether
TTT	1,3,5-triaza-triallyl-trione
U	Potential
UV	Ultraviolet
V	Volume
v	Velocity
$z_i$	Ion charge
$\phi$	Potential

# 1. Introduction

## 1.1 Water Contamination and Decontamination

Water is necessary for all living organisms' survival and so it is crucial to protect water sources. Water contamination is inevitable, whether it occurs via natural means or is anthropogenic. Various contaminants exist, from organic matter to microorganisms, to inorganics including heavy metals. Natural vectors of contamination include urban run-offs, soil erosion, and aerosol particulates, whereas anthropogenic means include mining operations, metal refineries and electroplating industries, agricultural industries, and nuclear power [1]. The resulting commonly discovered heavy metal contaminants in wastewater effluents include Pb, Hg, Cd, Zn, and Ni. Furthermore, the increased demand for heavy metals has led to an increase in human exposure to them, and heavy metal contamination causes a high level of serious health and environmental problems [1]. Studies have demonstrated a correlation between, for example, exposure to chromium (Cr) and cancer in animals and humans [2]. Specifically, hexavalent chromium [Cr(VI)] is classified as a human carcinogen and Cr(VI)-containing compounds are also known to cause asthma and renal damage [2]. Moreover, Ni is also a known human allergen and carcinogen. Consumption of Ni can lead to hepatitis, dermatitis, cardiovascular disease, pulmonary fibrosis, and central nervous system dysfunctions [3]. Consequently, development of purification techniques for metal-contaminated water is of paramount importance.

In order for positive change to occur towards producing cleaner water, wastewater bodies must be treated before discharge into the environment. The majority of metal-contaminated water originates from commercial, industrial, and domestic anthropogenic activities [4]. The resulting wastewater is mostly left untreated before its liberation into the environment. Source reduction of contaminants is the first step to providing cleaner water and minimizing waste generated. Along with limiting anthropogenic contamination, treating the contaminated water is crucial for many other reasons. First, it will recover metals to be used subsequently, which is a more sustainable approach than disregarding valuable metals as waste. For example, 18 metals out of 60 chemical elements, identified by the United

Nations as recycling targets, are currently recovered at a rate of 50% [5]. Other metals have a recycling rate of 1%, and this low rate is attributed to a lack of practical recycling methods [5]. Treating contaminated water will also generate large volumes of clean water to be reused. Desalination is a great example, since it removes salts from water, producing fresh water for further use. Furthermore, treating contaminated water will aid in decreasing waste volumes generated. Just like how landfill volume is reduced by separating out recyclable material, removing metal contaminants from water decreases the volume of waste for disposal and allows for recycling of metals.

Water treatment methods can be classified as primary, secondary, or tertiary treatments. Primary treatment consists of a preliminary physical filtration process. Secondary treatment is considered a biological method, and tertiary treatment is the advanced treatment process. The end-product of the first two methods enters the tertiary step, where water is converted into high quality water, ready for the specified use, such as drinking and industrial purposes. In the tertiary step, 90 to 99% of contaminants are eliminated. All three treatment steps are typically integrated in a complete water treatment plant [6].

Wastewater treatment methods are also subclassified as biological, physical, and chemical. A typical wastewater treatment employs all three to eliminate the various types of contaminants [6]. Biological methods employ microorganisms to reduce the dissolved organic content in the water, whereas physical and chemical methods use physical barriers and chemical reagents [7]. More recently, electrochemical methods have been introduced as a fourth sub-classification. The focus of this research is on an electrochemical decontamination technique, known as electrodialysis, which falls under the tertiary/physical techniques category [7]. Water is required for all living things and the scarcity of clean water is a real concern for the generations to come. However, before diving further into the focus of this research, this thesis introduces more well-understood and common water decontamination methods below.

## 1.2 Decontamination Methods

From the various classifications of water treatment methods mentioned above, only physical, chemical, and electrochemical methods are discussed in this report.

## 1.2.1 Physical Decontamination Methods

Physical methods for water treatment do not change the chemical nature of the contaminants. Instead, they use barriers such as screens and membranes to separate out the contaminants. Examples include screening and filtration, flotation, and membrane filtration.

### 1.2.1.1 Screening and Filtration

Screening removes large solid waste particles by using physical barriers, and it is typically the first step in a treatment plant. Screens of different sizes are used, as pre-treatment, to remove large bits of suspended material [8]. The size of the passageways through which the contaminants pass is used to classify the physical barrier. Screening is crucial because not only does it increase the efficiency of the biological and chemical methods, but it also ensures that the large waste particles do not impair any equipment used in the next treatment steps [8]. Pollutants removed during this stage include cans, wood, plastic, and paper. After the wastewater has been through the screening process, it typically undergoes filtration, which removes wastewater solids by permeating the water across granular media [9]. Filtration has different subcategories according to the insoluble contaminants' size (Table 1.1).

**Table 1.1. Various filtration techniques and the targeted particles' specifications.**

<b>Filtration Technique</b>	<b>Particle Size (<math>\mu\text{m}</math>)</b>	<b>Particle Characterization</b>
Particle filtration	1-1000	Macro to micro particle
Microfiltration	0.1-1	Macromolecular to cellular
Ultrafiltration	0.01-0.1	Molecular to macromolecular
Nanofiltration	0.001-0.01	Ionic to molecular
Reverse osmosis	0.0001-0.001	Ionic

### 1.2.1.2 Flotation

Flotation involves air bubbles transporting the suspended waste to the surface of the flotation tanks by agglomeration and adhesion to the bubbles [10]. Waste is removed subsequently from the surface of the tanks by a clearing device (skimmer). Moreover, finer bubbles lead to better accumulation of the particles and hence, higher efficiency [10]. This technique targets suspended solids and oils mostly and is common in conventional water treatment plants since it is very economical.

### 1.2.1.3 Membrane Filtration

Physical barriers with smaller passageways are considered part of a secondary treatment. This includes membrane filtration methods in which the targeted contaminants vary between 1 and 0.0001 micrometers in size [11].

Reverse osmosis (RO), also known as hyperfiltration, is an example of a membrane filtration technique which relies on hydraulic pressure and semi-permeable membranes. Water is pressurized across the membrane leaving behind ionic contaminant particles to be collected and removed [12]. It is considered the best, well-established water recycling method as it targets ionic contaminants [12]. Levels greater than osmotic pressure are applied, to concentrate and remove dissolved organic matter, viruses, and bacteria, producing ultrapure water [12]. Furthermore, this technique is considered as an economical technique for potable water generation from previously saline water. The main drawbacks of this technique are its cost and excessive requirement for equipment maintenance. Nonetheless, RO is one of the most common physical industrial water treatment methods used in the world today [13].

## 1.2.2 Chemical Decontamination Methods

Chemical decontamination methods involve the addition of chemical reagents which react to eliminate the contaminant. These methods are considered efficient, and the water generated is reused for industrial purposes. However, certain chemical decontamination methods may leave behind chemical residues in the water thus, not all of these techniques produce potable water [13]. Also, reagent consumption increase is another pitfall of these

methods. Precipitation, advanced oxidation, and ion exchange are examples discussed below.

### 1.2.2.1 Precipitation

Precipitation involves the addition of chemicals, such as ferric chloride, alum, and sodium bicarbonate to precipitate the dissolved contaminants [14]. This method has been applied for removal of heavy metals, like Ni, and in water softening. Removal rates of 40-60% for pollutants have been reported [14]. One complication of precipitation is the sludge volume generated requiring further action.

### 1.2.2.2 Advanced Oxidation

Advanced oxidation (AO) is a chemical method which converts organic contaminants and certain inorganics to water and carbon dioxide. AO is typically used to produce potable water [15]. Partial conversion to other compounds such as alcohols, aldehydes, and carboxylic acids is beneficial, as they are more biodegradable than their parent compounds [15]. Chlorine, ozone, peroxides, and potassium permanganate are examples of the chemical oxidants used. Ozone, for example, is produced from oxygen ( $O_2$ ) electrochemically or by UV radiation and attacks many organics and microorganisms [16]. Ozonation is a popular and preferred disinfection technique because it does not leave behind a residue of harmful chemicals. High costs associated with AO and the continuous need for chemicals decrease the desirability of this method and have limited the commercialization of it on a large scale.

### 1.2.2.3 Ion Exchange

The ion exchange method exchanges one ion for another of the same charge. Ion exchange resins have active sites on their surface to exchange cations or anions, depending on whether they are classified as cation or anion exchangers, respectively. Sodium silicates and zeolites are examples of ion exchangers [17]. This method can be used to soften water by removing magnesium and calcium ions. Ion exchange is a reversible process with low energy requirements. However, ion exchangers require regeneration, and this maintenance procedure introduces a hurdle in advancing this technique [17]. Another physical

manifestation of ion exchangers includes membranes, which will be discussed in section 1.3.

### 1.2.3 Electrochemical Decontamination Methods

Electrochemical treatment methods are considered tertiary, as they are aimed towards ionic species, micro suspended solids, and pathogenic bacteria [18]. In general, electrochemical techniques have gained more focus in the past decade due to their increased efficiency, ease of maintenance, zero requirement for chemical addition, and little sludge compared to alternative techniques. Electrochemical oxidation, electrocoagulation, and electrodialysis are examples of electrochemical treatment methods [18]. A key advantage of these methods is the recovery of metals, or resource recovery.

All electrochemical techniques require two electrodes (anode and cathode) and an electrolytic solution. Some advanced techniques require adjustments to be made to the system. For example, a membrane is added to any electrochemical membrane separation technique, such as in electrodialysis which is discussed below.

#### 1.2.3.1 Electrochemical Oxidation and Reduction

Oxidizing species are formed using current or potential difference to remove contaminants, in a method known as electrochemical oxidation (EO). The oxidants generated, such as hydrogen peroxide and hydroxy radicals, depend on the anode material. EO has been proven effective at degrading pollutants [19]. EO is typically used for organic contaminants and some inorganic compounds, whereas electrochemical reduction (ER) targets heavy metals. In ER, atoms or molecules at the cathode surface gain electrons when current is passed through the system. The metals are recovered after they are deposited on the cathode. A main drawback of this technique is the operation cost; the requirements of certain electrodes are often costly. Also, it is crucial to pay attention to the by-products formed as they can be toxic [19]. For example, chlorinated by-products may be generated and they can be more dangerous than the contaminant originally present in the water.

### 1.2.3.2 Electrocoagulation

Another electrochemical water decontamination method is known as electrocoagulation, in which multiple reactions take place concurrently. Metal ions dissipate in the water from the anode, whereas hydrogen gas and hydroxide ions are formed at the cathode. Electrons also move from the anode towards the cathode and this destabilizes surface charges on suspended solids in the water [18]. Suspended solids and heavy metals, along with other contaminants, coagulate to form flocs. Lastly, downstream filtration is used to separate the flocs from the water [18]. This technique has been shown to remove 90% of microplastics in simulated wastewater [19]. However, electrocoagulation is not ideal, since the electrodes are sacrificial and require replacement due to their corrosion with use over time.

### 1.2.3.3 Electrodialysis

Electrodialysis (ED) is a membrane-based electrochemical separation technique originally introduced as a desalination method and its uses have continued to grow over the years. Unlike the membrane techniques mentioned in 1.2.1.3, ED uses electrochemistry, rather than pressure, as a driving force to extract and transport ionic species in a solution. An ion exchange membrane (IEM) typically separates two, or more, solutions and the ion transport across the membrane is investigated. In a general ED system, an electric current is applied between the anode and cathode and the IEMs are paralleled between the electrodes. The electric current promotes the cations in solution to migrate towards the cathode and anions towards the anode [20]. IEMs facilitate the ions' movement from the diluate compartments to the concentrate compartments (from the side with initially a higher ion concentration to the side with the low ion concentration), respectively. On an industrial level, tens or hundreds of membranes are assembled in an ED stack [20]. However, for the purposes of simplification and to investigate the migration across the membrane of interest, this thesis work focused on an ED unit consisting of one cation exchange membrane.

The efficiency of ED processes can be evaluated via various measures. A common calculation used measures the energy consumption ( $EC$ ) of the process (Equation 1.1).  $U$  is the potential of the ED,  $I$  is the current,  $t$  is the duration of the ED process, and  $V$  is the

volume of solution treated. This measures the required energy to produce a unit volume of water. Increasing the efficiency of ED is directly linked to reducing the EC [21].

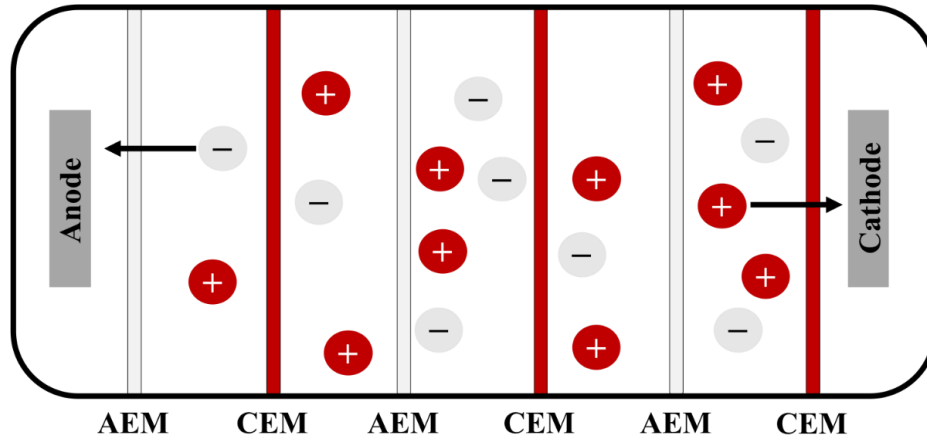


**Figure 1.1. Schematic of an ED stack. Positive symbols represent cations, and negative symbols represent anions. Arrows indicate direction of ion flow.**

$$EC = \frac{UIt}{V} \quad (1.1)$$

Productivity ( $P$ ) is another efficiency metric and it measures the amount of generated water, per unit time and membrane area ( $A_m$ ). This calculation gives information on the size requirement of the system.  $Q_d$  is the diluate flow rate per cell pair [22].

$$P = \frac{Q_d}{A_m} \quad (1.2)$$

A third ED efficiency measure evaluates the removal of the ion of interest, in percentage, and it can be calculated using the following equation,

$$Removal \% = \frac{C_{D,i} - C_{D,f}}{C_{D,i}} \times 100 \quad (1.3)$$

where  $C_{D,i}$  and  $C_{D,f}$  are the initial and final concentrations in the diluate compartment, respectively. In one study, ED was shown to remove 97% of contaminants, including Mg, Mn, sulfates, and fluorides, from an acid mine drainage [23]. In another study, ED was proven successful at removing contaminants, such as Cu, Zn, and Cr, from electroplating wastewater while simultaneously recovering water for use in the laboratory and pilot plants

[23]. There are more than 2000 ED plants worldwide for desalinating water. However, the capability of ED to effect metal decontamination is still under investigation, with a focus on enhancing the selectivity and proficiency of the process. Factors such as the potential difference applied and the IEM installed in the ED process are pivotal to its success.

### 1.3 Ion Exchange Membranes

IEMs are polymeric network films with ion exchange capabilities. Several subgroups of IEMs exist but the most common, and relevant to this research, are monopolar membranes, which include cation exchange membranes (CEMs) and anion exchange membranes (AEMs) [22]. IEMs have fixed groups, with either positive or negative charge, to facilitate ion transport. As the name suggests, CEMs exchange cations (counter-ions), since the fixed groups are negatively charged and impede negative ions (co-ions). Whereas anions are transported across AEMs with the facilitation of positively charged fixed groups. Figure 1.2 demonstrates how a CEM under the influence of an electric field separates cations from contaminated water to be captured on the other side of the membrane [24].

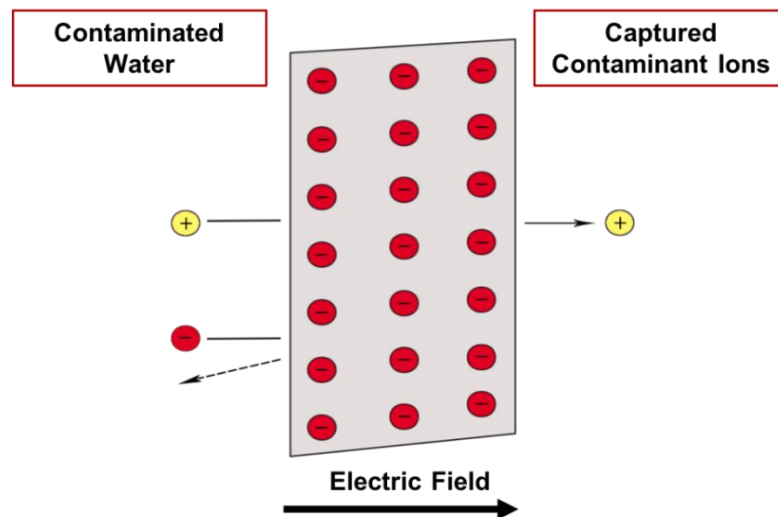


**Figure 1.2. CEM schematic under the influence of an electric field. Arrow indicates the direction of electric field, positive charges depict cations, and negative charges depict anions.**

Ions in electrolytes act as charge carriers and transport electric current, whereas in solid materials (i.e., metal) the charge carriers are usually electrons. The main difference

between electrons and ions as charge carriers is that ion conductivity is coupled with ionic mass transport in an electrolyte however, no mass is transported in an electron conductor [22]. The extended Nernst-Planck equation is used to describe ion transport in an electrolyte and IEMs:

$$J_i = -D_i \frac{dC_i}{dx} + -D_i \frac{Fz_i C_i}{RT} \frac{d\varphi}{dx} + vC_i \quad (1.4)$$

In this equation,  $J_i$  is the flux density of ion  $i$  with a concentration  $C_i$ ,  $z_i$  is the charge number,  $F$  is the Faraday constant,  $R$  is the electrical resistance,  $T$  is the temperature,  $\varphi$  is the potential,  $x$  denotes the coordinate across the membrane,  $D_i$  is the diffusion coefficient corresponding to  $i$ , and  $v$  is the linear convective velocity along  $x$ . The three main ion transport mechanisms in IEMs are represented by three terms in equation 1.4 and they are diffusion, migration, and convection [22]. Diffusion takes place when there is a concentration or chemical potential gradient, migration occurs via an electrical potential gradient, whereas convection occurs in response to a pressure gradient. The first term represents ionic diffusion, the second term refers to ion electromigration (migration by electrochemistry), and the third term represents convective transport of ions [22]. All three mechanisms contribute to the ion transport across membranes, nonetheless, only migration, specifically electromigration, plays a significant role in ED, since the electric field is the driving force.

Ion exchange membranes have numerous desired properties, including:

- High permselectivity: the membrane should be highly selective towards counterions but impermeable to co-ions.
- Low electrical resistance: this allows for maximum permeability of counterions.
- High stability (chemical and mechanical): the membrane should withstand any mechanical strain and must be stable across the entire pH range.

The semi-permeable polymeric films are applied in various fields, such as in energy conversion and energy storage, fuel cells, separation processes, and treatment of contaminated water and industrial effluents [25]. However, improvement of IEMs is necessary in order to increase selectivity towards the ions to be captured. For example, if a

CEM is installed in an ED unit to remove Ni from electroplating wastewater, the CEM will likely capture other cations, due to a lack of permselectivity, along with Ni, such as Na or Fe, hindering the process's efficiency. Factors behind selective ion transport across IEMs are not fully understood; however, specifics such as ion mobility and electrostatic attraction play a role.

The proficiency of IEMs to treat contaminated water is one of the research topics of interest, as utilizing IEMs and ED will decrease waste generated for disposal, reduce reagent consumption for wastewater treatment, and it will aid in the regeneration of clean water. Finally, this technique can prove its value in capturing radioactive contaminants, as discussed below.

## 1.4 Radioactive Contamination

Nuclear energy powers one in six Ontarians' electricity [26]. The waste generated by nuclear energy is categorized into three groups based on its activity: low-level, intermediate-level, and high-level radioactive waste [26]. 98.1% of the waste is considered low-level waste and is lightly contaminated with radioactive substances [26]. This includes tools, work clothes, and cleaning supplies from power plants. Intermediate-level waste originates from nuclear reactors including nuclear components and waste from the mining and processing of U [27], whereas the fuel used to power the plants becomes high-level waste. High-level waste is managed in interim storage facilities at the reactor sites, and a plan for its permanent disposal is under development by the Nuclear Waste Management Organization (NWMO, Toronto). Low- and intermediate-level waste is currently safely managed at the production sites; however, a long-term plan is still not finalized, as possible disposal methods continue to be investigated [27]. Various radionuclide removal techniques have been previously investigated [28, 29]. ED is one technique demonstrating promising results. For example, it was reported that 99.2% removal of radioactive cesium ( $^{137}\text{Cs}^+$ ) was achieved by ED [29].

Radioactive isotopes of Cs, I, and Sr are U fission by-products, and these isotopes are soluble in water [30]. When accidents occur, like at the Fukushima Daiichi Nuclear Power Plant, radionuclides can enter water streams, which is alarming, as radioactive waste is

dangerous to the environment and living organisms [31]. This research has great implications for the safe disposal of low-level and intermediate-level waste, since it can aid in removing radionuclides and recycling the previously contaminated water. For this reason, the capture of Sr was investigated in this study. Sr is naturally occurring in environments and the four stable non-radioactive isotopes are  $^{88}\text{Sr}$ ,  $^{86}\text{Sr}$ ,  $^{87}\text{Sr}$ , and  $^{84}\text{Sr}$  with natural abundances of 82.6%, 9.9%, 7.0% and 0.6%, respectively [30]. Sr has adverse health side effects including bone growth impairment and it is a carcinogen. The maximum acceptable concentration (MAC), per Health Canada's guidelines, for Sr in drinking water is 7.0 mg/L [30]. On the other hand, the most common radioactive isotopes of Sr are  $^{89}\text{Sr}$  and  $^{90}\text{Sr}$ , and they result from nuclear reactor operations [30]. Also, radionuclides of Sr are typically used in medical applications (i.e., in cancer radiotherapy and imaging). Thus, waste containing Sr is generated and disposal methods depend on the activity level, similar to other radioactive waste [31]. Low activity waste, or solid waste with less than 1.35 microcuries activity and liquid waste with less than one microcurie, are disposed of as ordinary waste and in a sanitary sewage system with plenty of water, respectively. Waste with medium activity is stored until the activity decays to low levels and then disposed of accordingly, whereas high activity waste is stored and buried in designated burial sites, as storing it until the activity decays is impractical [31]. Decreasing the waste volumes of medium and high activity waste decreases the need for long-term storage and burial of the waste. ED and IEMs have many potential applications for radioactive material and its waste, including cleanup of medical radioactive waste and cleanups of potential spills of radioactive material.

## 1.5 Gaps in Research and Research Objectives

The increase in demand for metals across multiple industries globally has resulted in an increase in metal presence in water systems and in waste streams. 71% of the world is water and only 1% is drinkable according to international standards [32]. Access to drinkable water is a worldwide concern for the twenty-first century. Even though research on water decontamination methods dates back to the 1800s, a lack of a universal method still exists. As outlined in section 1.1, water decontamination methods are generally grouped into three categories, which are primary, secondary, and tertiary treatments and subclassified as

biological, chemical, physical, and electrochemical methods. Electrochemical methods have gained more interest in the past decade, due to their many advantages, such as higher contaminant removal rates, lack of increase in reagent consumption, and ease of operation. These advantages deem electrochemical methods superior to competitor methods.

Although there have been many recent advancements regarding metal uptake research, there are some dark corners that require light to be shed on them [32, 33]. For example, the permselectivity towards the capture of certain metals is still lacking. Most methods facilitate the removal of contaminants based on type or size of contaminant but are not selective enough to the ionic speciation level. For example, CEMs are selective towards cations but there have not been reports of a certain CEM type that preferentially captures one cation over another. This is important in increasing efficiency and sustainability of ED processes, thus advancing water decontamination methods. Furthermore, rather than saturating a membrane and an ED stack with harmless and nontoxic ions, targeting health-endangering or radioactive contaminants is a better approach. ED of radioactive contaminants, to the best knowledge of the author, has not been investigated intensively. Sr was chosen as a metal of interest as it is a by-product of U fission and there has been great interest in the capture of Sr. Capture of Sr by zeolites was reported to provide 84-99% removal rates; however, leaching the Sr from the zeolites yielded low removal of 0.1-0.7% [34]. Therefore, other techniques, such as ED, must be investigated.

ED is a promising technique, and with a focus on improving its operation parameters, it can be very powerful in the water treatment field. Economical aspects are also important to consider. Most commercially available membranes are costly. As an example, Nafion polymers cost between \$700 and 3500/m<sup>2</sup> [35]. The gap in cheaper alternatives must be acknowledged. The phosphorus polymer (CapturePhos), introduced in section 2.5.2, is proposed as a solution to the mentioned problems. The ability to modify the network to tailor which cation it attracts and ligates increases its attractiveness as the next generation of CEMs.

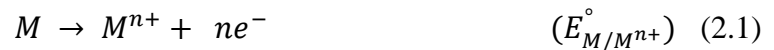
The objectives behind this research are the following. To further investigate ED as a metal decontamination technique and characterize its efficiency. Specifically, Ni and Sr were

chosen as the metals of interest due to their toxicity. Also, electrochemical capture of Sr has not been investigated profoundly and its capture is interconnected to its radionuclides, which is of great relevance to the nuclear industry. Selective membranes are unconventional and consequently, developing polymers that are ion-selective, allow electrochemical extraction of metal ions, are economical, and eliminate the need for chemicals would greatly advance the fields of waste management and water decontamination. Furthermore, testing a new class of polymers as potential CEMs is another objective to this research. The electrochemical behaviour of the polymer CapturePhos towards metal decontamination is characterized. The results from the CapturePhos polymer are compared to those of the commercial CEM, Nafion. The experimental design is discussed in the following section.

## 2. Methods and Materials

### 2.1 Fundamentals of Electrochemistry

Electrochemistry is the branch of chemistry that studies the relationship between electrical and chemical interactions. Species can be oxidized, via an anodic reaction, and reduced, via a cathodic reaction, in an electrochemical system. Furthermore, in a cathodic reaction there is a gain of electron(s) whereas in an anodic reaction a loss of electron(s) occurs [36]. Equations 2.1 – 2.3 present a typical anodic reaction, a cathodic reaction, and an overall reaction, respectively.  $M$  represents a material,  $n$  is the number of electrons ( $e^-$ ) transferred,  $Ox$  is the oxidant being reduced, and  $Red$  is the reduced species formed.



Neutral molecules can dissociate when dissolved in certain electrolyte producing cations, ions with positive charge, and anions, negatively charge ions. The ions can migrate in solution upon the application of an electric field, and they act as electrical charge-carriers [36, 37]. The cations move towards the cathode whereas the anions move oppositely towards the anode [37]. The transport of electrical current in a solution can be explained

by Ohm's law (Equation 2.4).  $E$  is defined as the potential difference,  $i$  is the current, and the resistance of the system is  $R$ .

$$E = iR \quad (2.4)$$

Ohm's law also correlates the cell potential to the current and a typical ED unit follows Ohm's law until a certain current density is reached, which is known as the limiting current density [38]. The concept of limiting current density will be discussed further below.

### 2.1.1 Concentration Polarization and ED Current-Potential Curves

Concentration polarization, defined as concentration gradient between the membrane surface and solution bulk, is a phenomenon observed in all membrane processes. In ED, the concentration changes as a result of ion migration and current flow, due to the electrochemical processes, across a membrane [38]. This leads to a concentration gradient adjacent to the membrane, an enrichment on one side and a depletion on the other. This phenomenon is observed at the limiting current density, which is an important concept in ED systems. Typical ED systems are operated below the limiting current density to optimize the ion transport across the membrane at the lowest consumed energy possible [39]. Figure 2.1 represents an ED system's, "S"-shaped, current-potential curve. The following three regions can be identified:

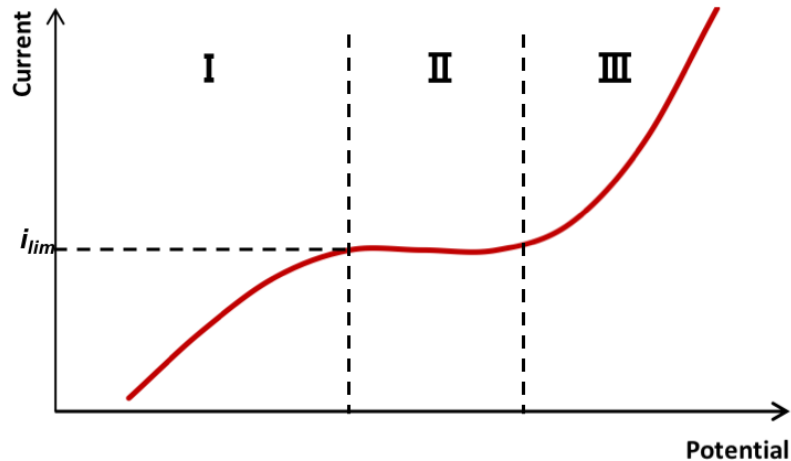


**Figure 2.1. Representation of a typical ED current-potential curve.**

I) Ohmic region: an initial linear region where the potential increases linearly with increasing currents, following Ohm's law. As current flows through the ion exchange membrane, the ion concentration increases on one side of the membrane and decreases on the other side [39].

II) Limiting current density region: a small region with a potential plateau. This corresponds to ion depletion adjacent to the membrane's surface [39].

III) Overlimiting current region: a second region with observed current and potential increase. This region is attributed to non-uniformity in the membrane and to electroconvection phenomena [39].

## 2.2 Electrochemical Techniques

### 2.2.1 Open Circuit Potential (OCP)

All electrochemical experiments had an initial open circuit potential measurement for ten-fifteen minutes in order to determine the system's natural potential before starting the next step of the experiment. At OCP, the cathodic and anodic reactions are equal in rate but opposite in sign [40]. As a result, there is no net current flowing through an external circuit. Measuring this potential provides an insight on the system under investigation before any external current or potential are applied, giving a baseline for the polarization measurements discussed below. Monitoring the OCP can provide an understanding of the stability of the system, with respect to time. This technique is typically used in combination with other electrochemical techniques.

### 2.2.2 Polarization Techniques

There are numerous electrochemical methods used to polarize a system away from its natural state. For example, current or potential, in static or dynamic modes, are possible polarization techniques. Galvanostatic mode applies constant current ( $i_{app}$ ) while monitoring the potential change over time, whereas in galvanodynamic polarization, the potential is monitored while  $i_{app}$  is scanned, at a fixed scan rate. This gives an insight into the effect of potential on the system [40].

### 2.2.2.1 Galvanostatic Polarization

Galvanostatic experiments were conducted to create an electrical field for the migration of the cation under investigation. the currents applied ranged from 0 to 30 mA, for varying durations.

### 2.2.2.2 Galvanodynamic Polarization

Galvanodynamic experiments were conducted to determine the system's limiting current density. The current was scanned anywhere from 0 to 40 mA, at different scan rates.

## 2.3 Surface and Solution Analysis Techniques

### 2.3.1 Scanning Electron Microscopy (SEM) and Energy Dispersive X-ray (EDX) Analysis

In scanning electron microscopy (SEM) a focused electron, primary, beam is accelerated by an electric field and focused by a series of magnets under vacuum. The beam interacts with the sample surface to generate various emissions, Figure 2.2 summarizes these electron-sample interactions [41]. The two-dimensional images, 50-100 nm in resolution, are produced when the secondary and backscattered electrons leave the sample and reach the detector. SEM provides information regarding the morphology and topography of the sample [42].

Secondary electrons (SE) are generated when the incident beam results in the ejection of a core electron from the atoms in the sample, creating a vacancy. Secondary electrons provide information regarding the sample topography, as these electrons escape from the first few nanometers of the surface [41].

Backscattered electrons (BSE) are a result of elastic scattering of the incident electron beam. Additional to topographic information, backscattered electrons reveal information about the atomic composition of the sample. Since heavy atoms are more efficient at scattering electrons than lighter atoms, heavy atoms produce higher signals and thus, brighter images.

A vacancy occurs in the core shell when a secondary electron is ejected, and so an outer shell electron will fall to fill the vacancy, minimizing the energy. This relaxation process emits X-ray photons. Analysis of the X-rays, which are characteristic of the elements associated with them, by energy dispersive X-ray (EDX) spectroscopy provides information regarding the sample's composition [43].

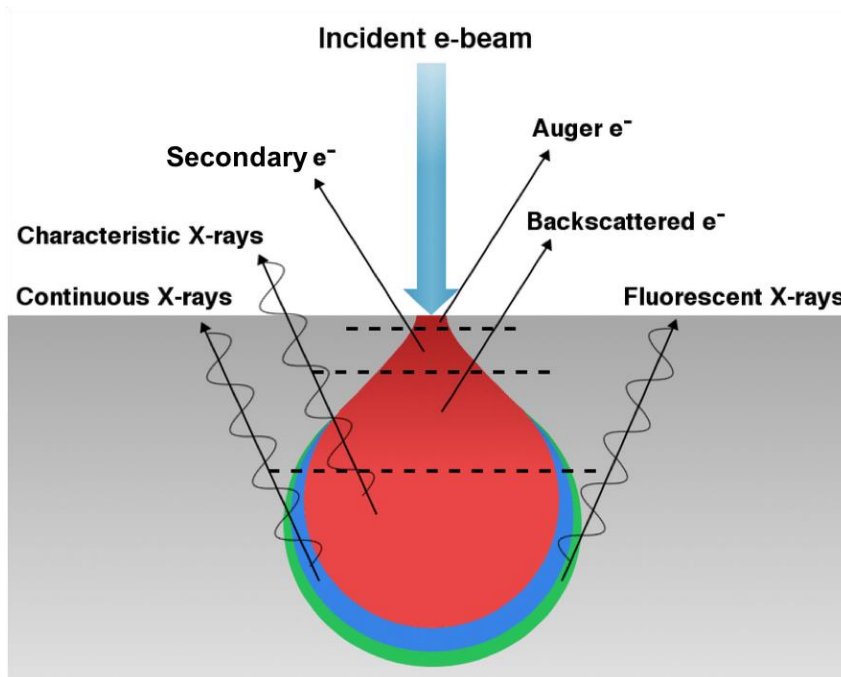


**Figure 2.2. Schematic of primary electron beam interactions with a specimen [41].**

Surface analysis of the membranes was conducted, to examine their morphologies and elemental compositions, using a Hitachi SU3900 large chamber variable pressure SEM coupled with an Oxford Ultim Max 65 SDD X-ray analyzer located at Surface Science Western. Micrographs were collected in both SE and BSE modes. The instrument was operated at an accelerating voltage between 10 and 20 kV.

### 2.3.2 Fourier Transform Infrared (FTIR) Spectroscopy

Fourier transform infrared (FTIR) spectroscopy is a non-destructive technique allowing insight into the vibrations of molecules in samples. FTIR uses an optical device called an interferometer, which has a beamsplitter, to split the incoming infrared beam into two beams oriented at a known angle (Figure 2.3). The beams are directed towards a fixed and

a movable mirror; which moves only a short distance. The beams are reflected back towards the beamsplitter to be recombined [44]. The resulting signal, or interferogram, is directed towards the sample compartment. The light is either reflected off of the sample or transmitted, with the majority traveling through the sample. The transmitted light carrying the sample's molecular information will be collected by the detector, producing an electronic signal, and decoded as an IR spectrum. IR spectra consist of a fingerprint region and a functional group region [44].

The spectral region for mid infrared is  $4000\text{-}400\text{ cm}^{-1}$  and it is most useful for studying fundamental stretching vibrations [44]. The stretching vibrations are modelled using the harmonic oscillator model and the chemical bond is embodied as two masses linked by a spring [44]. For a vibrational mode to be IR-active, it must have a net dipole moment. The electromagnetic waves interact with chemical bonds that are polar and if there is no dipolar moment, the infrared interaction is considered IR-inactive [44, 45].

FTIR Spectroscopy Bruker Tensor II system with Hyperion 2000 microscope instrument, located at Surface Science Western, was used to analyze the functional groups in the Nafion 117 membrane.

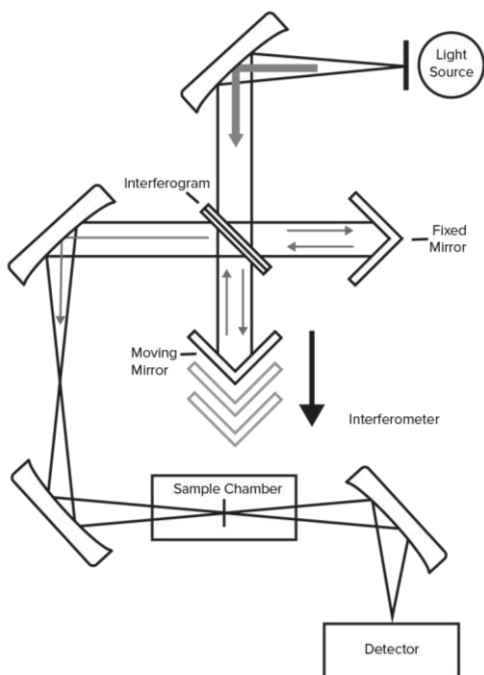


**Figure 2.3. Schematic of FT-IR spectrometer components [45].**

The instrument is outfitted with platinum micro-attenuated total reflectance (ATR) unit with a 2 mm × 2 mm diamond crystal. ATR-FTIR measures changes in a reflected IR beam as the beam hits the sample and this mode is ideal for thin films, including polymeric membranes [45].

### 2.3.3 Raman Spectroscopy

Raman spectroscopy is a non-destructive light scattering technique. A monochromatic laser irradiates a sample, exciting the molecules to an unstable virtual state. As de-excitation occurs, a photon is released through several potential transitions (Figure 2.4). Most photons return to the ground state, releasing the same energy level and this is known as elastic, or Rayleigh, scattering [46]. However, a small portion of the photons are inelastically scattered and they can be more energetic (anti-Stokes scattering) or less energetic (Stokes scattering) than the incoming light.

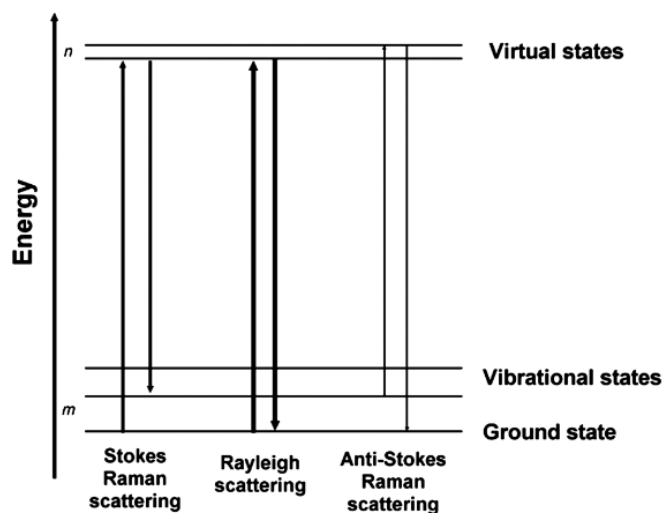


**Figure 2.4. Diagram of three possible transitions in Raman spectroscopy [46].**

The Raman spectrum produced is a chemical fingerprint of the molecules in the sample analyzed, as the vibrational modes of the molecules have discrete transitions, which are unique to the molecules' bonds. The spectrum provides information regarding the chemical structure and crystallinity of the sample.

Renishaw InVia Reflex Raman Spectrometer with 633 nm laser located at Surface Science Western was used. The spectrometer, which has a spatial resolution of 0.5-1  $\mu\text{m}$ , is coupled with an optical microscope to allow visualization of the sample before and after analysis.

### 2.3.4 Inductively Coupled Plasma-Mass Spectrometry (ICP-MS)

Inductively coupled plasma-mass spectrometry (ICP-MS) is an elemental analysis technique with detection levels of milligrams to nanograms per liter. The solutions are sampled using an autosampler, and consequently the elements are atomized and ionized by a nebulizer in the sample interface. The resulting ions are deflected through to the detector [47]. The signal is collected and generated based on the ions' mass-to-charge ratios. A schematic of the ICP-MS components is presented in Figure 2.5.

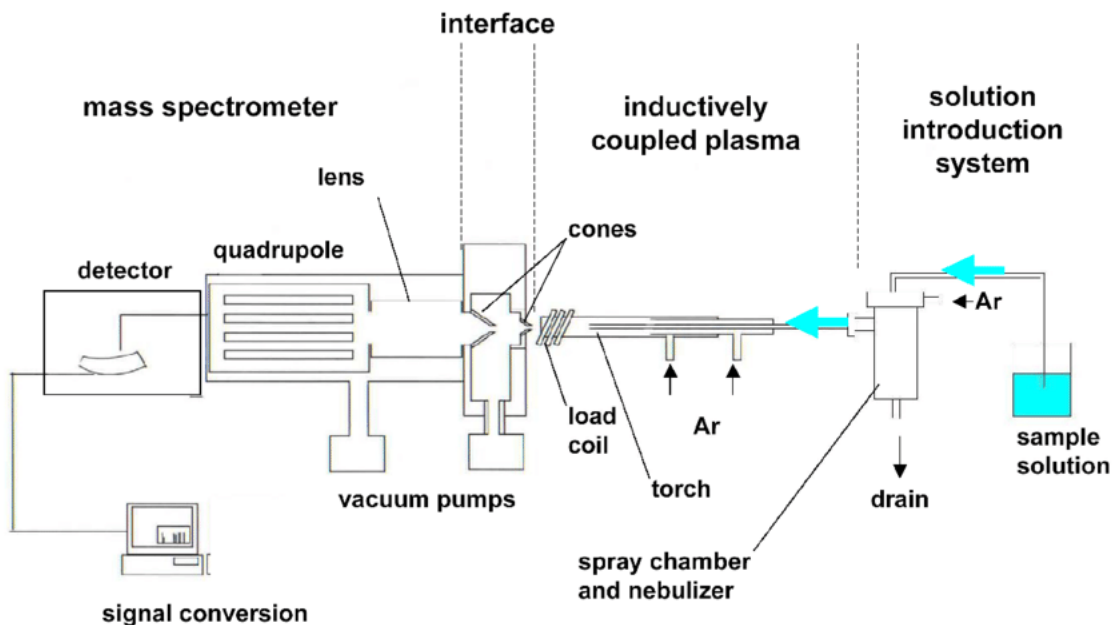


**Figure 2.5. Schematic of ICP-MS instrument components [47].**

The solutions collected before, after, and during experiments were analyzed, to determine dissolved metal concentrations, using an Agilent 7700 Series ICP-MS located in the Department of Chemistry at Western University. All solutions were diluted and acidified with 2%  $\text{HNO}_3$  except for the HCl samples, Type I deionized (DI) water was used. Numerous standards with concentrations ranging from 1 ppb to 500 ppb were prepared and run prior to the analysis of any samples to establish the calibration curve, an example is

presented in Figure 2.6. The samples were run as unknowns and the signal intensities were compared to the calibration curve generated in order to calculate the concentration of the samples.  $R^2$  values obtained from the calibrations were always between 0.9997 and 1.000.

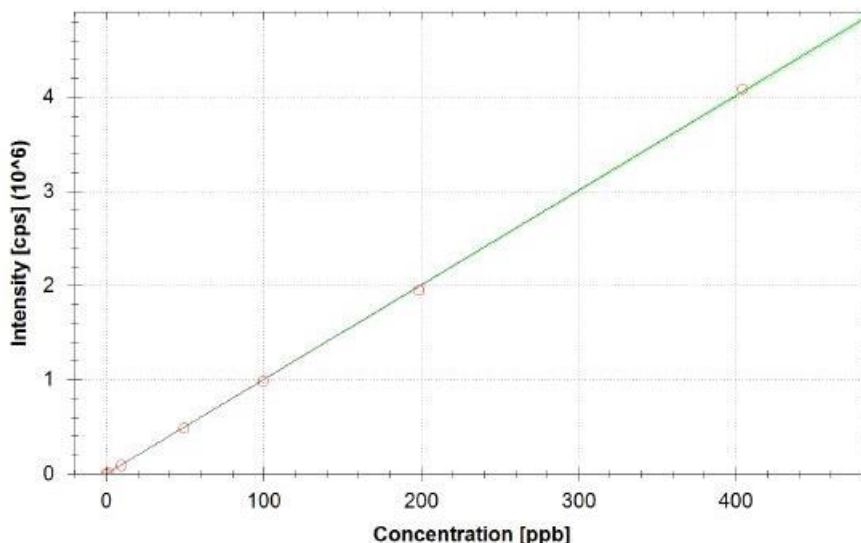


**Figure 2.6. Example calibration curve generated from ICP-MS standards with  $\text{Ni}^{2+}$  concentrations between 1 ppb and 400 ppb.**

## 2.4 Experimental Conditions and Setup

All experiments were performed at room temperature (25 °C). Experimental solutions were prepared using reagent grade NaCl (Caledon Laboratory Chemicals, Georgetown, ON), reagent grade stock HCl (Caledon Laboratory Chemicals, Georgetown, ON), reagent grade  $\text{NiCl}_2 \cdot 6\text{H}_2\text{O}$ , reagent grade  $\text{SrCl}_2 \cdot 6\text{H}_2\text{O}$ , and Type-1 DI water. Electrochemical benchtop measurements were carried out using a 2100 Analytical Modulab (Solartron Analytical, Hampshire, UK), whereas glovebox measurements were carried out using a 1287 Electrochemical Interface (Solartron Analytical, Hampshire, UK) and a Keithley 2260B DC power supply (Tektronix, US).

### 2.4.1 Benchtop Experiments

Electrochemical experiments were performed using a four-electrode cell (Figure 2.7). The cell utilizes two saturated calomel electrodes (SCE) as the reference electrodes (0.241 V

vs. SHE) and platinum sheets connected with platinum wires as the anode and cathode, which were placed in the major cell compartments. The membrane investigated was placed in the middle to separate the two major compartments. The reference electrodes were housed in separate compartments, using Luggin capillaries to decrease any IR drop effects, and they monitored the potential across the membrane.

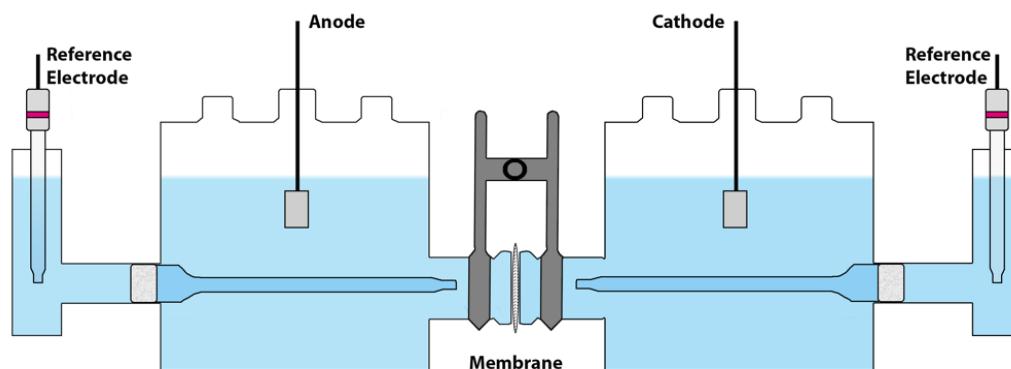


**Figure 2.7. Four-electrode electrochemical cell setup.**

## 2.4.2 Glovebox Experiments

Experiments with the CapturePhos membrane were conducted in a glovebox, due to the oxygen sensitivity of the membrane. The cell used was 3D-printed using polyvinylidene fluoride (PVDF). Experimental solutions were prepared in the same manner as for benchtop experiments and they were pre-sparged with Ar for approximately one hour prior to introduction to the glovebox. The membranes were introduced into the glovebox in a container packaged under N gas.

## 2.5 Materials

### 2.5.1 Nafion 117 Membrane

Nafion 117 was the commercial CEM chosen for experimentation. Nafion 117 has a tetrafluoroethylene backbone and perfluorovinyl ether groups on side chains terminated with sulfonic acid groups (Figure 2.8). The membrane is 183  $\mu\text{m}$  thick and has a resistance of 2.0  $\Omega\cdot\text{cm}^2$ . The membrane was received as a 15  $\times$  15  $\text{cm}^2$  sheet in the acidic ( $\text{H}^+$ ) form from Ion Source. A round cutter was used to create the samples with different diameters.

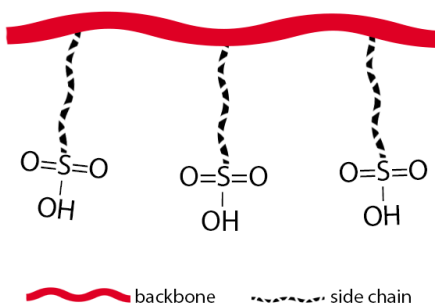


**Figure 2.8. Schematic of Nafion 117 structure.**

Prior to electrochemical measurements, the membrane was either subjected to a pre-treatment procedure of two thirty-minute consecutive immersions in 1 M HCl, followed by Type-1 DI water at  $75 \pm 3$  °C, or soaked in the experimental metal solution for a set duration. The membrane was soaked for varying amounts of time in a 1 M HCl solution post electrochemical experiments. This step ensured that the membrane was back to its original  $H^+$  form.

## 2.5.2 CapturePhos

A new class of phosphorus-based polymers, known as CapturePhos, were first polymerized at Western University by Cuthbert et al. [48]. The polymeric network was prepared using a primary phosphine, 1,3,5-triaza-triallyl-trione (TTT), and tetra ethylene glycol diallylether (TEGDAE). A reaction scheme is presented in Figure 2.9. TTT was used as a cross-linker and TEGDAE as a chain extender, which is needed in order for the network to not be too densely packed and brittle [49].

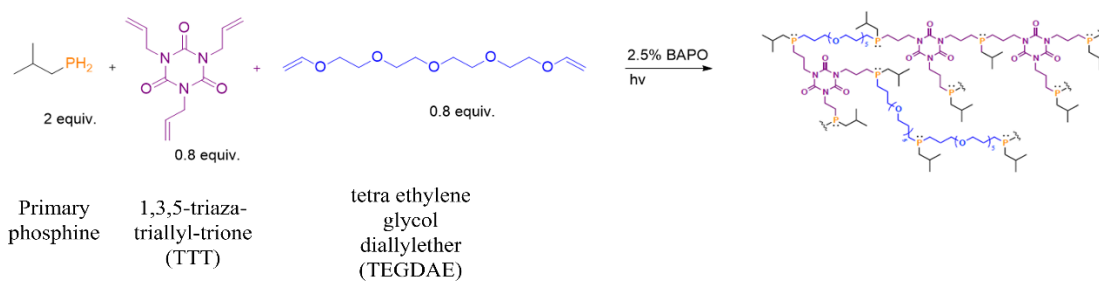


**Figure 2.9. Chemical reaction scheme for the preparation of the CapturePhos network.**

The metal uptake of this network towards Ru and Rh was previously investigated by soaking in the respective metal ion solutions. It was reported that 30% of the Ru<sup>2+</sup> was removed in twenty minutes and 97% after twenty-four hours, while 99.8% of the Rh<sup>2+</sup> was removed in twenty-four hours [48]. The CapturePhos networks are relatively easy to manufacture, economical, and their ligand system is tunable. Interchanging the functional groups installed into the polymer allows for selectivity towards specific ions. By achieving better ion-selectivity, CapturePhos will fill a gap in ED metal uptake research. The electrochemical behaviour of the CapturePhos is investigated here.

Several formulations, with varying ratios of the starting materials, and formulation amounts, of the final gel product, cured were tested to find the optimal formula for metal uptake (Table 2.1). The polymers were preconditioned in the experimental metal solutions and soaked in various solutions post experimentation to test the solutions' desorption strength.

**Table 2.1. Formulation ratios and amounts cured for CapturePhos polymers tested.**

<b>Generation</b>	<b>Polymer Name</b>	<b>Formulation Amount (g)</b>	<b>iBuPH<sub>2</sub>:TTT:TEGDAE</b>
<b>1</b>	<b>P-91</b>	3.1	2:1:0.5
<b>2</b>	<b>P-99</b> <b>P-05</b>	1.7	2:0.8:0.8
<b>3</b>	<b>P-22</b> <b>P-40</b>	2.5	2:0.8:0.8
<b>4</b>	<b>P-65</b>	1.7	2:1:0.5

The following section presents the data collected from experiments performed, results obtained from membrane characterization and surface analysis work, and a discussion of the results.

### 3. Results and Discussion

The results presented in this chapter are divided into two sections, Nafion experiments and CapturePhos experiments. Each section includes data from chemical sequestration,

electrochemical sequestration, and membrane characterization. Discussion and conclusions follow at the end of each section and end of the chapter.

### 3.1 Nafion Experiments

The experiments performed investigated the uptake of divalent metal ions  $\text{Ni}^{2+}$  and  $\text{Sr}^{2+}$ . Parameters such as ED duration, current effect, pre-treatment and desorption methods, agitation effect, and pH were investigated. The results from within and between the testing scenarios were compared, based on the removal efficiency of the metal ion of interest, recovery of the ion, and energy consumption, to evaluate the overall ED performance.

#### 3.1.1 Chemical Sequestration

A polymeric sample was soaked in solutions of various concentrations, at various agitation rates, and for different time periods to characterize the sequestration behaviour of the Nafion chemically. The results for the  $\text{Ni}^{2+}$  solution experiments are listed in Table 3.1, whereas experiments with the  $\text{Sr}^{2+}$  solution are listed in Table 3.2. Chemical sequestration experiments were performed by immersing a polymeric specimen in 100 mL of solution, at the specified conditions, followed by a rinse stage in DI  $\text{H}_2\text{O}$  and the polymer was then placed in the exchange solution. The removal efficiency was calculated based on the difference in the  $\text{Ni}^{2+}$  or  $\text{Sr}^{2+}$  concentration in solution.

Experiments A-D in Table 3.1 show an interesting trend. At three hours and 250 rpm, the highest removal percentage was observed (experiment A) and when the soak time was increased to six and twenty-four hours, the removal efficiency decreased (experiments B and C). Experiment C had no actual change in the concentration. Increasing the agitation rate significantly improved the removal efficiency for the twenty-four-hour soak periods, experiment D, however the removal efficiency was lower than that for the three-hour soak with the low agitation speed.

**Table 3.1. Chemical sequestration data for 1000 ppm Ni<sup>2+</sup> solution for various durations and agitation speeds.**

Experiment	Ni <sup>2+</sup> concentration (ppm)		Duration (hours)	Agitation speed (rpm)	Removal efficiency (%)
	Initial	Final			
A	1046	923.7	3	250	11.7
B	1127	1017	6	250	9.74
C	1078	1105	24	250	-2.50
D	1023	939.0	24	500	8.23

For the tests performed, a maximum exchange capacity between H<sup>+</sup> and Ni<sup>2+</sup> was reached between three and six hours at the low agitation rate. With time, and due to the stagnant nature of the solution, the Ni<sup>2+</sup>, absorbed by the polymer leached out from the polymer and back into solution, increasing the Ni<sup>2+</sup> concentration measured in solution and decreasing the removal efficiency. Neither increasing the soak time nor the agitation speed, overall, increased the removal of the metal ion, demonstrating the impracticality of treating contaminated water with an IEM, using a chemical method only.

**Table 3.2. Chemical sequestration data for 500 ppm Sr<sup>2+</sup> solution for various durations and agitation speeds.**

Experiment	Sr <sup>2+</sup> concentration (ppm)		Duration (hours)	Agitation speed (rpm)	Removal efficiency (%)
	Initial	Final			
A	526.0	341.4	10	250	35.1
B	520.2	446.0	20.5	-	14.3
C	503.0	410.2	24	250	18.5
D	512.0	414.1	24	500	19.1

For the Sr<sup>2+</sup> sequestration experiments, not stirring the solution led to the lowest removal efficiency, which is expected. Similar to the Ni<sup>2+</sup> system, increasing the soak period did not increase the amount of Ni<sup>2+</sup> or Sr<sup>2+</sup> removed from solution as the shortest soak period had the highest removal rate (experiment A) and agitation at 500 rpm did not significantly increase the removal of Sr<sup>2+</sup> from solution (experiment D), compared to the low agitation speed. However, higher removal efficiency was achieved for Sr<sup>2+</sup> than for Ni<sup>2+</sup>.

### 3.1.2 Electrochemical Sequestration

Electrochemical investigations included control experiments and LCD determination, and numerous ED operation parameters were tested to further investigate their effect on the ED performance.

#### Control Experiments

Two control experiments were performed to investigate the effect of electrochemistry and to investigate the effect of the membrane. In the first experiment, presented in Figure 3.1, the same setup (Figure 2.7) was used; however, no electric field was applied to document the likelihood of ions migrating across the membrane due to electrostatic attraction alone. During the three-hour period, the  $\text{Ni}^{2+}$  concentration in the diluate cell with NaCl showed a minor increase, accompanied by a slight decrease in  $[\text{Ni}^{2+}]$  in the concentrate. This can be attributed to the electrostatic attraction between the positive  $\text{Ni}^{2+}$  ions and the negatively charged end groups on the polymeric network. This increase is slight and not significant compared to the  $\text{Ni}^{2+}$  concentration change noted in the electrochemical experiments performed with the same setup, presented below, for example Figure 3.13.

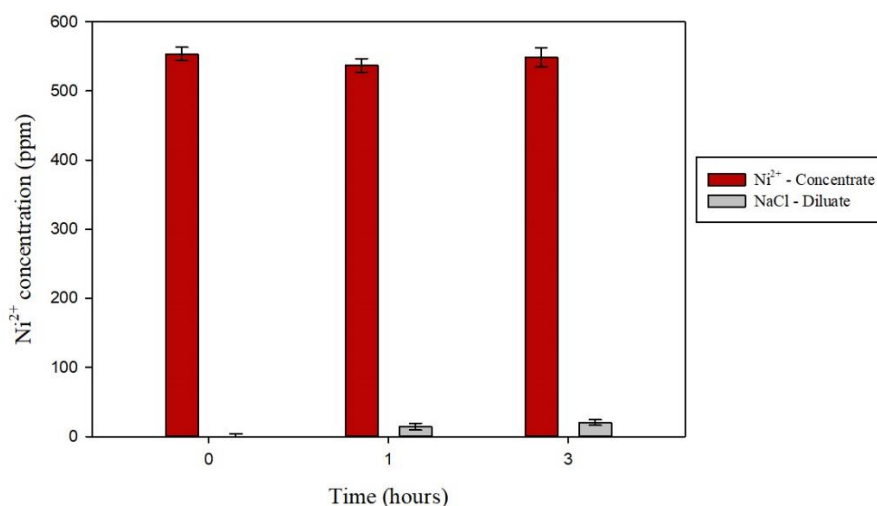


**Figure 3.1. Change in  $\text{Ni}^{2+}$  concentration from a 500 ppm  $\text{Ni}^{2+}$  control experiment performed without an electric field.**

The second control experiment had a PTFE sheet installed in place of the membrane. The lack of CEM impeded the  $\text{Ni}^{2+}$  ions' migration from the concentrate to the diluate cell

during the three-hour period, as the  $\text{Sr}^{2+}$  concentration in the diluate cell was negligible and no significant decrease was noted in the concentrate's  $\text{Sr}^{2+}$  amount (Table 3.3 and Figure 3.2).

**Table 3.3. Concentrations in the concentrate and diluate compartments for the three-hour experiment, with standard deviation values.**

Compartment	Duration (hours)	$\text{Sr}^{2+}$ concentration (ppm)	Standard deviation
Concentrate	0	518.8	4.42
	3	522.5	1.75
Diluate	3	0.014	0.003

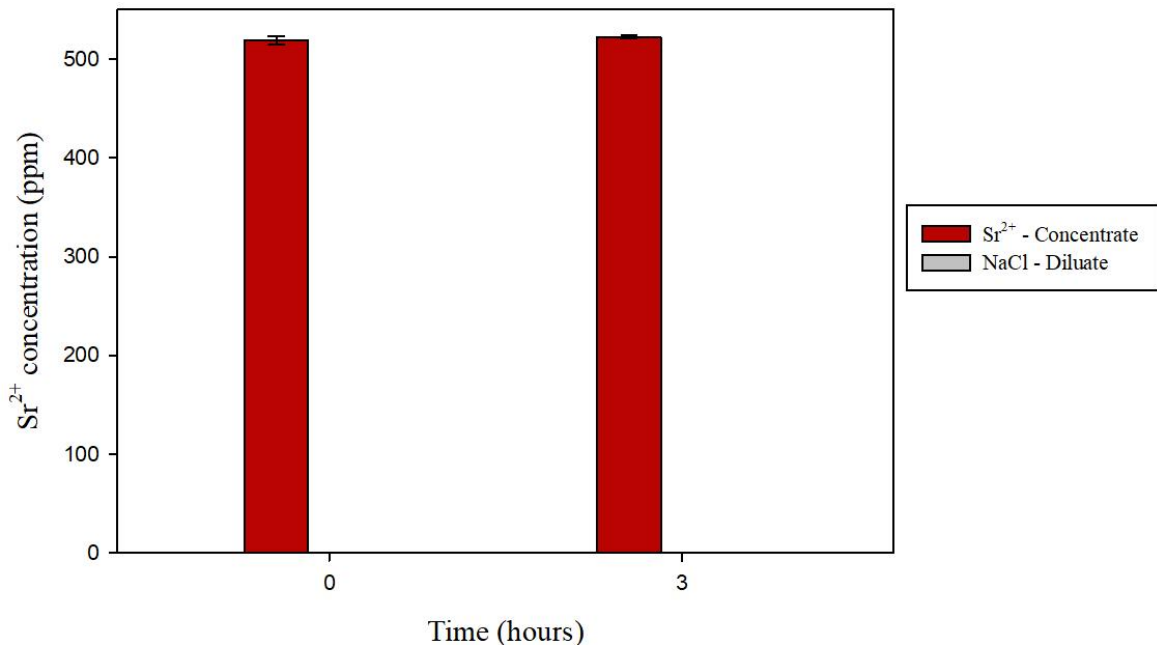


**Figure 3.2. Change in  $\text{Sr}^{2+}$  concentration from a 500 ppm  $\text{Sr}^{2+}$  control experiment performed with a PTFE sheet instead of the Nafion 117 polymer.**

### LCD Determination

The initial set of experiments involving a sweep of the potential response, for a specified current range, was performed to determine the LCD. The LCDs for all experimental solutions were determined, and they are reported in Table 3.4 and Figure 3.3 below.

**Table 3.4. Measured limiting current densities (LCD) for the solutions listed.**

Solution	LCD (mA/cm <sup>2</sup> )	Standard deviation
100 ppm Ni <sup>2+</sup>	0.40	0.041
500 ppm Ni <sup>2+</sup>	0.78	0.055
1000 ppm Ni <sup>2+</sup>	0.80	0.030
500 ppm Sr <sup>2+</sup>	0.35	0.021

It is evident that for the Ni<sup>2+</sup> system, the LCD increases with the increase in concentration, although this increase is minor between 500 and 1000 ppm Ni<sup>2+</sup>. The Sr<sup>2+</sup> system had the lowest LCD, even lower than 100 ppm Ni<sup>2+</sup>, indicating that for different ions, factors other than the concentration play a role in determining the LCD.

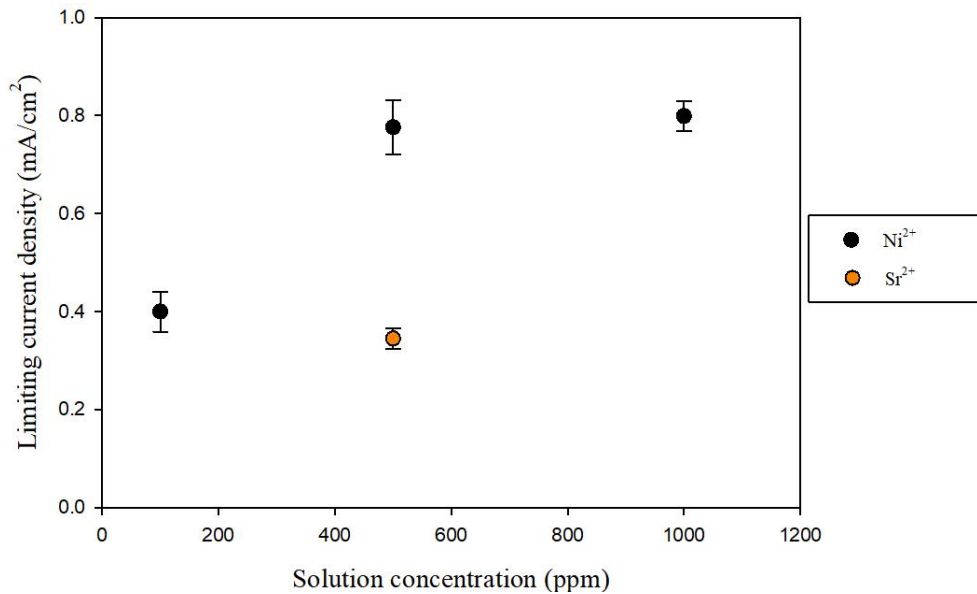


**Figure 3.3. Limiting current densities (LCD) for the four solutions investigated.**

Furthermore, the higher the LCD, the greater the freedom in the ED operation. As noted below, there is more opportunity with the 1000 ppm  $\text{Ni}^{2+}$  system to initiate cation migration across the CEM, as the threshold for applied CD is higher, compared to the other systems with lower LCDs.

### OCP Measurements

OCP was recorded for all experiments to demonstrate the stability of the system prior to the static/dynamic polarizations. Examples of OCP transients for the  $\text{Ni}^{2+}$  (100 ppm, 500 ppm, and 1000 ppm) and  $\text{Sr}^{2+}$  (500 ppm) solutions are displayed in Figure 3.4. The OCP for all tests performed, depending on the solution used, varied in the range of  $\pm 15$  mV from the data presented in the figures. Once the OCP was recorded and the system's stability was insured, the experiment proceeded to the next step.

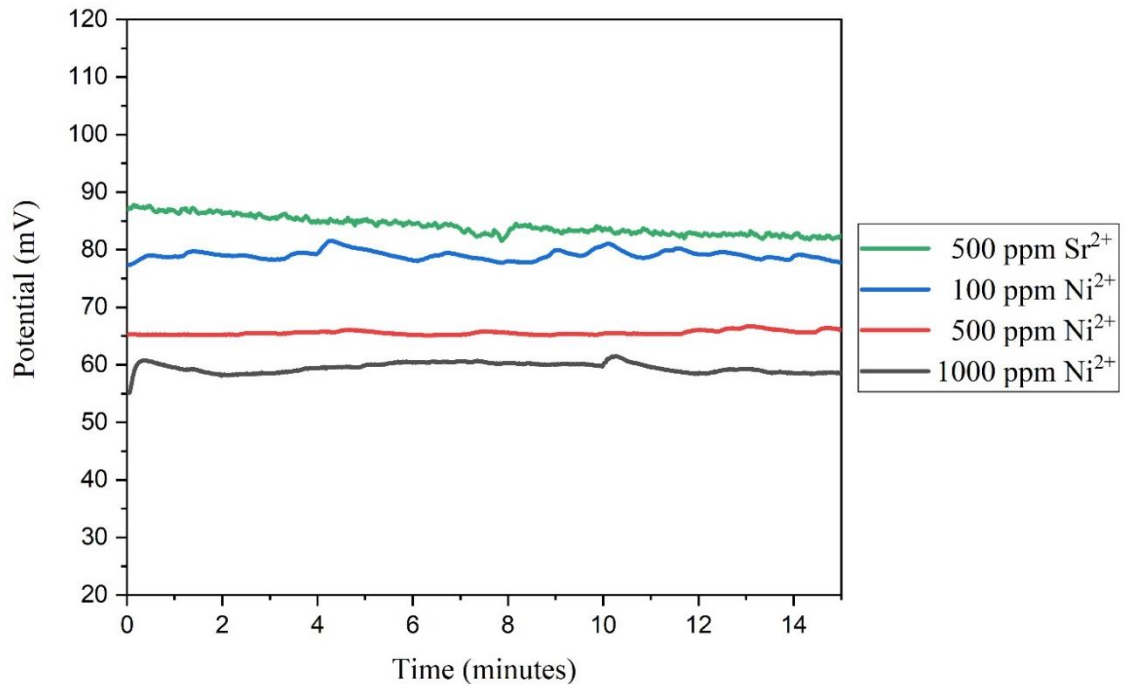


**Figure 3.4. Example open circuit potential (OCP) transients for the four solutions investigated.**

### Potential-time Curves

Potential-time (E-t) curves for select experiments from 1000 ppm  $\text{Ni}^{2+}$ , 500 ppm  $\text{Ni}^{2+}$ , 100 ppm  $\text{Ni}^{2+}$ , and 500 ppm  $\text{Sr}^{2+}$  testing solutions are provided in Figures 3.5, 3.6, 3.7, and 3.8 respectively. The GS experiments recorded the potential drop across the membrane as the cation,  $\text{Ni}^{2+}$  or  $\text{Sr}^{2+}$ , migrated across it.

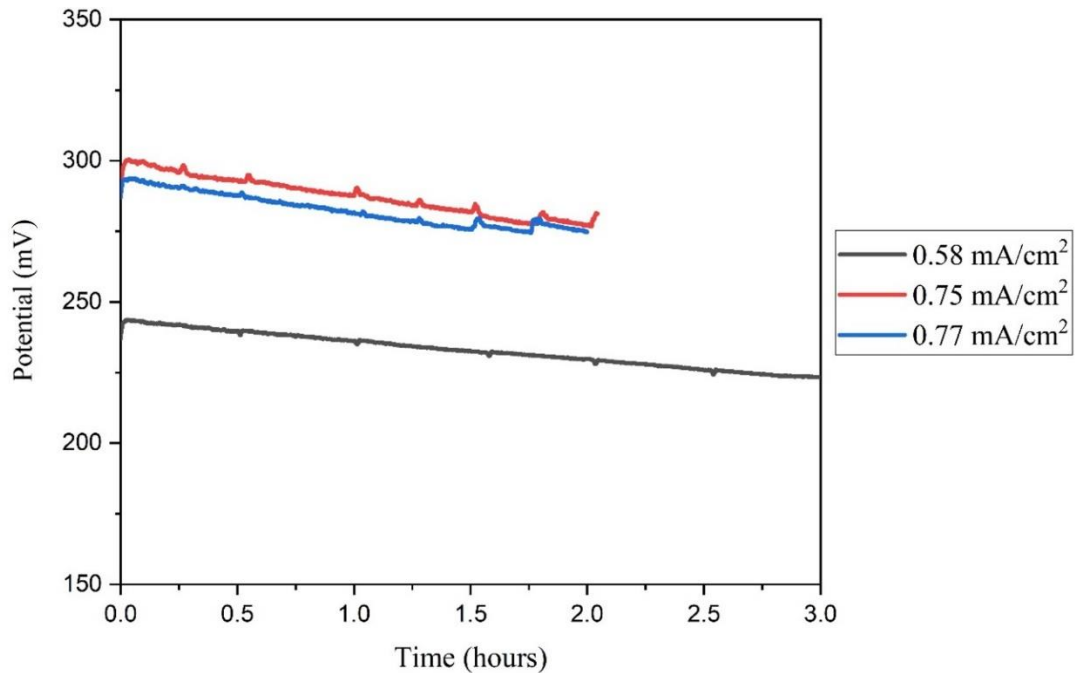


**Figure 3.5. Example potential-time curves corresponding to the indicated applied current densities for the experiments performed in 1000 ppm  $\text{Ni}^{2+}$  solution.**

In general, as the applied CD increased, the potential recorded also increased. It was noted that the agitation rate also impacted the potential response, Figure 3.6. For 500 ppm and 1000 ppm solutions, the potential response falls between 200 mV and 450 mV, whereas the 100 ppm system experienced higher potentials, between 550 and 800 mV. According to Ohm's law (Equation 2.4), higher potential is indicative of higher resistance. This can hinder the ED operation and its efficiency.

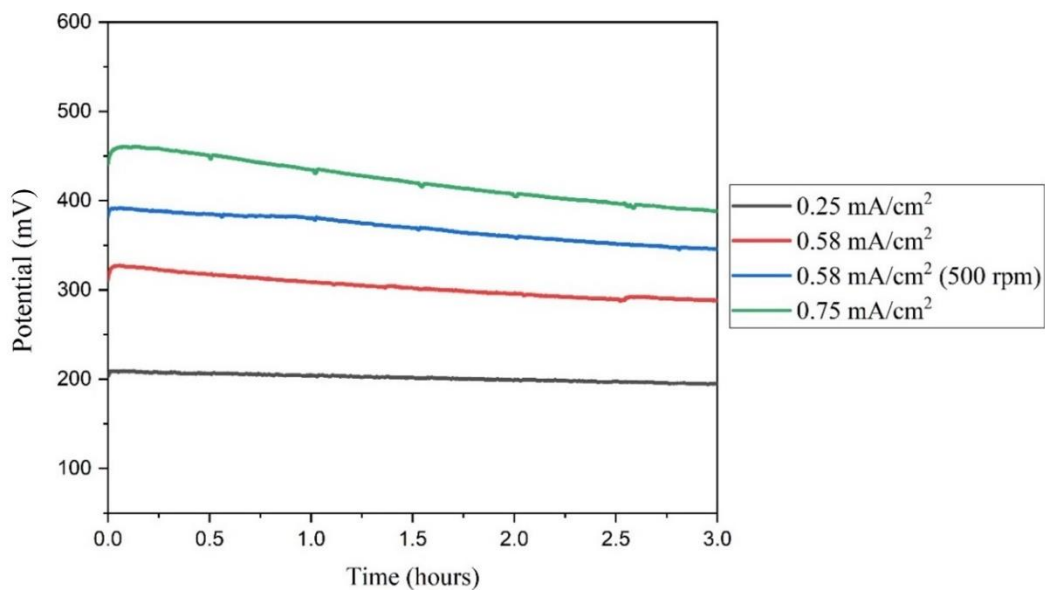


**Figure 3.6. Example potential-time curves corresponding to the indicated applied current densities for the experiments performed in 500 ppm Ni<sup>2+</sup> solution.**

The potential range for the Sr<sup>2+</sup> system aligns with that of the Ni<sup>2+</sup> system. In general, higher CDs resulted in a more significant potential drop during the ED experiment.

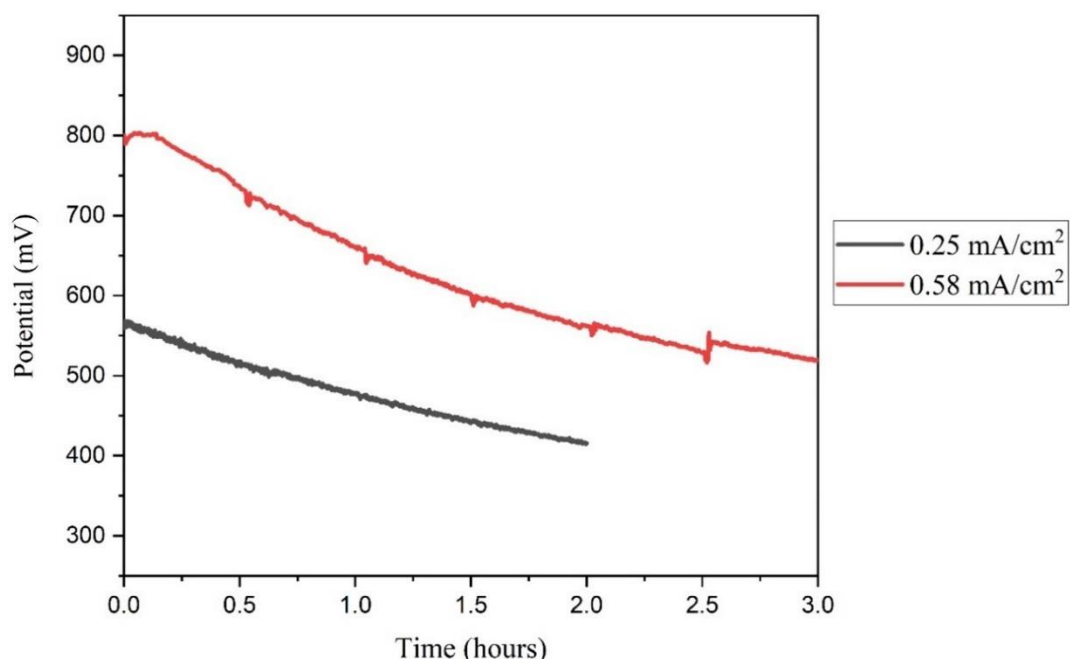


**Figure 3.7. Example potential-time curves corresponding to the applied current densities for the experiments performed in 100 ppm Ni<sup>2+</sup> solution.**

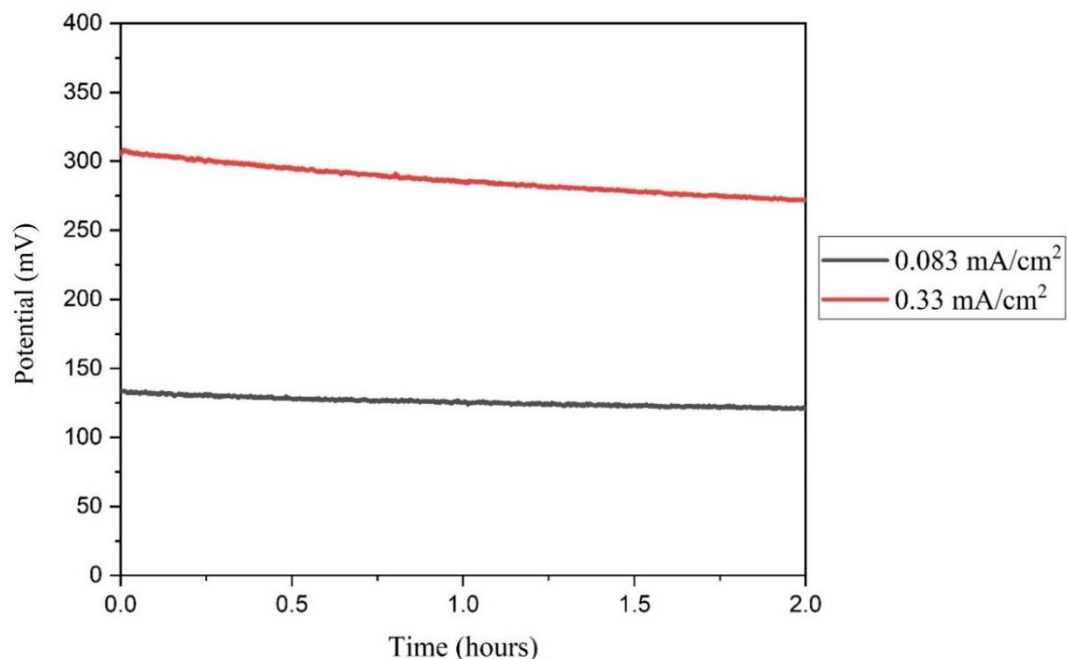


**Figure 3.8. Example potential-time curves corresponding to the applied current densities for the experiments performed in 500 ppm Sr<sup>2+</sup> solution.**

#### Effect of Pre-Treatment

It is important to ensure that the polymer is clean and free of the metal ions prior subjecting it to experimentation to truly have a clear picture of the effect of the parameters tested. Various pre-treatments were investigated, including treatments with 1 M HCl, DI H<sub>2</sub>O, and the same ionic solution as in the testing criteria (i.e., 500 ppm Ni<sup>2+</sup>); Table 3.5. Each test consisted of a polymer soak in 500 ppm Ni<sup>2+</sup> solution for three hours post an initial soak in the respective solution, at the conditions listed. All pre-treatment solutions were stirred at 250 rpm.

The table provides removal efficiency percentages corresponding to the Ni<sup>2+</sup> concentration decrease in the test solution at the end of each test. The amount of Ni<sup>2+</sup> removed from the solution corresponds to an estimate of the Ni<sup>2+</sup> amount in the polymer. As noted in Table 3.5, pre-treatment test C had the best outcome with the highest removal efficiency, in terms of preparing the CEM for the ED experiments. A desorption stage, consisting of the same conditions and steps as test C, was also performed post experiments. The solutions were

also sampled at thirty minutes, and it was noted that the removal efficiency did not significantly increase afterwards. So, the final pre-treatment and post-treatment consisted of a shortened variation of the pre-treatment test C.

**Table 3.5. Various pre-treatments tested, for Nafion 117 subjected to 500 ppm Ni<sup>2+</sup> test solution.**

Pre-treatment Test	Solution	Duration (hours)	Temperature (° C ± 2)	Removal efficiency (%)
A	DI H <sub>2</sub> O	1	75	31.1
B	1 M HCl	1	75	67.9
C	1 M HCl	1	75	88.6
	DI H <sub>2</sub> O	1	75	
D	1 M HCl	24	20	74.4
E	Ion solution (i.e., 500 ppm Ni <sup>2+</sup> )	18	20	79.4

Data for the following sections are presented as bar graphs, similar to Figures 3.1 and 3.2. The bar graphs illustrate the concentration changes of the metal ion, Ni<sup>2+</sup> or Sr<sup>2+</sup>, in the two compartments, concentrate and diluate. The removal efficiency and/or EC are overlaid on the figures, providing a better representation for data interpretation.

In order to verify the LCD theory, experiments were performed at current densities below and above the measured value, Table 3.4 and Figure 3.3 [38, 39].

#### Effect of Applied CD: Experiments Above the LCD

The following test was performed to further investigate the extent of the role the pre-treatment has and to investigate operating the ED unit at high current, above the LCD. Figure 3.9 displays two experiments in 1000 ppm Ni<sup>2+</sup> solution, performed at 1.67 mA/cm<sup>2</sup> for two hours, the first with no pre-treatment performed. The second data set had a pre-

treatment of two consecutive thirty-minute soaks in 1 M HCl and DI H<sub>2</sub>O (pre-treatment test C).

**Table 3.6. Removal efficiency and energy consumption data for two experiments, with and without pre-treatment, for 1000 ppm Ni<sup>2+</sup> systems performed at 1.67 mA/cm<sup>2</sup> for two hours.**

<b>Experiment</b>	<b>Removal efficiency (%)</b>	<b>EC (Wh/m<sup>3</sup>)</b>
1.67 mA/cm <sup>2</sup> (no pre-treatment)	7.01	32.5
1.67 mA/cm <sup>2</sup> (pre-treatment)	3.95	30.5

Solutions in both data sets had relatively low removal efficiencies, with the “no pre-treatment” experiment’s removal more than double that of the “pre-treatment” experiment. The EC values were very high but close in range for the two testing conditions, Table 3.6. Although the “pre-treatment” had lower removal of the Ni<sup>2+</sup>, the amount of Ni<sup>2+</sup> recovered in the diluate is slightly higher than from the solution in the other data set. This shows that the pre-treatment enhanced the ability of the ions to migrate across the membrane into the NaCl solution, rather than the Ni<sup>2+</sup> being removed from the concentrate and remaining static in the polymeric network. Also, it is plausible that the degree of the pre-treatment’s success was diminished due to the high CD applied, further demonstrating that CD’s role overshadows other factors, to an extent.

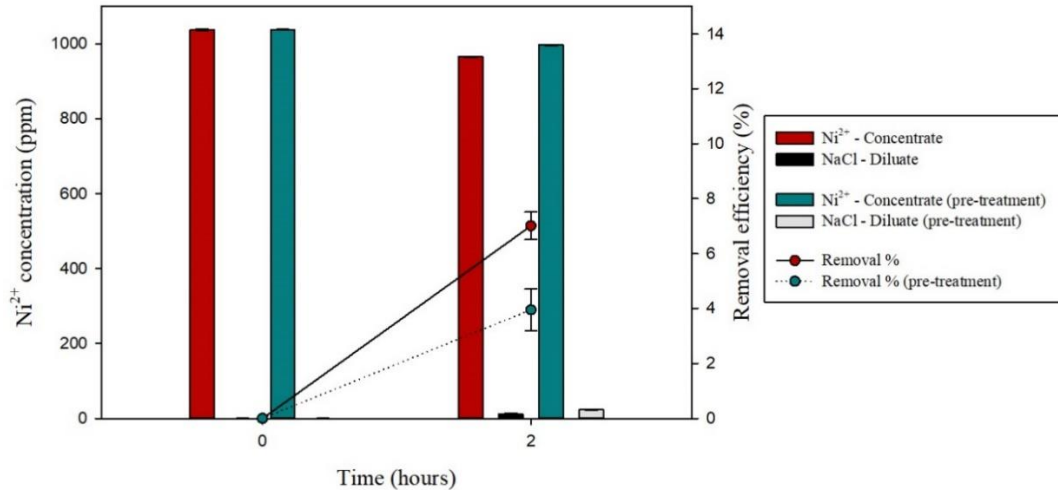


**Figure 3.9. Ni<sup>2+</sup> concentration and removal efficiency changes from two experiments performed using 1000 ppm Ni<sup>2+</sup> solutions, with and without pre-treatment, at 1.67 mA/cm<sup>2</sup> for two hours.**

#### Effect of applied CD: Experiments Below the LCD

From the data set presented above, operating the ED unit past the LCD is not economical, especially at the commercial scale, since high energy is required and very minimal cations are captured. The following section dives deeper into the effect of certain parameters (i.e., solution agitation rate, ED duration, CD applied, pH control, etc.) at CDs below the limiting values.

#### Effect of Agitation Rate

Diffusion in solution and its rate can be impacted by numerous factors. Here, the effect of stirring was investigated by running three sets of experiments: without stirring, with a low stirring rate (250 rpm), and with a high stirring rate (500 rpm). The first data set, Figure 3.10, compares an experiment without any solution agitation to one in which the solution was agitated at 250 rpm.

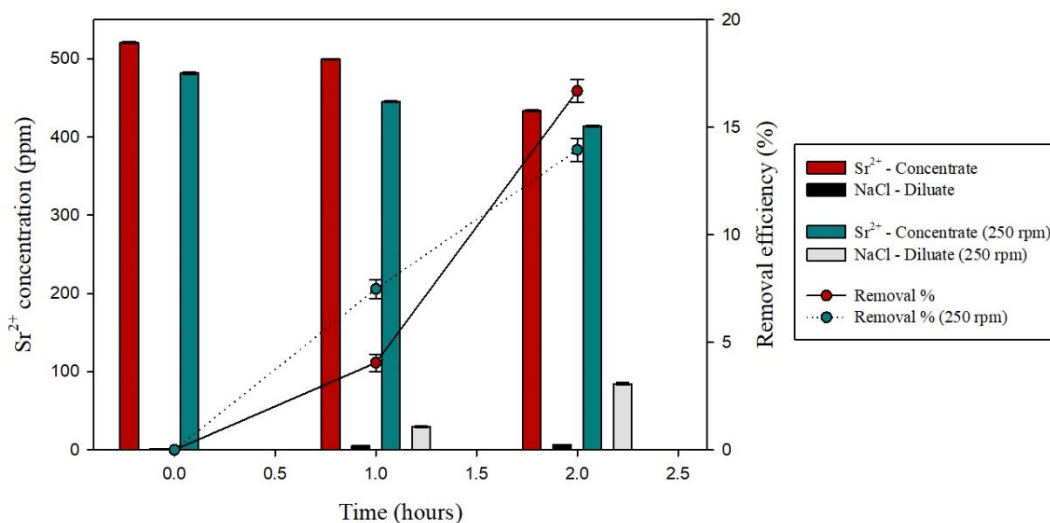


**Figure 3.10. Sr<sup>2+</sup> concentration and removal efficiency changes from stationary (no stirring) and stirred experiments, agitation speed of 250 rpm, performed using 500 ppm Sr<sup>2+</sup> solution at 0.083 mA/cm<sup>2</sup>, for two hours.**

The stirred experiment displayed a higher amount of Sr<sup>2+</sup> removed (%) at the midpoint but was later surpassed. Although the removal rates were comparable for the two experiments, the stirred solution had more Sr<sup>2+</sup> recovered in the diluate compartment. When the diluate solution is stagnant for a period of time, the layer near the polymer's surface in the concentrate will equilibrate with the ions in solution and impede further effective migration. This in return, will negatively impact the removal efficiency.

The second data set in Figure 3.11, compares 250 and 500 rpm agitation rates for experiments performed using 500 ppm Ni<sup>2+</sup> solutions at an applied current density of 0.58 mA/cm<sup>2</sup> for three hours. The high agitation rate slightly improved the removal efficiency and it led to a higher Ni<sup>2+</sup> recovery (grey versus black bars), further confirming the importance of solution agitation.

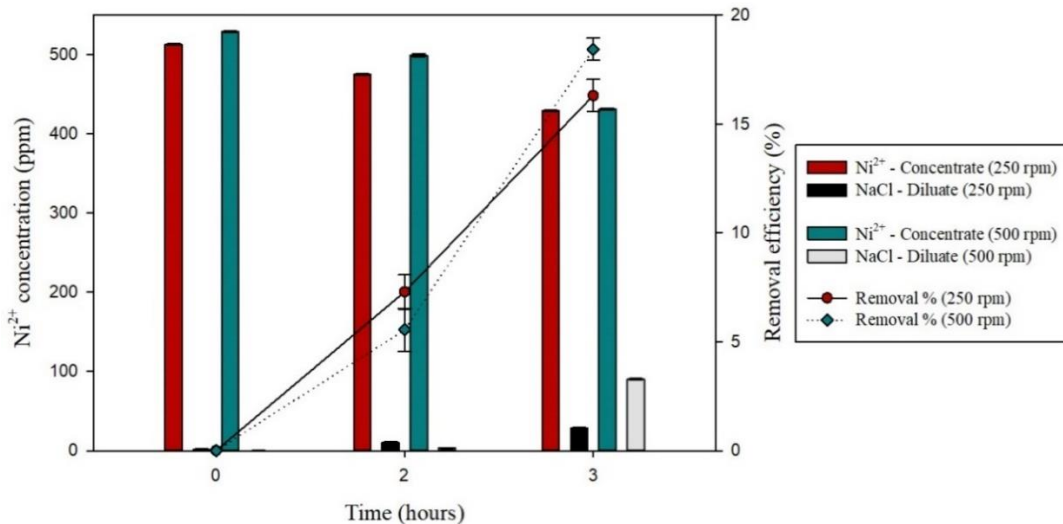


**Figure 3.11. Ni<sup>2+</sup> concentration and removal efficiency changes from two experiments, with agitation speeds of 250 and 500 rpm, performed using 500 ppm Ni<sup>2+</sup> solution at 0.58 mA/cm<sup>2</sup>, for three hours.**

#### Effect of Initial Concentration

In order to examine any differences in operation efficiency linked to the initial metal ion concentration, at a CD suitable for both systems, the same testing parameters were applied to experiments with 500 ppm and 1000 ppm Ni<sup>2+</sup> solutions. Overall, the experiment performed in a 1000 ppm Ni<sup>2+</sup> solution had removal efficiency higher than that of the experiment performed with 500 ppm Ni<sup>2+</sup> solution, by a factor of four, at an applied CD of 0.75 mA/cm<sup>2</sup> (Figure 3.12). However, by comparing the Ni<sup>2+</sup> concentration in the diluate compartment for the 1000 ppm Ni<sup>2+</sup> experiment (grey bar) to that of the 500 ppm Ni<sup>2+</sup> experiment (black bar), it was evident that the amount of Ni<sup>2+</sup> recovered was higher for the lower concentration experiment. Interestingly, the trend was reversed at the midpoint of the experiment, as the removal efficiency for the 500 ppm Ni<sup>2+</sup> experiment was higher. 0.75 mA/cm<sup>2</sup> is closer to the 500 ppm Ni<sup>2+</sup> system's LCD, which is 0.78 mA/cm<sup>2</sup>, than to that of the 1000 ppm Ni<sup>2+</sup> system, 0.80 mA/cm<sup>2</sup>. The better removal observed for the experiment performed with 1000 ppm Ni<sup>2+</sup> solution demonstrates that the closer the applied CD to the LCD, the worse the performance of the ED unit. Further proving that high CD values, above or close to the LCD, should be avoided.

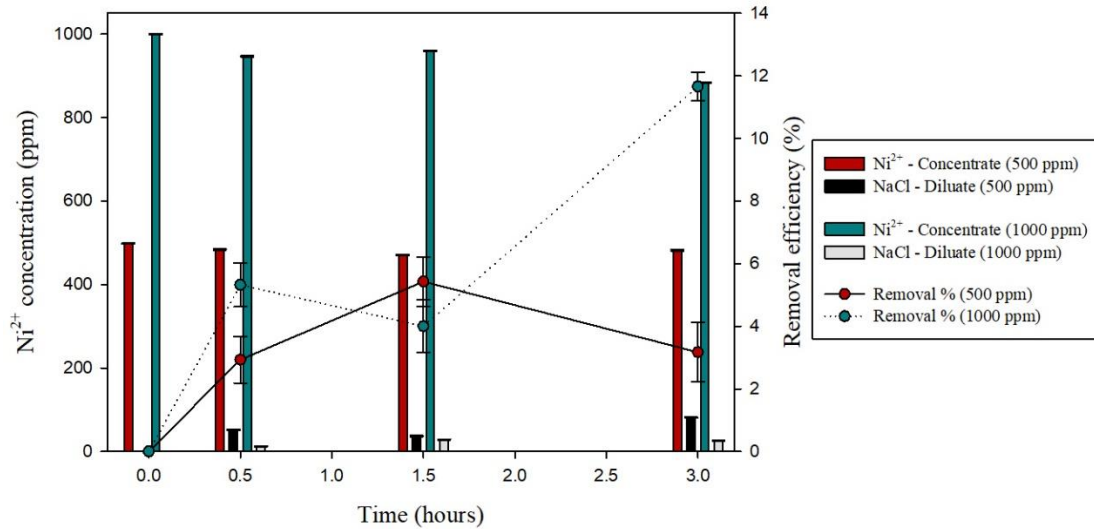


**Figure 3.12. Ni<sup>2+</sup> concentration and removal efficiency changes for two experiments performed in 500 ppm and 1000 ppm Ni<sup>2+</sup> solutions, at 0.75 mA/cm<sup>2</sup> for three hours and 250 rpm agitation speed.**

#### Effect of Applied CD

To further investigate the effect of applied CD, two CD values below the LCD, 0.75 and 0.77 mA/cm<sup>2</sup>, were chosen and experiments were performed, results are presented in Figure 3.13, which show the changes in Ni<sup>2+</sup> concentrations and removal efficiencies for the 1000 ppm Ni<sup>2+</sup>. The results from both CDs indicated similar removal and recovery of the Ni<sup>2+</sup>, with the higher CD performing slightly better, although it is closer to the LCD of the system. Unlike for experiments performed with the 500 ppm Ni<sup>2+</sup> solution, the experiments performed using 1000 ppm Ni<sup>2+</sup> solution allowed for CD closer to the LCD, without negatively impacting the removal efficiency.

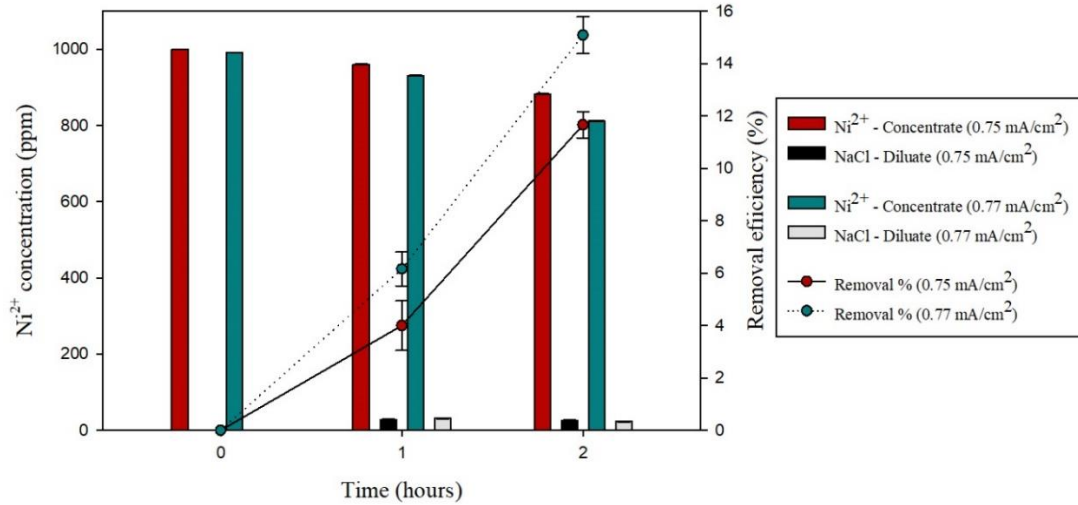


**Figure 3.13. Ni<sup>2+</sup> concentration and removal efficiency changes for two experiments performed using 1000 ppm Ni<sup>2+</sup> solutions at two current densities, 0.75 and 0.77 mA/cm<sup>2</sup> for two hours.**

#### Effect of Metal Ion

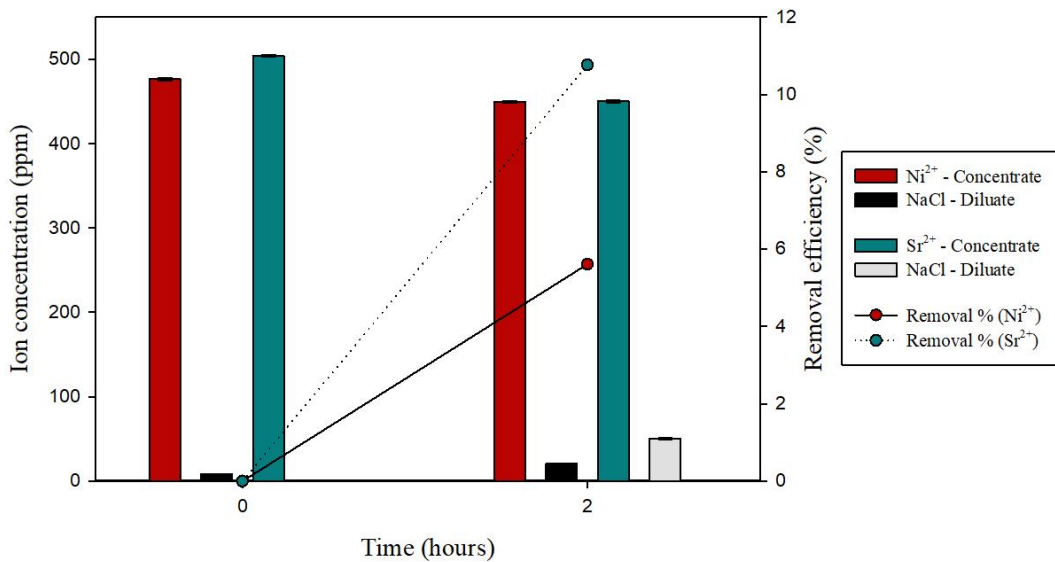


**Figure 3.14. Ni<sup>2+</sup> and Sr<sup>2+</sup> concentration and removal efficiency changes from two experiments performed using 500 ppm Ni<sup>2+</sup> and 500 ppm Sr<sup>2+</sup> solutions at 0.33 mA/cm<sup>2</sup> for two hours.**

To further investigate the effect of low CDs but for the metal cations, the same concentration solutions for Ni<sup>2+</sup> and Sr<sup>2+</sup> were compared, with 0.33 mA/cm<sup>2</sup> CD applied

(Figure 3.14). The experiment performed in  $\text{Sr}^{2+}$  had nearly double the removal value of the experiment performed in  $\text{Ni}^{2+}$  solution as well as higher recovery in the diluate compartment.

Effect of Generating an Electric Field: Galvanostatic (GS) or Potentiostatic (PS)

Two of the many methods of applying an electric field in an ED operation, constant potential (CV) or constant current (CC) were investigated, also referred to as potentiostatic (PS) and galvanostatic polarization (GS), respectively. The difference between CV versus CC was briefly investigated. An experiment was performed, in the 500 ppm  $\text{Sr}^{2+}$  solution, at 300 mV, since this potential corresponds to a CD below the LCD and thus, falls within the safe window for ED operation.

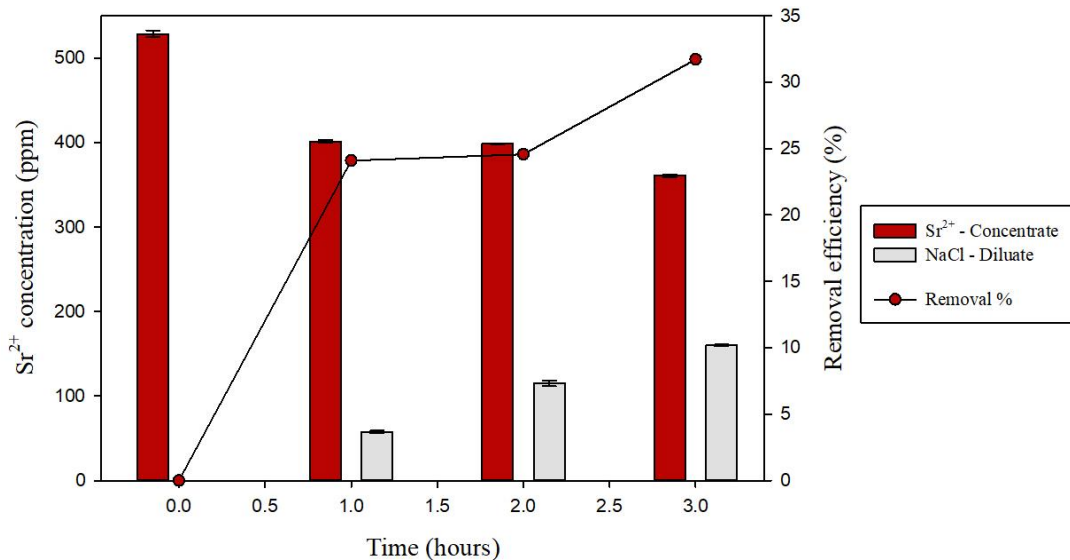


**Figure 3.15.  $\text{Sr}^{2+}$  concentration and removal efficiency changes from an ED experiment performed using 500 ppm  $\text{Sr}^{2+}$  solution, at a constant potential of 350 mV, 250 rpm agitation speed, and for three hours.**

CV is a suitable method for creating electric field required in an ED unit, Figure 3.15. It proved successful in removing and recovering the  $\text{Sr}^{2+}$  ions from the concentrate, with a removal efficiency of 31.71%. The  $\text{Sr}^{2+}$  recovered in the diluate compartment (184.11 ppm) exceeds the  $\text{Sr}^{2+}$  removed from the concentrate (167.67 ppm) by 16.44 ppm. A potential source of the extra  $\text{Sr}^{2+}$  ions is the polymer, meaning that the post-treatment after the previous experiment did not extract all the  $\text{Sr}^{2+}$  in the network. However, this does not

impact the removal efficiency, as the calculation only considers the initial and final metal ion concentrations in the concentrate side of the ED unit. This discrepancy in the concentrations can also be indicative of better removal of the  $\text{Sr}^{2+}$  from the polymer and into the NaCl solution. The experiments performed with the different electric field generation methods seemed to result in different removal efficiencies, favouring PS over GS. One explanation would be that when applying CV, the electric field generated remains stable and relatively low with duration of the experiment.

**Table 3.7. Removal efficiency and energy consumption data for an experiment performed using 500 ppm  $\text{Sr}^{2+}$  solution at a constant potential of 300 mV, 250 rpm agitation speed, and for three hours.**

CV (mV)	Duration (hours)	Removal efficiency (%)	EC (Wh/m <sup>3</sup> )
300	3	31.7	8.83

#### Effect of ED Duration

In order to study the effect of ED duration, the 500 ppm  $\text{Sr}^{2+}$  solution was chosen and two experiments, with the same parameters, were run but for different lengths of time. Figure 3.16 presents the data from the two experiments, performed at 0.33 mA/cm<sup>2</sup>, 250 rpm agitation speed, and for three and five hours. With the increase in ED duration, an increase in  $\text{Sr}^{2+}$  recovery was noted, as well as an increase in removal efficiency. Over the span of the five hours, the  $\text{Sr}^{2+}$  in the concentrate decreased, with a reciprocated increase in the diluate compartment.

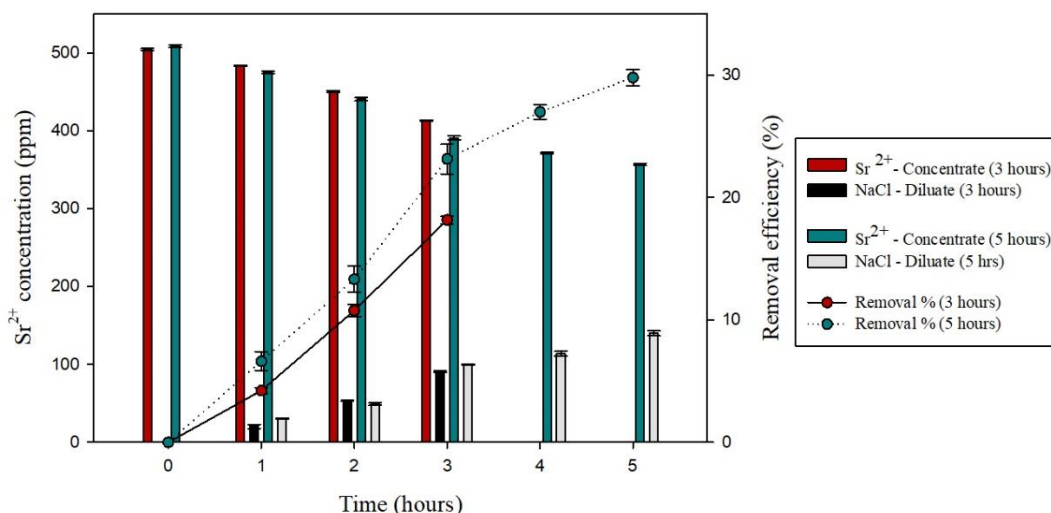


**Figure 3.16.  $\text{Sr}^{2+}$  concentration and removal efficiency changes for experiments performed using 500 ppm  $\text{Sr}^{2+}$  solution at 0.33 mA/cm<sup>2</sup> for three and five hours.**

However, other factors such as the EC need to be considered to better evaluate the extent of the ED duration. From Table 3.8, increasing the ED duration for these experiments almost doubled the EC, which is still relatively low. Increasing the ED length has positive and negative components of the process as both the removal efficiency and the EC are increased.

**Table 3.8. Removal efficiency and energy consumption for experiments performed using 500 ppm  $\text{Sr}^{2+}$  solution at 0.33 mA/cm<sup>2</sup> for three and five hours.**

CD (mA/cm <sup>2</sup> )	Duration (hours)	Removal efficiency (%)	EC (Wh/m <sup>3</sup> )
0.33	3	18.2	7.47
0.33	5	29.8	11.3

Since the increase in ED duration had an overall positive impact with respect to removal and recovery of the metal ion, an even longer experiment was run for the 1000 ppm  $\text{Ni}^{2+}$  system. This experiment, presented in Figure 3.17 and Table 3.9, was initially planned to run for twenty-four hours but it was terminated at twenty hours, for reasons outlined below. A CD of 0.167 mA/cm<sup>2</sup> was chosen because it was tested before, for three hours, and it provided a comparison point for the efficiency and impact of the longer ED duration.

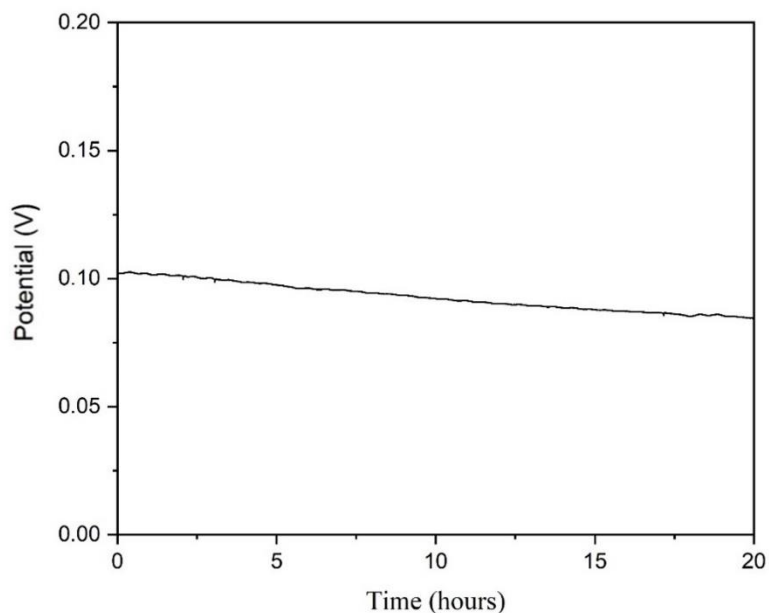


**Figure 3.17. Time-potential curve for an experiment performed using 1000 ppm Ni<sup>2+</sup> solution at 0.167 mA/cm<sup>2</sup>, 250 rpm stirring speed, and for twenty hours.**

The potential was recorded for twenty hours and the starting potential was 0.10 V, slightly decreasing with time. At the twenty-hour mark, a great amount of green precipitate was noted in the diluate cell and thus, the experiment was terminated early. The solutions were sampled at various time intervals and a portion of the precipitate was collected for further testing (data in section 3.1.3). The pH change documented in both compartments is presented in Table 3.10, and the data reflect an increase in the diluate compartment's pH and a decrease in the concentrate solution's pH. The impact of pH is discussed further below. Unlike in the previous experiment, increasing the duration did not positively impact the removal efficiency and it led to a fivefold increase in the EC (Table 3.9).

**Table 3.9. Removal efficiency and EC data for experiments performed using 1000 ppm Ni<sup>2+</sup> solution at 0.167 mA/cm<sup>2</sup> for three and twenty hours.**

CD (mA/cm <sup>2</sup> )	Duration (hours)	Removal efficiency (%)	EC (Wh/m <sup>3</sup> )
0.167	3	15.1	0.81
0.167	20	17.5	4.95

## Effect of pH

Pourbaix diagrams, or potential-pH diagrams represent the thermodynamically stable species at given potentials, pH values, and temperature for various systems [50]. According to the Pourbaix diagram for  $\text{Ni}^{2+}$ , Figure 3.18, the stability window for  $\text{Ni}^{2+}$  in solution extends from pH 0 to approximately pH 8, and in alkaline environments  $\text{Ni}(\text{OH})_2$  forms [51]. The potential for the experiment, equivalent to 0.341 V versus SHE, falls within the range where  $\text{Ni}(\text{OH})_2$  is stable. Equations 3.1 and 3.2 illustrate the reactions which took place and resulted in the precipitation of the hydroxide, Figure 3.19. Moreover, the hydrogen evolution reaction (HER) contributed to the pH increase in the diluate compartment (Equation 3.1).

**Table 3.10. pH measured in the concentrate and diluate compartments, over the span of the twenty-hour experiment.**

<b>Sampling Time (Hours)</b>	<b>Compartment</b>	<b>pH</b>
0	Concentrate - $\text{NiCl}_2$	3.58
4	Concentrate - $\text{NiCl}_2$	3.20
20	Concentrate - $\text{NiCl}_2$	2.70
0	Diluate - $\text{NaCl}$	2.98
4	Diluate - $\text{NaCl}$	4.63
20	Diluate - $\text{NaCl}$	10.02

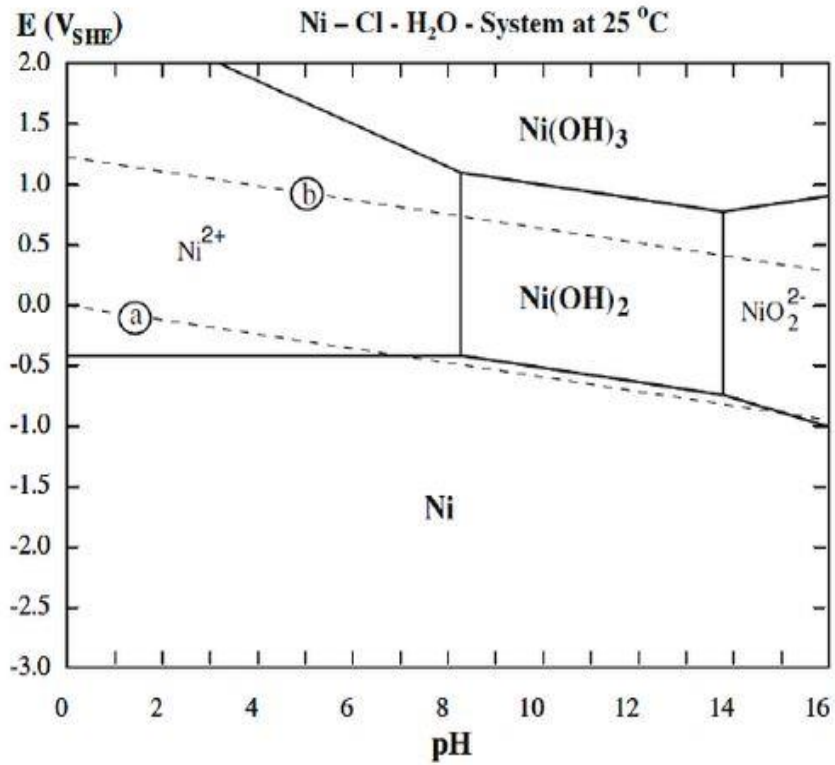


**Figure 3.18.** Pourbaix diagram for Ni-Cl system at 25 °C, indicating water stable region (dashed lines) and stable species at the given potential and pH values [50].

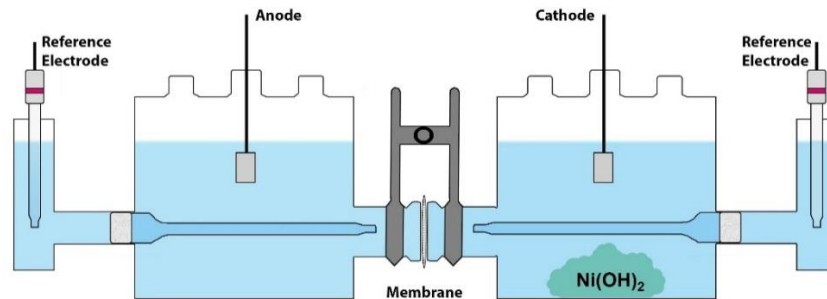
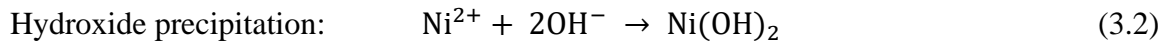
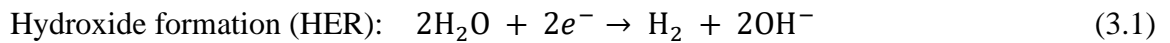


**Figure 3.19.** Electrochemical cell diagram demonstrating the precipitation of nickel hydroxide.

Precipitation can be an effective method of recovering the metal after decontamination. These conditions and reactions formed  $\text{Ni}(\text{OH})_2$ , which in turn recycles the  $\text{Ni}^{2+}$  removed from the concentrate. Nonetheless, it will likely cost more energy than avoiding the precipitation by pH adjustment. It is more practical to control the pH during the ED operation, precipitate the metal, or recover it in other ways, as a means of recycling, post the ED process rather than concurrently with the ED step.

The effect of pH was investigated by maintaining a pH of 2, for an experiment with 500 ppm  $\text{Ni}^{2+}$ , in the diluate compartment at the start of the experiment and adjusting the pH accordingly every thirty minutes for three hours. 1 M HCl was added to adjust the solution pH. Again, the same experiment was performed, without altering the pH, as a comparison point. From Figures 3.20 and 3.21, it is evident that controlling the pH resulted in a steep increase in  $\text{Ni}^{2+}$  removal and an EC of  $5.16 \text{ Wh/m}^3$ , which was the lowest EC obtained between all the experiments.

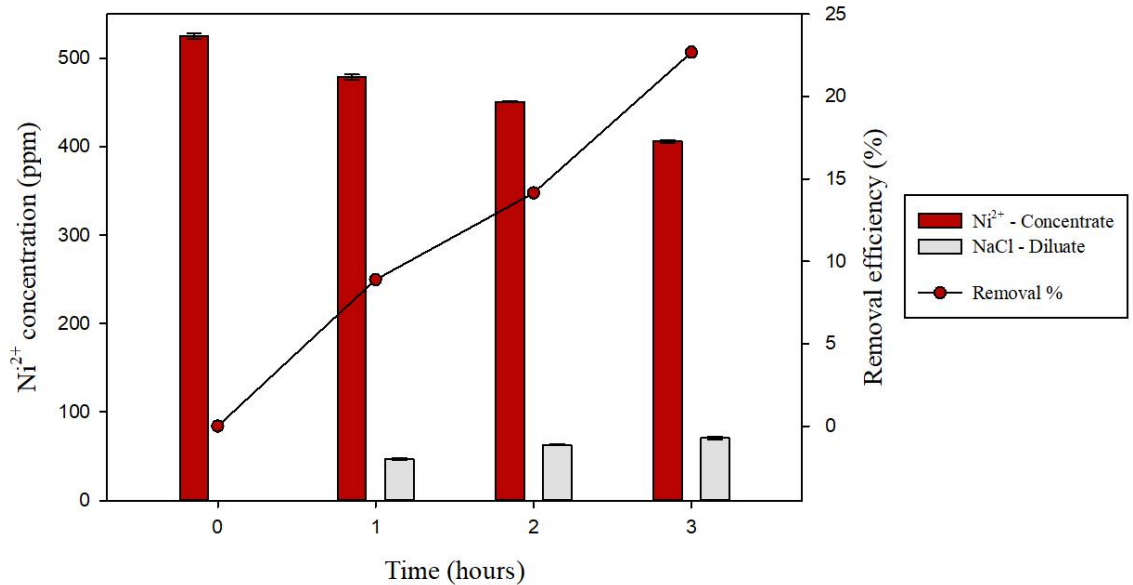


**Figure 3.20.  $\text{Ni}^{2+}$  concentration and removal efficiency changes for a pH-controlled experiment performed using 500 ppm  $\text{Ni}^{2+}$  solution at  $0.58 \text{ mA/cm}^2$ , 250 rpm agitation speed, and for three hours.**

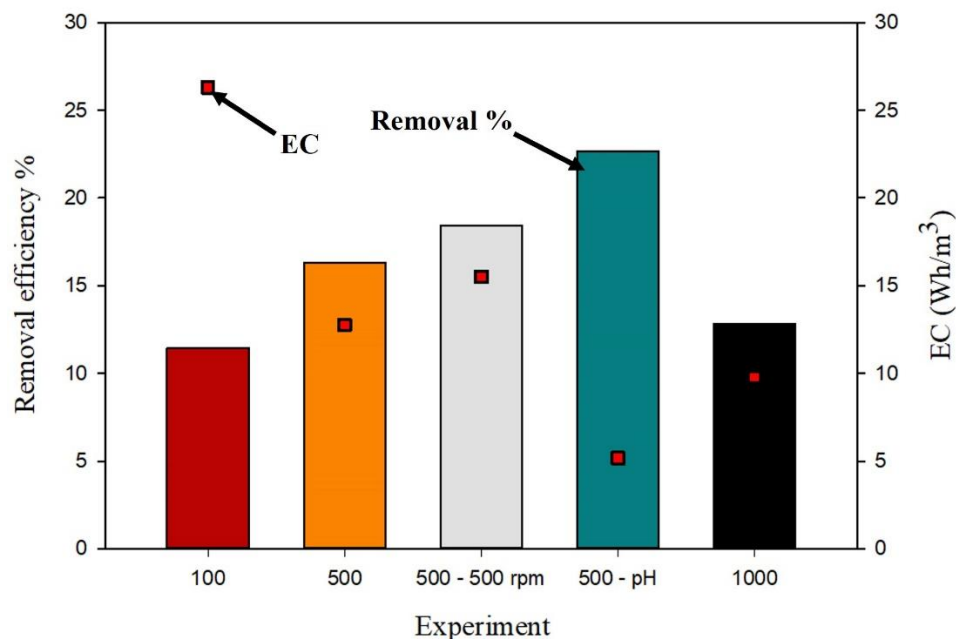


**Figure 3.21. Comparison between the removal efficiency and EC for 100 ppm, 500 ppm, and 1000 ppm Ni<sup>2+</sup> solutions investigated, at an applied CD of 0.58 mA/cm<sup>2</sup>, 250 rpm, 500 rpm, and pH controlled at 2.**

Compilation of experiments investigating the effect of pH, 250 rpm agitation rate, and 500 rpm agitation rate at the same CD for the various Ni<sup>2+</sup> concentrations was documented and compared in Figure 3.21. All experiments were performed for three hours and except for one (grey bar), all were stirred at 250 rpm. In general, 500 ppm had the highest Ni<sup>2+</sup> removal compared to 100 and 1000 ppm systems. The 100 ppm Ni<sup>2+</sup> system experienced high resistance, as noted from the E-t curves. In return, this increased the EC, leading to the highest energy requirement between the other concentrations and solutions investigated. Moreover, increasing the agitation speed from 250 rpm to 500 rpm slightly improved the removal efficiency; the most practical factor to enhance Ni<sup>2+</sup> removal is controlling the pH. By increasing the acidity of the solution, more H<sup>+</sup> ions were readily available in the concentrate compartment, alleviating the pressure on the anode to produce more H<sup>+</sup> via the oxygen evolution reaction [52].

The various testing parameters play different roles in the removal and recovery efficiency of the metal ion. These parameters convey insights into the factors that need to be

considered when deciding on the ED operation conditions to ensure effective and economical runs.

### 3.1.3 Surface Analysis and Membrane Characterization

The Nafion 117 polymer was analyzed with various analytical techniques including FT-IR and SEM/EDX. The precipitate collected from a twenty-hour experiment performed with 500 ppm Ni<sup>2+</sup> solution was also characterized by Raman spectroscopy and the following sections present the results obtained.

#### FT-IR

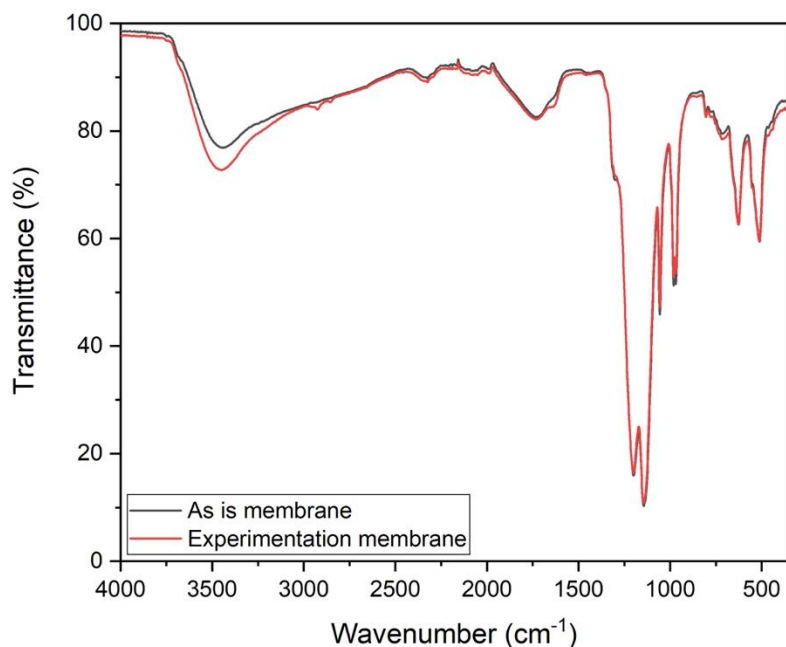


**Figure 3.22. FT-IR spectra of an as-received Nafion 117 membrane and a Nafion 117 membrane post experimentation.**

FT-IR spectra of an as-received membrane and a membrane used in electrochemical experiments are displayed in Figure 3.22. There was a large similarity between the peaks in both spectra, such as the peaks between 500 and 2500 cm<sup>-1</sup>. The peak at 1100 cm<sup>-1</sup> was assigned to the C-F stretch, the peak at 1150 cm<sup>-1</sup> was assigned to the C-O stretch, and that at 1300 cm<sup>-1</sup> was assigned to the S=O stretch [53, 54]. The membrane used for experimentation had a larger transmittance for the O-H stretch at 3500 cm<sup>-1</sup> compared to

the as-received membrane, and this may be an indication of a greater hydration level within the membrane. The high correlation between the two spectra indicated that the membrane's structure was not altered during the experimentation and that the pre-treatment step successfully expelled any ions sequestered by the membrane during experimentation. In order to ensure the reliability of the results and to also ensure that the observed changes were caused by changes in the parameters used in the latest experiment rather than the consequence of an accumulation of changes during previous experiments, the structure of the membrane must be the same between each experiment, and this was corroborated by the results presented above. Further analyses were performed to further characterize the morphology and composition of the Nafion 117 membrane.

### SEM/EDX

The Nafion 117 polymer was analyzed top-down and in cross-section by SEM/EDX. The top-down BSE micrographs show a relatively clean surface of the Nafion sample, Figure 3.23. The micrographs show the homogeneity of the membrane, as there no inclusions or regions with different texture present.

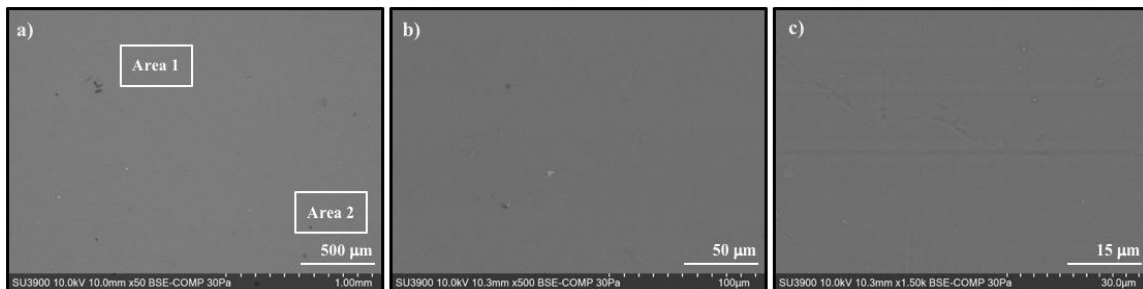


**Figure 3.23. BSE micrographs of Nafion 117. Areas marked correspond to EDX areas in Table 3.11.**

The semi-quantitative EDX analysis of two areas on the membrane, Table 3.11, indicated the presence of carbon, fluorine, oxygen, and sulfur, which correspond to the structure of the polymer comprising a tetrafluoroethylene backbone and perfluorovinyl ether group side chains, terminated with sulfonic acid groups. Trace amounts of potassium were also detected, likely a contaminant from sample handling.

**Table 3.11. EDX semi-quantitative elemental analysis of Nafion 117.**

Spectrum Label	Elemental Composition (wt. %)				
	C	F	O	S	K
Area 1	21.9	66.1	8.5	3.3	0.2
Area 2	21.6	67.5	7.9	2.7	0.2

The fracture pattern and homogeneity of the sample were evident in the cross-sectional BSE micrographs, Figure 3.24. The homogeneity of the Nafion 117 membrane in cross-section is consistent with previous literature reports [55]. The thickness of the Nafion 117 polymer was 185  $\mu\text{m}$ , which was slightly thicker than what the supplier stated (183  $\mu\text{m}$ ) [56]. This small deviation could be a result of different moisture levels in the polymer, temperatures, or relative humidities.

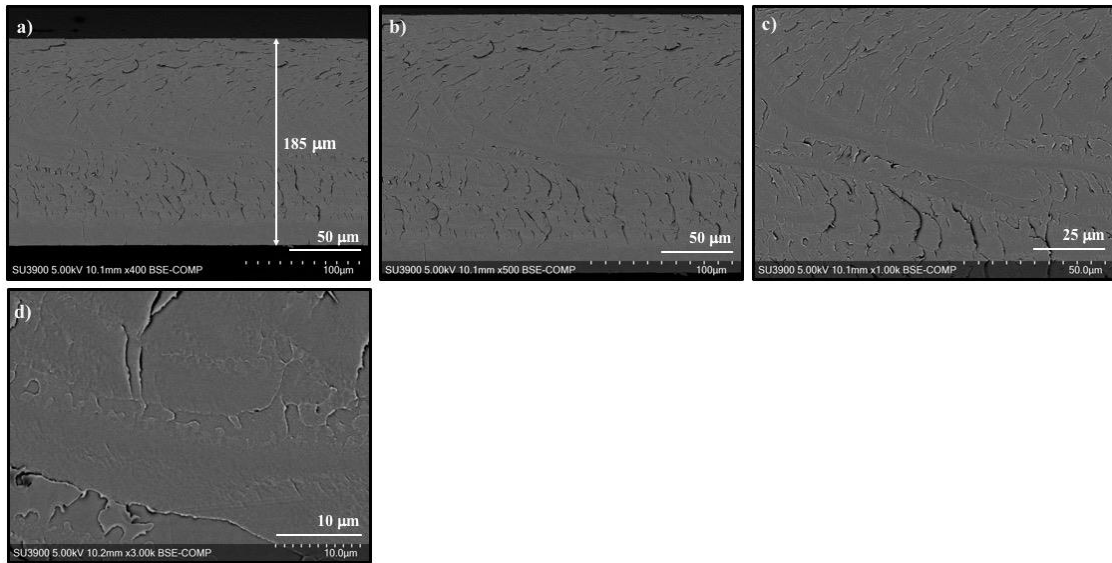


**Figure 3.24. Cross-section BSE micrographs of Nafion 117.**

After characterization of the Nafion 117 polymer by FT-IR and SEM/EDX was complete, the precipitate collected from the long-term experiment performed with 500 ppm  $\text{Ni}^{2+}$  was analyzed by Raman spectroscopy.

## Raman

The precipitate noted in the twenty-hour long experiment (section 3.1.2) was collected from solution, concentrated by a centrifuge, and analyzed by Raman spectroscopy (Figure 3.25).

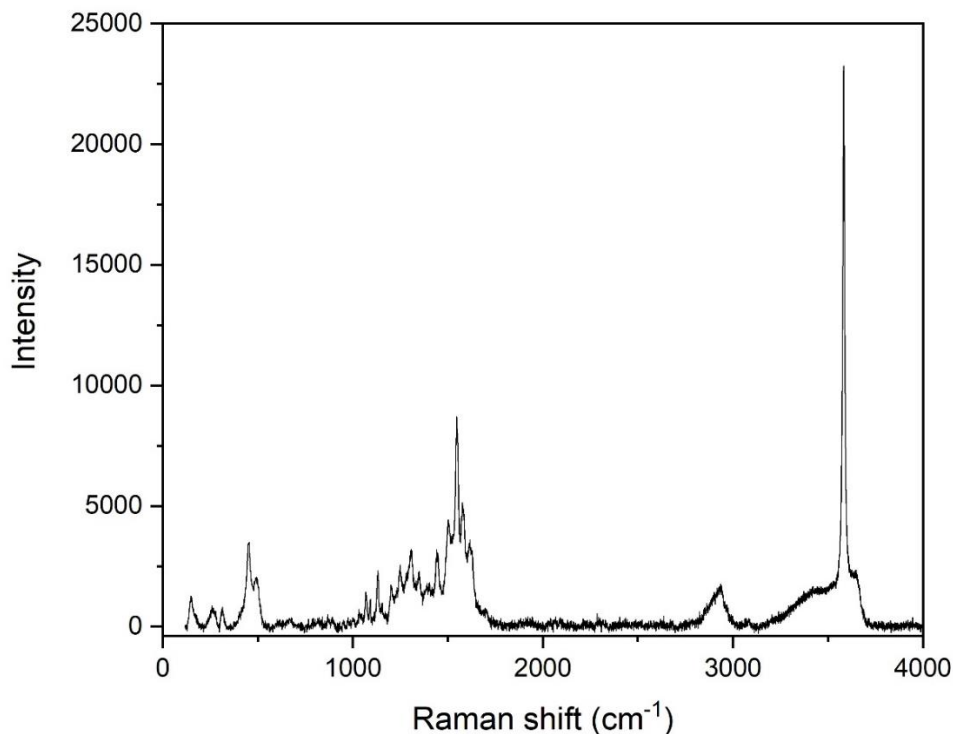


**Figure 3.25. Raman spectrum of the collected and centrifuged Ni(OH)<sub>2</sub> precipitate.**

Raman-active transitions reported in literature for Ni(OH)<sub>2</sub> match the peaks in the Raman spectrum of the precipitate and they appear around 450 cm<sup>-1</sup>, 1200 cm<sup>-1</sup>, and 3600 cm<sup>-1</sup> [57]. The Raman data further prove the composition of the precipitate and clarify the importance of controlling the pH for experiments performed with Ni<sup>2+</sup> solutions.

## Discussion

Chemical and electrochemical sequestration of Ni<sup>2+</sup> and Sr<sup>2+</sup> by Nafion 117 were investigated and numerous trends were observed. The chemical sequestration data proved that that chemical treatment alone would not be an effective method of treating contaminated water, especially at an industrial scale. For the electrochemical sequestration

study, numerous factors were investigated, including LCD determination, pre-treatment effects, agitation rates, CD applied (above and below the LCD), metal ion preference, initial solution concentration, experiment duration, and pH effects. In summary, the tested parameters contributed differently to the removal and recovery efficiencies of  $\text{Ni}^{2+}$  and  $\text{Sr}^{2+}$ . For example, agitating the test solution increased the ionic migration rate and in return, increased the removal efficiency; similar results were reported in literature [58]. However, the effect of other testing conditions, such as the pH of the solution, overshadowed the effect of solution agitation for solutions containing  $\text{Ni}^{2+}$ . Controlling the pH of the 500 ppm  $\text{Ni}^{2+}$  solution increased the removal efficiency by 10% and decreased the EC by a factor of five.

In terms of pre-treatment effects, a two-step pre-treatment (test C in Table 3.5), consisting of thirty-minute soaks in 1 M HCl and DI  $\text{H}_2\text{O}$  at 75 °C, yielded the best outcome. In some instances, the removal percentage was higher than the recovery percentage, meaning that not all  $\text{Ni}^{2+}$  or  $\text{Sr}^{2+}$  removed from the concentrate cell was recovered in the diluate cell. An explanation for this would be that, depending on the pre-treatment and post-treatments tested, a portion of the ionic species sometimes remained in the polymeric network. Furthermore, desorption investigations showed that longer soak durations did not result in higher recovery of the ions of interest and rather, the desorption solution had a maximum threshold for the containment of the metal ionic species. In other words, the desorption solution must be renewed multiple times to remove all of the ions from the networks of the polymer. Another potential pre-treatment that was not investigated, but reported in literature, involved the same idea of refreshing the HCl solution, every thirty minutes to an hour, for a set amount of time until all the ions of interest were removed from the membrane [59]. As the availability of fresh  $\text{H}^+$  ions increased in solution, it allowed for a higher exchange with the metal ions in the membrane, bringing the polymer back to its protonated form. Also, this would be a better alternative to increasing the acid concentration, as this option would degrade the polymer faster, decreasing its lifetime in the ED operation.

Increasing the ED duration by few hours significantly increased the EC but when the duration was extended further, the removal rate reached a maximum. The highest removal efficiency noted was for an experiment performed at a CD of 0.33  $\text{mA}/\text{cm}^2$  and a solution

containing 500 ppm  $\text{Sr}^{2+}$ , for five hours. A similar removal value was calculated for a chemical sequestration experience performed for twenty-four hours. Since the electrochemical experiment only took five hours compared to twenty-four hours, this verified the applicability and advantage of electrochemical means over chemical means for water decontamination. In practice, long-term experiments with  $\text{Sr}^{2+}$  provided better removal efficiency. This was a result of the higher affinity of Nafion 117 for  $\text{Sr}^{2+}$ . Also, formation and precipitation of  $\text{Sr}(\text{OH})_2$  was not a concern, as extremely basic solutions (pH 14) would be required, as apparent from the Pourbaix diagram presented in Figure 3.26. A bigger pH range of  $\text{Sr}^{2+}$  stability versus that of  $\text{Ni}^{2+}$  allowed for higher removal of  $\text{Sr}^{2+}$  without the need for pH adjustments.

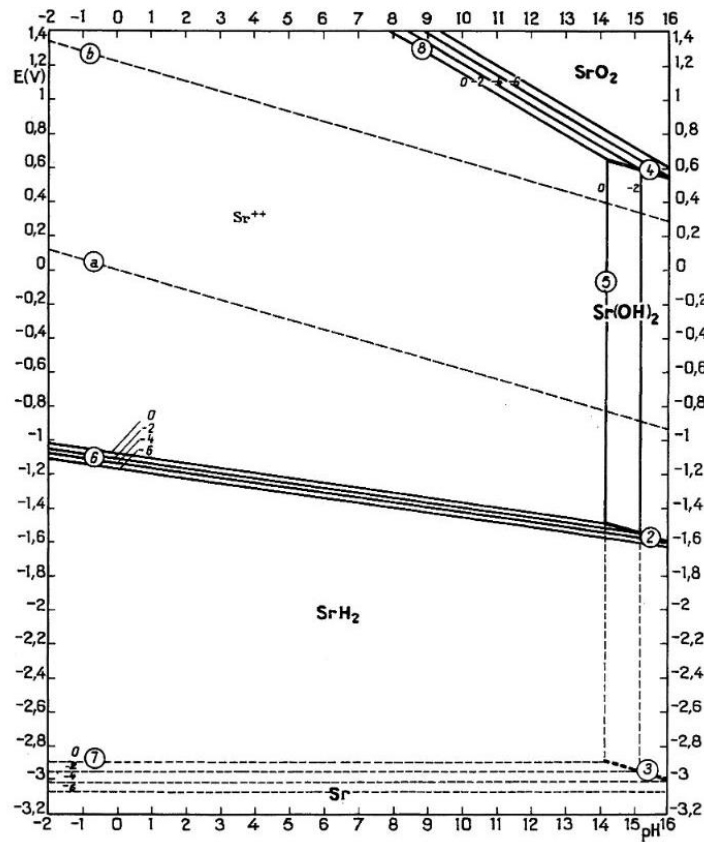


**Figure 3.26. Pourbaix diagram for Sr-Cl system at 25 °C, indicating the water stability region (lines a and b) and stable species at the given potential and pH values [60].**

It is evident from the results in sections 3.1.1 and 3.2.2 that the Nafion 117 polymer has a higher affinity for  $\text{Sr}^{2+}$  than for  $\text{Ni}^{2+}$ . Both ions are divalent, eliminating the effect of charge on the polymer's affinity towards them.  $\text{Sr}^{2+}$  has a larger ionic radius of 132 pm compared to an ionic radius of 83 pm for  $\text{Ni}^{2+}$  [61]. The higher affinity of the Nafion polymer for  $\text{Sr}^{2+}$  is explained by higher coulombic attraction between the larger ion and the oppositely charged fixed groups in the IEM.

The second part of this research project consisted of testing and characterizing the novel CapturePhos polymers mentioned in section 2.5.2 and the results can be found in section 3.2, below.

## 3.2 CapturePhos Experiments

Different formulations of the CapturePhos polymers were tested (Table 2.1). The first two designs (P-91 P-99, and P-05) were not mechanically stable, as they punctured when they were installed in the electrochemical cell; however, their chemical sequestration performance was still investigated. To improve the mechanical strength and stability of the polymer, the ratio of the cross-linker to chain-extender was changed and the formulation amount cured was also changed. However, initial attempts focused on adjusting the cross-linker to chain-extender ratio, followed by decreasing the formulation amount used to reduce the thickness of the polymer.

### 3.2.1 Chemical Sequestration

The polymers were soaked in 500 ppm  $\text{Ni}^{2+}$  solutions for various durations in order to investigate their capture behaviour and later compare the results to the electrochemical sequestration results.

**Table 3.12. Chemical sequestration data for first-generation CapturePhos polymer (P-91).**

Duration (hours)	$\text{Ni}^{2+}$ concentration (ppm)	Removal efficiency %
0	498.2	NA
0.5	490.1	1.63
1	500.3	-0.41
5	502.8	-0.92
24	451.6	9.36

P-91, from the first-generation of polymers tested, was soaked for twenty-four hours (Table 3.12). The Ni<sup>2+</sup> concentration and the removal efficiency fluctuated throughout the soak period. The fluctuations indicated a lack of preference and attachment between the Ni<sup>2+</sup> and the CapturePhos network. The final removal achieved was 9.36%.

**Table 3.13. Chemical sequestration data for second-generation CapturePhos polymer (P-05).**

<b>Duration (hours)</b>	<b>Ni<sup>2+</sup> concentration (ppm)</b>	<b>Removal efficiency (%)</b>
0	527.1	NA
1	526.7	0.08
3	522.8	0.82
24	516.6	2.00

The chemical uptake of the second-generation of polymers was also investigated, Table 3.13. This formulation led to worse preference for the Ni<sup>2+</sup>, compared to P-91, since only 2% was removed from the solution after twenty-four hours. Since both the formulation and the amount used were altered for the second-generation, only the formulation amount of polymer cured was further changed for the 3.0 generation (Table 3.14).

**Table 3.14. Chemical sequestration data for third-generation CapturePhos polymer (P-40).**

<b>Duration (hours)</b>	<b>Ni<sup>2+</sup> concentration (ppm)</b>	<b>Removal efficiency (%)</b>
0	518.3	NA
24	506.8	2.20

However, increasing the formulation amount did not positively impact the removal efficiency, as the same removal efficiency was noted for polymers P-05 and P-40. Instead, agitating the solution at the low rate of 250 rpm had a more positive impact. The removal efficiency was increased by 400%. The solutions were sampled at the midpoint and the end of the soak, and the removal was not significantly impacted by leaving the polymer in the solution for an additional twelve hours.

**Table 3.15. Chemical sequestration data for third-generation CapturePhos polymer (P-40) to investigate the effect of agitating the solution at 250 rpm.**

Duration (hours)	Ni <sup>2+</sup> concentration (ppm)	Removal efficiency (%)
0	536.5	NA
12	489.1	8.84
24	484.4	9.72

The chemical sequestration behaviour of the last CapturePhos generation, polymer P-65, was tested in a four-day long soak, Table 3.16. The duration of the experiment was increased by a factor of four to determine whether longer soak durations resulted in better removal of the Ni<sup>2+</sup>.

**Table 3.16. Chemical sequestration data from a ninety-six hour soak of the fourth-generation CapturePhos polymer (P-65).**

Duration (hours)	Ni <sup>2+</sup> concentration (ppm)	Removal efficiency (%)
0	482.3	NA
24	464.6	3.66
96	461.3	4.35

After ninety-six hours of soaking, 4.35% of the Ni<sup>2+</sup> was removed by the polymer. All the chemical experiments with the CapturePhos, excluding data of P-91, proved that increasing the soak time did not result in better removal of the Ni<sup>2+</sup>.

The ability of NaCl solution at desorption was also investigated and the data did not indicate strong desorption behaviour, Table 3.17. Trace amounts of Ni<sup>2+</sup> were leached out of the polymer soaked in NaCl for two hours, which is an indication of the lack of the ion in the network and the poor strength of NaCl for removing any residual Ni<sup>2+</sup> in the network.

**Table 3.17. Amount of Ni<sup>2+</sup> desorption in NaCl post soak experiment for P-40.**

Duration (hours)	Ni <sup>2+</sup> concentration (ppm)
0	0.140
1	0.220
2	0.495

Electrochemical testing followed investigations of the chemical sequestration behaviour of the four CapturePhos polymers, and the results are presented below.

### 3.2.2 Electrochemical Sequestration

Every generation of the polymers was tested for their electrochemical sequestration behaviour. The first two generations of polymers tested were too brittle, and punctured when installed in the ED cell, as they were too thick and not mechanically stable (Figure 3.27), whereas the third and fourth-generation polymers did not puncture immediately; however, they caused a high resistance in the cell and a potentiostat could not be used to create the electric field required. Instead, a high-voltage DC power supply was used.



**Figure 3.27. Digital image of the punctured P-91 polymer after a failed electrochemical experiment.**

A current density of  $9.2 \text{ mA/cm}^2$  was applied to polymer P-65 for only fifteen minutes before the polymer collapsed. The recorded potential was around 74 V at the start of the experiment; it increased to 110 V around eight minutes and returned to 86 V by the end of the fifteen minutes.

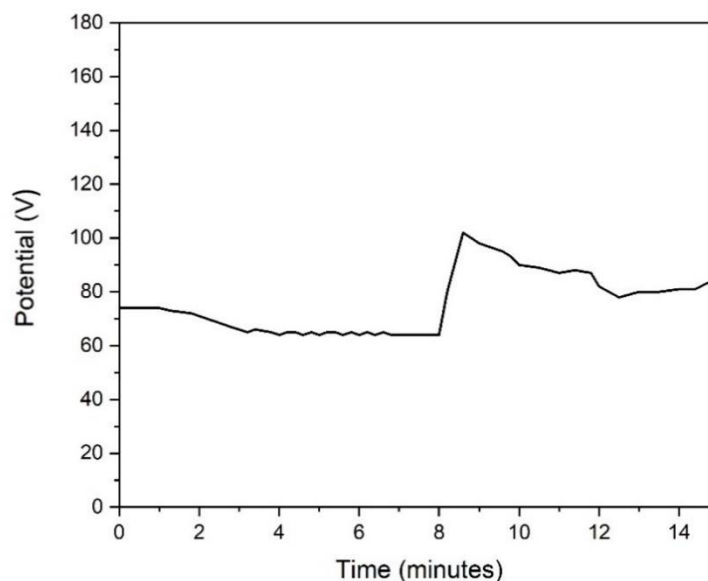


**Figure 3.28. Potential recorded for fifteen minutes in response to the application of 9.2 mA/cm<sup>2</sup> for polymer P-65.**

The Ni<sup>2+</sup> removal efficiency calculated for the experiment was 5.06% (Table 3.18). In comparison to the 4.35% that was removed by ninety-six hours during the chemical sequestration experiment, 5.06% of the Ni<sup>2+</sup> was removed by the polymer at the end of the electrochemical step, further proving the enhanced removal of electrochemical techniques such as ED compared to chemical experiments. Surface analysis of the polymer was performed in an attempt to further understand the brittleness and high resistance of the polymers.

**Table 3.18. Measured Ni<sup>2+</sup> concentrations and removal efficiency for the electrochemical sequestration experiment performed at 9.2 mA/cm<sup>2</sup> for fifteen minutes, on a fourth-generation CapturePhos polymer (P-65).**

Duration (hours)	Ni <sup>2+</sup> concentration (ppm)	Removal efficiency (%)
0	478.3	NA
0.25	454.1	5.06

### 3.2.3 Surface Analysis and Membrane Characterization

Various samples of the CapturePhos polymer were characterized by FT-IR and SEM/EDX spectroscopy techniques and the results can be found below.

#### FTIR

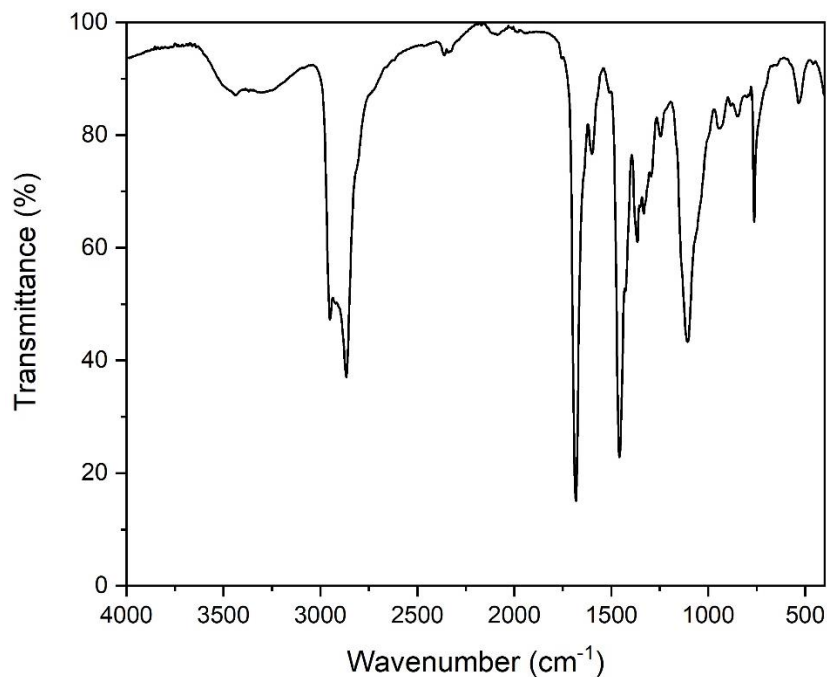


**Figure 3.29. FT-IR spectrum of polymer P-40.**

The FT-IR spectrum for polymer P-40 was collected and presented in Figure 3.29. Peaks at  $1100\text{ cm}^{-1}$ ,  $2850\text{ cm}^{-1}$ ,  $3000\text{ cm}^{-1}$ ,  $2300\text{ cm}^{-1}$ ,  $1690\text{ cm}^{-1}$ , and  $1340\text{ cm}^{-1}$  were assigned to the C-O stretch, alkane C-H stretch, alkene C-H stretch, P-H stretch, amide C=O stretch, and aromatic C-N, respectively [53, 54]. Similar to the Nafion 117 FT-IR spectra, an O-H stretch was observed around  $3490\text{ cm}^{-1}$ , although the O-H stretches in the Nafion FT-IR spectra were more pronounced. This peak could be an indication of polymer hydration, as it was not oven-dried post experimentation and before the FT-IR analysis. Furthermore, FT-IR provided information on the bonding on the polymer, however additional analytical techniques, such as SEM/EDX, were required to visualize the polymers, and determine their morphology/texture and their chemical composition.

## SEM/EDX

Numerous samples of the four polymer generations were examined top-down and in cross-section by SEM/EDX. The thickness of the polymers was measured for the samples analyzed after the SEM micrographs were recorded. The resistance observed in the CapturePhos experiments can be partially explained by the thickness of the polymers. Moreover, SEM micrographs for many of the polymers showed the presence of voids in the polymer, which were also evident in Figure 3.27.

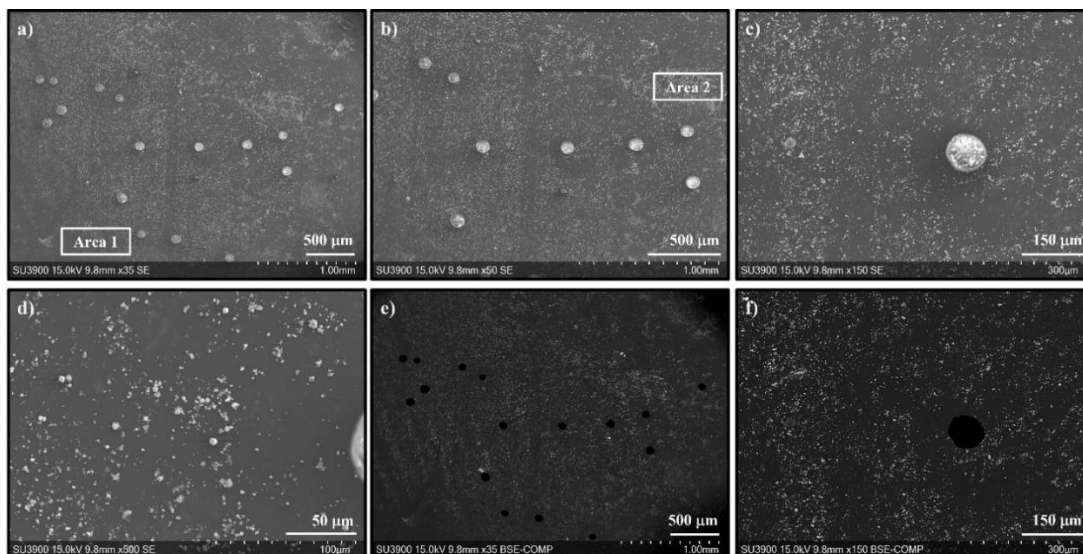


**Figure 3.30. Top-down SEM micrographs of a first-generation CapturePhos polymer (P-91). The areas marked indicate the EDX areas in Table 3.19**

The SE and BSE micrographs of a first-generation CapturePhos polymer P-91 are shown in Figure 3.30. A large number of small voids, in the form of bubbles, are evident, and they appear to be filled with uncured polymer. The cross-section micrographs, Figure 3.31, show a uniform polymer, with a thickness of 2.18 mm. The semi-quantitative EDX analysis of the polymer indicates that the surface of P-91 mostly consists of C, O, and P. Minor trace amounts of  $\text{Ni}^{2+}$  were detected on the surface of the polymer, along with various impurities, such as Al, Mg, K, and Ca, most likely from handling.

**Table 3.19. EDX semi-quantitative data for P-91.**

Spectrum Label	Elements Detected (wt. %)												
	C	O	P	Ni	Si	Cl	Al	Na	Ba	Mg	K	Fe	Ca
Area 1	64.9	15.1	19.2	0.5	0.1	0.3	-	-	-	-	-	-	-
Area 2	28.2	40.5	1.9	1.8	11.6	1.2	10.8	2.6	0.5	0.3	0.3	0.2	0.1

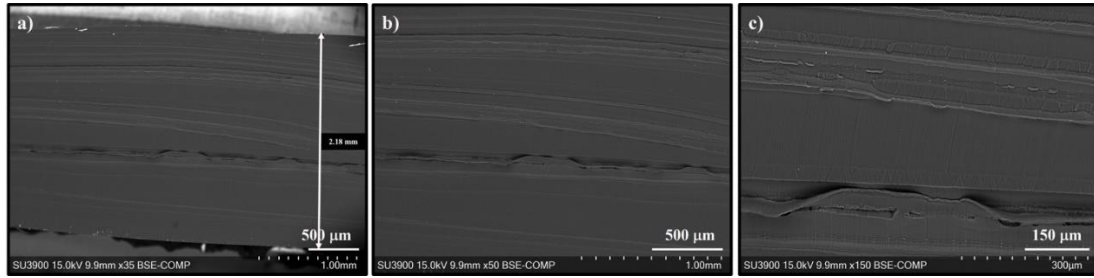


**Figure 3.31. Cross-section SEM micrographs of a first-generation CapturePhos polymer (P-91).**

Figures 3.32 and 3.33 exhibit top-down and cross-section micrographs of a second-generation CapturePhos formulation (P-05), respectively. Large voids, between 250 and 500  $\mu\text{m}$ , are noticeable in both Figures. The top-down micrographs indicate a textured and non-uniform surface, which could negatively impact the migration of ions across the polymer. This non-uniformity is further observed in the cross-section micrographs. The thickness of the polymer varied between 1.65 and 1.85 mm (Figure 3.23 (a)).

**Table 3.20. EDX semi-quantitative data for P-05.**

Spectrum Label	Elements Detected (wt. %)							
	C	O	P	Si	F	Cl	Na	Al
Area 1	65.4	23.6	10.7	0.2	0.1	-	-	-
Area 2	61.3	18.8	17.2	2.0	0.4	0.2	0.1	0.1

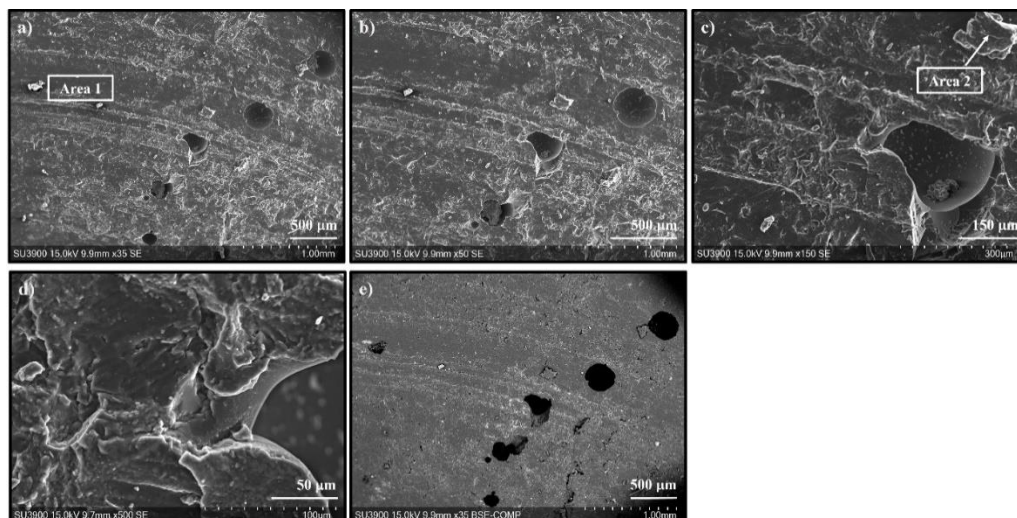


**Figure 3.32. Top-down SEM micrographs of a second-generation CapturePhos polymer (P-05). The areas marked indicate the EDX areas in Table 3.20.**

Similar composition data was obtained for the second-generation polymer compared to the first-generation polymer.

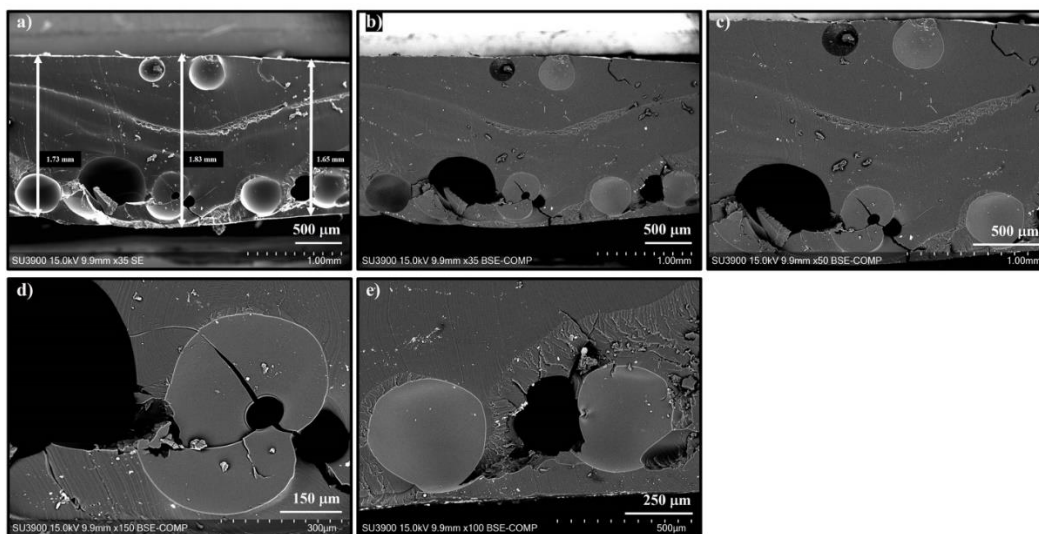


**Figure 3.33. Cross-section SEM micrographs of a second-generation CapturePhos polymer (P-05).**

Two of the third-generation polymers were imaged and analyzed by SEM/EDX; top-down and cross-section micrographs of P-40 were recorded, Figures 3.34 and 3.35, and micrographs of the cross-section of P-46 were also recorded and presented in Figure 3.36.

With this formulation, fewer voids were noticed top-down and in cross-section, an indication of an improved polymer preparation technique.

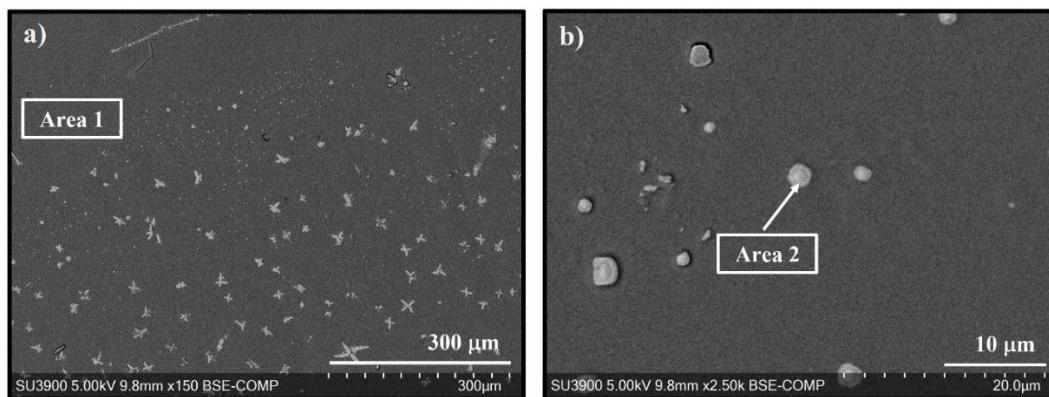


**Figure 3.34. Top-down SEM micrographs of a third-generation CapturePhos polymer (P-40). The areas marked indicate the EDX areas in Table 3.21.**

Crystals composed mostly of O, Na, P, and S were formed on the surface of the P-40 polymer and only this polymer displayed this pattern of crystallization on the surface. Since the cross-section did not indicate a similar pattern, the crystallization seemed to be a result of the experimentation and of the sample handling, rather than of the polymer preparation step.

**Table 3.21. EDX semi-quantitative data P-40.**

Spectrum Label	Elements Detected (wt. %)				
	C	O	P	Na	S
Area 1	66.5	23.6	10.0	-	-
Area 2	4.0	46.1	17.9	25.3	6.7

Moreover, the cross-section of P-40 was mostly homogenous, with only two voids located near the edge of the cross-section. This was an indication that the bubbles were escaping from the main body of the gel to the surface of the mount as the gel was curing.

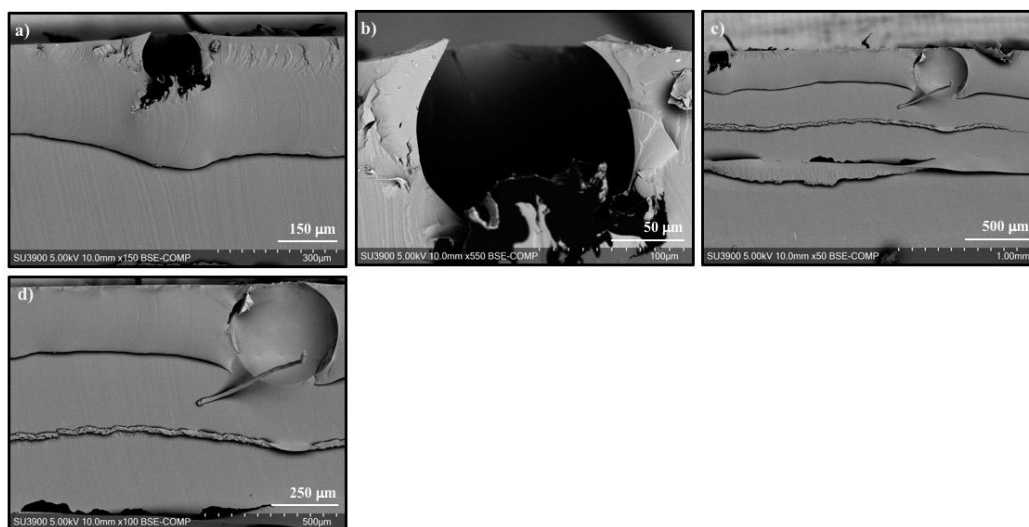


**Figure 3.35. Cross-section SEM micrographs of a third-generation CapturePhos polymer (P-40).**

The second polymer from the third-generation group, P-46, was cross-sectioned and analyzed. The thickness of P-46 was determined to be 2.12 mm and only one shallow void was found in the cross-section.

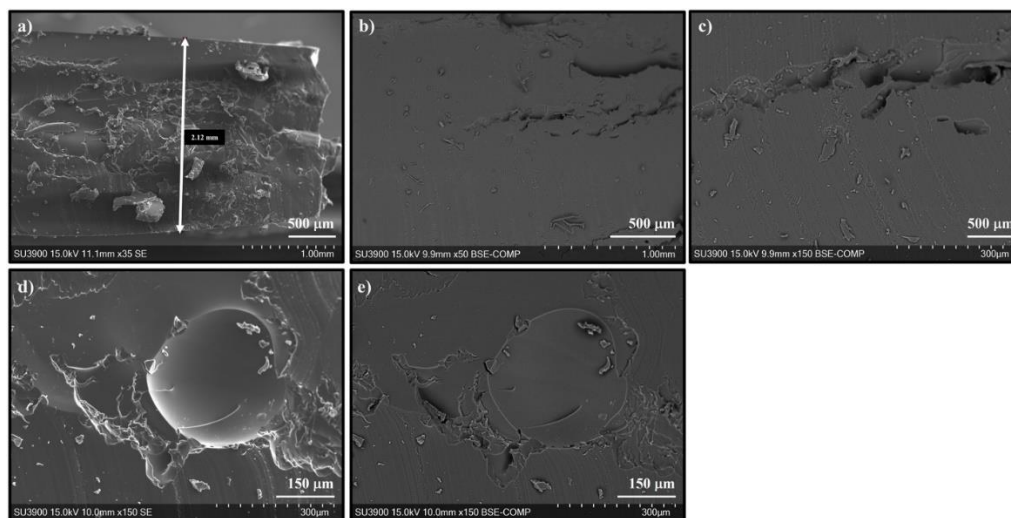


**Figure 3.36. Cross-section SEM micrographs of a third-generation CapturePhos polymer (P-46).**

The last polymer analyzed, top-down and in cross-section, by SEM/EDX was from the last generation of the CapturePhos polymers. Some impurities were obvious from the top-down micrographs as well as shallow inclusions of uncured polymeric sites (Figure 3.37).

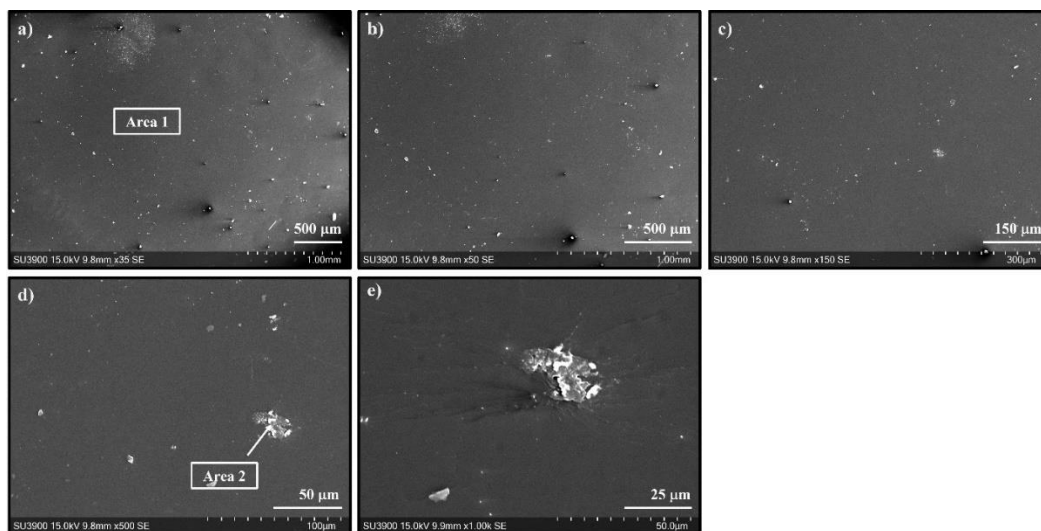


**Figure 3.37. Top-down SEM micrographs of a fourth-generation CapturePhos polymer (P-65). The areas marked indicate the EDX areas in Table 3.22.**

The semi-quantitative EDX analysis, presented in Table 3.22, was consistent with the previous data for the other CapturePhos polymers.

**Table 3.22. EDX semi-quantitative data for P-65.**

Spectrum Label	Elements Detected (wt. %)						
	C	O	P	Cl	Ca	Na	Si
Area 1	65.8	16.3	17.8	0.1	-	-	-
Area 2	65.4	24.0	9.6	0.2	0.1	0.6	0.1

The thickness of the cross-section was 944  $\mu\text{m}$ , deeming P-65 the thinnest polymer analyzed. In general, the cross-section seemed fairly clean and homogenous, with the exception of a small 50  $\mu\text{m}$  void.

With the different generations, it was noticeable that the polymers were improved, since fewer voids and cleaner cross-sections were imaged. However, the SEM micrographs of the surface and cross-sections of the polymers showed the heterogeneous nature of the polymers, overall, as a number of the polymers had uncured polymeric sites. This provided an insight on the reason behind the high resistance of the polymer and the large electric field required. Furthermore, the thicknesses of the polymers did not facilitate ion migration, as a thicker membrane did not necessarily indicate more fixed group sites available for temporary ion attraction.

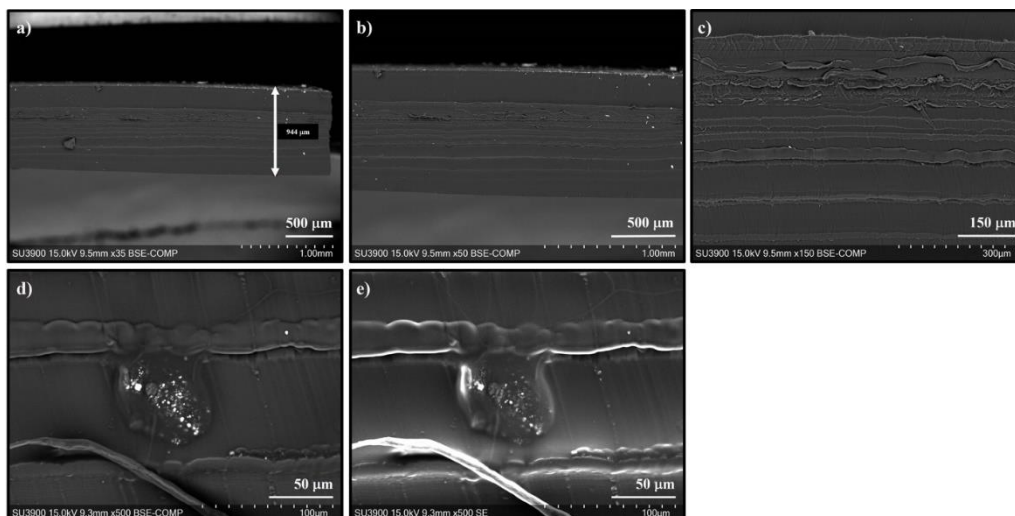


**Figure 3.38. Cross-section SEM micrographs of a fourth-generation CapturePhos polymer (P-65).**

In order for a polymer to classify as an IEM, it has to meet certain criteria. These include mechanical strength, electrical stability, low electrical resistance, high chemical stability, and most importantly, ion exchange capabilities. Electrochemically, all generations of CapturePhos polymers demonstrated high resistance, and poor electrical stability; significant  $\text{Ni}^{2+}$  ion migration was not documented for the polymers. However, decreasing the polymer's thickness improved its electrical resistance.

### Discussion

Previous reports, of CapturePhos's ability to capture ionic species that led to this research, were performed with a gel form rather than a polymeric sheet [13]. The high uptake noted for  $\text{Rh}^{2+}$  and  $\text{Ru}^{2+}$  opened the door to the possibility that, with some modifications, CapturePhos can potentially be employed as an IEM. However, challenges emerged as the testing of the various polymer formulations proceeded. The first problem encountered was the thickness of the polymers. The typical thickness of IEMs falls in the micrometer range, whereas the majority of the CapturePhos polymers, apart from P-65, had a thickness in the millimeter range [17]. As evident from the various attempts at installing these polymers in the ED unit testing scenarios, as well as from literature, the large thickness of the polymers caused high electrical resistance, rendering them impractical as IEMs [33]. Similarly, the majority of the CapturePhos polymers did not portray the mechanical strength required for

IEMs, as shown in Figure 3.27. The curing and polymerization steps seemed to alter the performance of the CapturePhos polymer compared to the gel form.

In real-world applications, ED IEMs encounter various chemical environments and mechanical stresses, depending on the specific application of the ED operation. Therefore, researchers looking to develop and commercialize novel polymers, such as CapturePhos, should consider the conditions an ED IEM would be subjected to for example, environments with high or low pH, physical strain of the ED equipment, flow of contaminated solution in the cell, and the pressure of pumping contaminated solution and/or rinse solutions in the cells, among other considerations. Thus, further polymer modifications would be required in order to classify the CapturePhos polymers as IEMs and utilize them in ED processes.

Finally, the research presented here illustrated the first attempts at forming polymeric membranes from the CapturePhos formulation and the challenges encountered. Suggestions on advancing future work can be found in the section below.

## 4. Conclusions and Future Work

### 4.1 Conclusions

In this work, the chemical and electrochemical sequestration performance of a commercially available polymer, Nafion 117, and a novel polymer, CapturePhos, were investigated. Two types of metal ion were chosen for the investigation,  $\text{Ni}^{2+}$  and  $\text{Sr}^{2+}$ , for their toxicity;  $\text{Sr}^{2+}$  was also chosen because its electrochemical capture had not been investigated previously. Also,  $\text{Sr}^{2+}$  was chosen because the obtained results can be correlated to the capture of its radionuclides and also because of its relation to radioactive waste. This research is of great relevance to the nuclear industry, as decontamination methods that capture dissolved radionuclides are lacking. Specifically, no water decontamination techniques selective at the ionic speciation level exist today.

Factors affecting the performance of the polymers in ED-simulated experiments, such as the pre-treatment effect, CD applied, and pH, were investigated. The removal efficiency was calculated for each experiment along with the EC.

Several pre-treatments performed with DI H<sub>2</sub>O and 1 M HCl were tested. A pre-treatment consisting of thirty-minute soaks in the two solutions, at 75 °C, was found to result in the highest desorption of the Ni<sup>2+</sup> ions, as 88% of the ions were removed from the sample.

The LCD was determined for the four testing solutions (100 ppm Ni<sup>2+</sup>, 500 ppm Ni<sup>2+</sup>, 1000 ppm Ni<sup>2+</sup>, and 500 ppm Sr<sup>2+</sup>). The solution tested with 500 ppm Sr<sup>2+</sup> demonstrated the lowest LCD and the values increased with increasing Ni<sup>2+</sup> concentrations for the other three solutions. Experiments were performed with CDs above and below the LCDs in order to verify the true extent of the effect of the LCD on the ED performance. It was shown that CDs applied above the LCD indeed yielded low removal of the ion of interest whereas experiments performed with CDs below the LCD performed in an opposite manner.

Controlling the pH proved helpful in experiments performed with Ni<sup>2+</sup> solutions. An experiment was performed at a CD of 0.58 mA/cm<sup>2</sup> and the pH of the concentrate solution was controlled at 2 by the addition of HCl, as needed. The removal efficiency measured was the highest from that group of experiments and this experiment demonstrated the lowest EC as well.

Nafion 117 had a stronger affinity, and better removal efficiency, for Sr<sup>2+</sup> than for Ni<sup>2+</sup>. This was consistently observed in chemical and electrochemical experiments. In fact, experiments performed with 500 ppm Sr<sup>2+</sup> had the highest removal efficiencies, overall. This could be explained by the larger ionic radius of Sr<sup>2+</sup>.

The Nafion polymer was successfully regenerated post-experimentation as shown by the FT-IR data. Two spectra were collected, one of an as-received membrane and one of a membrane which had been used in prior experiments. Both FT-IR spectra were almost identical, with the exception of increased hydration noted in the experimentation sample.

The first CapturePhos polymer (P-91) had the best chemical sequestration, whereas the polymer with the final formulation (P-65) showed the best electrochemical performance, although it displayed extremely high electrical resistance.

The higher electric field required for the CapturePhos can be attributed to the presence of voids and to the thickness of the polymer. The chemical composition of the samples was consistent among the four generations.

The fourth and last generation of the CapturePhos polymers tested demonstrated their ability to be used as possible IEMs. Some aspects of the polymers must be optimized; however, the CapturePhos polymers showed strong promise for their use as IEMs, nonetheless. The ability to modify the network, by installing different ligand systems, and tailor which cation it attracts and ligates increases its attractiveness as the next generation of CEMs.

## 4.2 Future Work

This research laid the groundwork for future studies on the electrochemical removal of metal ions from contaminated wastewater, via ED and IEMs. The novel formulation of CapturePhos was investigated for the first time, in polymeric form, as IEMs. In the future, it would be beneficial to investigate the following:

- Effect of flow cell on the removal efficiency of the polymers. Most real-world ED operations use setups similar to that of a flow cell and so evaluating the performance of the Nafion 117 and CapturePhos polymers in such a setup would be of value. Attempts at designing and printing numerous 3D flow cells were made however, the final cell made had some functional errors and due to time limitations, this part of the project was not investigated further. Thus, it would be beneficial to modify the flow cell and investigate the many factors associated with it, such as the effect of flow rate, electrode rinse solutions, and recycling the water past the membrane during variety of ED experiment lengths.
- Concentrations of  $\text{Sr}^{2+}$  other than 500 ppm. Only one concentration of  $\text{Sr}^{2+}$  was investigated, and it would be helpful to repeat experiments performed, starting from LCD determination, to investigating the other factors for solutions with more and less than 500 ppm  $\text{Sr}^{2+}$ . Also, the reproducibility of the results should be verified for some of the experiments, i.e., the p-H controlled experiment, as repeat experiments were not performed.

- The effect of electric field generation method. It was demonstrated that a PS experiment had a high removal efficiency of  $\text{Sr}^{2+}$  however, this was not investigated further.
- The sequestration behaviour of the polymers towards monovalent and other divalent ions. The uptake  $\text{Ni}^{2+}$  and  $\text{Sr}^{2+}$  was investigated for the Nafion polymer and only the uptake of  $\text{Ni}^{2+}$  was investigated for CapturePhos. For example, it would be worthwhile to investigate the chemical and electrochemical uptake of  $\text{Rh}^{2+}$  and  $\text{Ru}^{2+}$  by the CapturePhos membranes, since previous reports only studied the uptake of these elements by the gel form of the CapturePhos formulation.
- Studies focusing on multi-component solutions to verify the effect of the presence of other ions and the competitions between them on the effectiveness of the CapturePhos compared to other IEMs. In reality, contaminated solutions consist of many ionic species and contaminants. For this reason, adding other metal ions to the test solutions can demonstrate the true efficiency of the polymers and would provide insight into which potential contaminants the polymers have strong affinity towards.
- Modify the chain-extender and cross-linker in the CapturePhos formulation. The ratio of the two components in the polymers and the formulation amount cured can adjust the mechanical strength and thickness of the polymers, respectively. It was reported that installing a siloxane cross-linker as opposed to TTT increased the stability of the network [62] and so, it would be of value to test samples of the polymer with the siloxane cross-linker as IEMs in an ED setup.
- Functionalize the parent CapturePhos formulation. Once the correct components and amounts are identified and a polymer resembling an IEM more closely is formed, install into the polymer and test various possible functional groups. The functionalization of the polymer allows for selectivity towards specific contaminant ions, which is an area still under research for ED applications. This was another key feature of the polymeric network that ignited interest in their use as IEMs.

## 5. References

- [1] Sillanpää, M.; Shestakova, M. Introduction. In *Electrochemical Water Treatment Methods: Fundamentals, Methods and Full Scale Applications*; Elsevier Inc., 2017; pp 1–46.
- [2] Ghernaout, D.; Elboughdiri, N. Electrochemical Technology for Wastewater Treatment: Dares and Trends. *Open Acc. J. lib.* **2020**, *7*, e6020.
- [3] Tchounwou, P. B.; Yedjou, C. G.; Patlolla, A. K.; Sutton, D. J. Heavy Metals Toxicity and the Environment. *Mol. Clin. Environ. Toxicol.* **2012**, *101*, 133–164.
- [4] Coman, V.; Robotin, B.; Ilea, P. Nickel Recovery/Removal from Industrial Wastes: A Review. "Resources, *Conserv. Recycl.* **2013**, *73*, 229–238.
- [5] Barakat, M. A. New Trends in Removing Heavy Metals from Industrial Wastewater. *Arab. J. of Chem* **2011**, *4* (4), 361–377.
- [6] Sjøgaard, E. G. *Chemistry of advanced environmental purification processes of water: fundamentals and applications*; Elsevier: Amsterdam, 2014.
- [7] Wastewater Treatment. *Environmental Science and Technology*; 1995; Vol. 29, p 240.
- [8] States, U. How Wastewater Treatment Works... The Basics. **1998**.
- [9] Sharma, S.; Bhattacharya, A. Drinking Water Contamination and Treatment Techniques. *Appl. Water Sci.* **2017**, *7* (3), 1043-1067.
- [10] McFee, J.; Krishnan, R.; Piao, H.; Randall, P. Decontamination Methods for Drinking Water Treatment and Distribution Systems. *Wiley Handb. Sci. Technol. Homel. Secur.* **2009**.
- [11] Membrane Filtration. Minnesota Rural Water Association, <https://www.mrwa.com/WaterWorksMnl/Chapter 19 Membrane Filtration.pdf> (accessed July 19, 2022).
- [12] Li, N. N.; Fane, A. G.; Ho, W. S. W.; Matsuura, T. *Advanced Membrane Technology and Applications*; 2008.
- [13] Biesheuvel, P. M.; Porada, S.; Elimelech, M.; Dykstra, J. E. Tutorial Review of Reverse Osmosis and Electrodialysis. *J. Memb. Sci.* **2022**, *647*, 1–58.
- [14] Liu, Y.; Deng, Y. Y.; Zhang, Q.; Liu, H. Overview of Recent Developments of Resource Recovery from Wastewater via Electrochemistry-Based Technologies. *Sci. Total Environ.* **2021**, *757*, 143901.
- [15] Sirés, I.; Brillas, E.; Oturan, M. A.; Rodrigo, M. A.; Panizza, M. Electrochemical Advanced Oxidation Processes: Today and Tomorrow. A Review. *Environ. Sci. Pollut. Res.* **2014**, *21* (14), 8336–8367.
- [16] Ghernaout, D.; Elboughdiri, N. Electrochemical Technology for Wastewater Treatment: Dares and Trends. *Open Access J. ibrary* **2020**, *7*, e6020.
- [17] Strathmann, H.; Grabowski, A.; Eigenberger, G. Ion-Exchange Membranes in the Chemical Process Industry. *Ind. Eng. Chem. Res.* **2013**, *52* (31), 10364–10379.

- [18] Sillanpää, M.; Shestakova, M. Electrochemical Water Treatment Methods. In *Electrochemical Water Treatment Methods: Fundamentals, Methods and Full Scale Applications*; Elsevier Inc., 2017; pp 74–87.
- [19] Shahedi, A.; Darban, A. K.; Taghipour, F.; Jamshidi-Zanjani, A. A Review on Industrial Wastewater Treatment via Electrocoagulation Processes. *Curr. Opin. Electrochem.* **2020**, *22*, 154–169.
- [20] Strathmann, H. Electrodialysis, a Mature Technology with a Multitude of New Applications. *Desal.* **2010**, *264* (3), 268–288.
- [21] Scarazzato, T.; Barros, K. S.; Benvenuti, T.; Rodrigues, M. A. S.; Espinosa, D. C. R.; Bernardes, A. M. B.; Amado, F. D. R.; Pérez-Herranz, V. Achievements in Electrodialysis Processes for Wastewater and Water Treatment. In *Current Trends and Future Developments on (Bio-) Membranes: Recent Achievements in Wastewater and Water Treatments*; Elsevier Inc., 2020; pp 127–160.
- [22] Martí-Calatayud, M.C.; Buzzi, D.C.; García-Gabaldón, M.; Bernardes, A.M.; Tenório, J.A.S.; Pérez-Herranz, V. Ion Transport Through Homogeneous and Heterogeneous Ion-Exchange Membranes in Single Salt and Multicomponent Electrolyte Solutions. *J. Memb. Sci.* **2014**, *466*, 45–57.
- [23] Costis, S.; Mueller, K. K.; Coudert, L.; Neculita, C. M.; Reynier, N.; Blais, J. F. Recovery Potential of Rare Earth Elements from Mining and Industrial Residues: A Review and Cases Studies. *J. Geochemical Explor.* **2021**, *221*, 106699.
- [24] Luo, T.; Abdu, S.; Wessling, M. Selectivity of Ion Exchange Membranes: A Review. *J. Memb. Sci.* **2018**, *555*, 429–454.
- [25] Tanaka, Y. *Ion Exchange Membranes Fundamental and Applications*, 12th ed.; Elsevier: Oxford, UK, 2007.
- [26] Nuclear Waste Management Organization. <https://www.nwmo.ca/> (accessed November 7, 2022).
- [27] Canadian Radioactive Waste Summit. Integrated Strategy on Radioactive Waste What We Heard Report (1); Online, March 30-April 1, 2021; 1-25.
- [28] Sugimoto, S. I. Removal of Radioactive Ions from Nuclear Waste Solutions by Electrodialysis. *J. Nucl. Sci. Technol.* **1978**, *15* (10), 753–759.
- [29] Sugimoto, S. I. Removal of Radioactive Ions from Nuclear Waste Solutions by Electrodialysis. *J. Nucl. Sci. Technol.* **1978**, *15* (10), 753–759.
- [30] Horr, C. A. *Chemistry of Strontium in Natural Water*; 1959.
- [31] Walters, W. R.; Weiser, D. W.; Marek, L. J. Concentration of Radioactive Aqueous Wastes. Electromigration Through Ion-Exchange Membranes. *Ind. Eng. Chem.* **1955**, *47* (1), 61–67. <https://doi.org/10.1021/ie50541a027>.
- [32] Søggaard, E. G. *Chemistry of advanced environmental purification processes of water: fundamentals and applications*; Elsevier: Amsterdam, 2014.

- [33] Tzanetakis, N.; Taama, W. M.; Scott, K.; Jachuck, R. J. J.; Slade, R. S.; Varcoe, J. Comparative Performance of Ion Exchange Membranes for Electrodialysis of Nickel and Cobalt. *Sep. Purif. Technol.* **2003**, *30*, 113–127.
- [34] Smičiklas, I.; Coha, I.; Jović, M.; Nodilo, M.; Šljivić-Ivanović, M.; Smiljanić, S.; Grahek, Ž. Efficient Separation of Strontium Radionuclides from High-Salinity Wastewater by Zeolite 4A Synthesized from Bayer Process Liquids. *Sci. Rep.* **2021**, *11* (1), 1–14.
- [35] Nafion N115, N117, N1110 Ion Exchange Materials. Product Bulletin P-12, 2016. Fuel Cell Store. <https://www.fuelcellstore.com/spec-sheets/chemours-nafion-115-117-1110-spec-sheet.pdf> (accessed May 21, 2022).
- [36] Kelly, G. R.; Scully, R. J.; Shoesmith, D. W.; Buchheit, G. R. *Electrochemical Techniques in Corrosion Science and Engineering*; Marcel Dekker: New York, 2013.
- [37] Marcus, F.; Mansfield, F. *Analytical Methods in Corrosion Science and Engineering*; [Online]; CRC Press: Florida, 2006.
- [38] Ibanez, R.; Stamatialis, D. F.; Wessling, M. Role of Membrane Surface in Concentration Polarization at Cation Exchange Membranes. *J. Memb. Sci.* **2004**, *239* (1), 119–128.
- [39] La Cerva, M.; Gurreri, L.; Tedesco, M.; Cipollina, A.; Ciofalo, M.; Tamburini, A.; Micale, G. Determination of Limiting Current Density and Current Efficiency in Electrodialysis Units. *Desal.* **2018**, *445*, 138–148.
- [40] Electric current in electrolyte solutions and Ohms law. Climate Change Watchers. <https://www.climate-policy-watcher.org/reverse-osmosis/electric-current-in-electrolyte-solutions-and-ohms-law.html> (accessed June 10, 2022).
- [41] Whiteside, Paul & Chininis, Jeffrey & Hunt, Heather. (2016). *Techniques and Challenges for Characterizing Metal Thin Films with Applications in Photonics. Coatings.*
- [42] Rybak, A.; Rybak, A. Characteristics of Some Selected Methods of Rare Earth Elements Recovery from Coal Fly Ashes. *Metals (Basel)*. **2021**, *11* (142), 1–27.
- [43] Virtual labs. Basics of Scanning Electron Microscopy: Secondary Electron and BSE Imaging Mode. <http://vlabs.iitb.ac.in/vlabs-dev/labs/electron-microscopy/experiments/sem-basics-iitk/theory.html> (accessed July 2, 2022).
- [44] Skoog, D. S.; et al. *Principles of Instrumental Analysis*, 6th ed.; Thomson Brooks: Belmont, CA, 2007; 430–470.
- [45] Theophanides, T. *Introduction to Infrared Spectroscopy, Infrared Spectroscopy - Materials Science, Engineering and Technology*; Theophanides, T. Ed; InTech ,2012; 1-10.
- [46] Carrero, J. A.; Arana, G.; Madariaga, J. M. Spectroscopic Properties of Inorganic and Organometallic Compounds. The Royal Society of Chemistry 2014, 178-210.
- [47] Ralph Müller, R. Instrumental Methods of Chemical Analysis. *Industrial & Engineering Chemistry Analytical Edition* **1941** *13* (10), 667-754

- [48] Cuthbert, T. J.; Evoy, E.; Bow, J. P. J.; Guterman, R.; Stubbs, J. M.; Gillies, E. R.; Ragogna, P. J.; Blacquiere, J. M. CapturePhos-A Phosphorus-Rich Polymer as a Homogeneous Catalyst Scavenger. *Catal. Sci. Technol.* **2017**, *7* (13), 2685–2688.
- [49] Guterman, R.; Rabiee Kenaree, A.; Gilroy, J. B.; Gillies, E. R.; Ragogna, P. J. Polymer Network Formation Using the Phosphane-Ene Reaction: A Thiol-Ene Analogue with Diverse Postpolymerization Chemistry. *Chem. Mater.* **2015**, *27* (4), 1412–1419.
- [50] Huang, L-F.; Hutchison, M. J.; Santucci Jr., R. J.; Scully, J. R.; and J. M. Rondinelli, M. Improved Electrochemical Phase Diagrams from Theory and Experiment: The Ni–Water System and Its Complex Compounds. *The Journal of Phys Chem.* **2017** *121* (18), 9782-9789.
- [51] Gayer, K. H.; Woontner, L. The Solubility of Ferrous Hydroxide and Ferric Hydroxide in Acidic and Basic Media at 25°. *J. Phys. Chem.* **1956**, *60* (11), 1569–1571.
- [52] Nasef, M. M.; Yahaya, A. H. Adsorption of some Heavy Metal Ions from Aqueous Solutions on Nafion 117 Membrane. *Desalination*, **2009**, *249*, 677–681.
- [53] Berthomieu, C.; Hienerwadel, R. Fourier transform infrared (FTIR) spectroscopy. *Photosynth Res* **2009**, *101*, 157–170.
- [54] Millipore Sigma. 2020. IR Spectrum Table and Chart. <https://www.sigmaaldrich.com/technical-documents/articles/biology/ir-spectrum-table.html> (accessed December 1, 2022).
- [55] Barros, K. S.; Martí-Calatayud, M. C.; Pérez-Herranz, V.; Espinosa, D. C. R. A Three-Stage Chemical Cleaning of Ion-Exchange Membranes Used in the Treatment by Electrodialysis of Wastewaters Generated in Brass Electroplating Industries. *Desalination* **2020**, *492* (July), 114628.
- [56] Ion Power. Nafion 117. <https://ion-power.com/product/nafion-n117/> (accessed December 1, 2022).
- [57] Nickel Hydroxide. PubChem. <https://pubchem.ncbi.nlm.nih.gov/compound/Nickel-hydroxide#section=Uses> (accessed July 1, 2021).
- [58] Le, X. T.; Bui, T. H.; Viel, P.; Berthelot, T.; Palacin, S. On the Structure-Properties Relationship of the AMV Anion Exchange Membrane. *J. Memb. Sci.* **2009**, *340* (1–2), 133–140.
- [59] Kuwertz, R.; Kirstein, C.; Turek, T.; Kunz, U. Influence of Acid Pretreatment on Ionic Conductivity of Nafion® Membranes. *J. Memb. Sci.* **2016**, *500*, 225–235.
- [60] Skilbred, Ellen Synnøve. (2016). Corrosion of Nickel-Aluminium Bronze - How does the different alloying elements effect the corrosion properties. 10.13140/RG.2.2.22278.57922.
- [61] Dardel, F. D.; Arden, T. V. Ion Exchangers. In *Ullmann's Encyclopedia of Industrial Chemistry*; Wiley, 2012; pp 473–545.

[62] Duggan, Kelly C., "Synthesis and Characterization of Phosphorus Containing Polymers for the Purpose of Polymer Derived Ceramics" (2022). *Electronic Thesis and Dissertation Repository*. 8387. <https://ir.lib.uwo.ca/etd/8387>.

# Baian Almusned

## Education

---

<b>Master of Science</b> , Analytical/Physical Chemistry <i>Western University – London, ON</i>	<b>2020 – 2023</b>
<b>Bachelor of Science</b> , Honors Specialization in Chemistry and Minor in Psychology <i>Western University – London, ON</i>	<b>2013 – 2018</b>

## Graduate Courses

---

9524A – Electrochemistry	<b>92%</b>
9674A – Spectroscopy and Microscopy	<b>91%</b>
9525B – Corrosion	<b>AUD</b>

## Relevant Experience

---

<b>Research Scientist</b> <i>Surface Science Western – London, ON</i>	<b>June 2022 – Present</b>
<b>Research Assistant</b> <i>Surface Science Western – London, ON</i>	<b>May 2018 – Dec 2019</b>
<b>Undergraduate Thesis Student</b> <i>Western University – London, ON</i>	<b>Sep 2017 – Apr 2018</b>
<b>Summer Research Student</b> <i>Western University – London, ON</i>	<b>May 2017 – Aug 2017</b>
<b>Vice-President</b> <i>Electrochemical Society (ECS) Student Chapter at Western University – London, ON</i>	<b>Feb 2021 – June 2022</b>
<b>Graduate Teaching Assistant</b> <i>Western University – London, ON</i>	<b>Sep 2020 – Dec 2021</b>
<b>Outreach Officer</b> <i>Electrochemical Society (ECS) Student Chapter at Western University – London, ON</i>	<b>Mar 2020 – Jan 2021</b>

## Honours and Awards

---

• Marie Sklodowska Curie Fellowship Program recipient, International Atomic Energy Agency (IAEA)	<b>2021</b>
• 1 <sup>st</sup> Place, Poster Session, NACE Southern Ontario Student Section 11 <sup>th</sup> Annual Symposium	<b>2021</b>
• 1 <sup>st</sup> Place, Analytical Division, 46 <sup>th</sup> Southern Ontario Undergraduate Student Chemistry Conference	<b>2018</b>
• Dean's Honour List	<b>2014</b>
• Entrance Scholarship	<b>2013</b>

## Publications

---

J.D. Henderson, B. Almusned, M. Momeni, S. Anderson, V. Dehnavi, D. Zagidulin, D.W. Shoesmith, and J.J. Noël, "Investigating the influence of Cr and Mo additions to commercial Ni-based alloys exposed to neutral and acidic chloride solutions", *J. Electrochem. Soc.*, **167** (2020) 131512.

## Conference Presentations

---

• <b>Water Decontamination via Electrodialysis</b> <i>Western Research Forum– Virtual</i> <u>B. Almusned</u> and J.J. Noël	<b>March 15 –16, 2022</b>
• <b>Electrodialysis Study of Ni<sup>2+</sup> Uptake Using Nafion 117 Membrane</b> <i>NACE Southern Ontario Student Section 11<sup>th</sup> Annual Symposium – Virtual</i> <u>B. Almusned</u> and J.J. Noël	<b>July 22 – 23, 2021</b>
• <b>Analysis of Ni-Cr-Mo Super Alloys Using X-ray Photoelectron Spectroscopy Imaging</b> <i>Gordon Research Conference on Aqueous Corrosion – New London, NH</i> M. Badley, J.D. Henderson, <u>B. Almusned</u> , B.A. Kobe, M.C. Biesinger, D.W. Shoesmith, and J.J. Noël	<b>July 8 – 13, 2018</b>

# Baian Almusned

---

- **Corrosion of Nickel-Chromium-Molybdenum Alloys**

March 24, 2018

*46<sup>th</sup> Southern Ontario Undergraduate Student Chemistry Conference – Waterloo, ON*

B. Almusned, J.D. Henderson, M. Badley, B.A. Kobe, D.W. Shoesmith, and J.J. Noël

## Conferences

---

- Western Research Forum **2022**
- Electrochemical Society (ECS) 5<sup>th</sup> Annual Student Symposium **2021**
- NACE Southern Ontario Student Section 11<sup>th</sup> Annual Student Symposium **2021**
- Canadian Radioactive Waste Summit **2021**
- Corrosion Science webinar series (CorroZoom) **2021**
- NACE Southern Ontario Student Section 10<sup>th</sup> Annual Student Symposium **2020**
- Electrochemical Society (ECS) 4<sup>th</sup> Annual Student Symposium **2020**
- NACE Southern Ontario Student Section 8<sup>th</sup> Annual Student Symposium **2018**
- 46<sup>th</sup> Southern Ontario Undergraduate Student Chemistry Conference **2018**